

Towards a Quieter World: Three-Dimensional Printed Acoustic Metamaterials for Noise Control

Cecilia Casarini

Centre for Ultrasonic Engineering
Department of Electronic & Electrical Engineering
University of Strathclyde

A thesis submitted for the degree of
Doctor of Philosophy

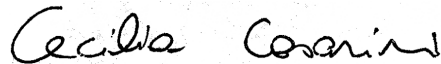
August 2021, Glasgow, UK.

Declaration

This thesis is the result of the author's original research. It has been composed by the author and has not been previously submitted for examination which has led to the award of a degree. The copyright of this thesis belongs to the author under the terms of the United Kingdom Copyright Acts as qualified by University of Strathclyde Regulation 3.50. Due acknowledgement must always be made of the use of any material contained in, or derived from, this thesis.

Date: 1 April 2021

Signed:

Handwritten signature of Cecilia Corrin in black ink.

Abstract

Environmental noise impacts the everyday life of millions of people and it represents a growing concern for the health of the world's population. To mitigate this impact, noise reducing materials such as foam or barriers are employed extensively with effective results. However, the efficacy of such materials is limited by the inverse relationship between the frequency of the attenuated waves and materials characteristics like thickness and density, as described by the mass-law. In order to overcome this fundamental limitation, a new challenge in acoustic engineering has emerged to design and manufacture lightweight and subwavelength materials that can break the mass-law. A potential solution to this challenge is represented by a recently discovered family of materials, called acoustic metamaterials, which show properties typically not found in nature. These materials are made of resonant building blocks that are smaller than the wavelength of the attenuated acoustic wave. When these building blocks are combined to form a metamaterial, they lead to the formation of band gaps - near their resonance frequency - that deeply attenuate the incident sound. The manufacturing of noise reducing acoustic metamaterials could also largely benefit from recent advances in three-dimensional printing technologies, as they offer the possibility to fabricate abstract shapes and to carefully choose some properties of the printed materials. The work presented in this thesis describes the modelling, fabrication and measurement of noise reducing acoustic metamaterials based on Helmholtz resonators, thin plates and active piezoelectric plates. These materials have been produced through original and innovative three-dimensional printing techniques. The results of this thesis can be applied to noise control in audio applications such as headphones, hearing aids and smart speakers. Similarly, other fields like aerospace and automotive industry or architectural acoustics could also greatly benefit from lightweight subwavelength noise reduction.

Acknowledgements

First and foremost special thanks to my supervisors Dr. Joseph Jackson and Prof. James Windmill. Thank you for giving me the opportunity to be a PhD researcher and for always providing precious feedback during these years. I am grateful not only for your constant help, but also because you gave me the freedom to shape this journey in a way that best reflected my research interests and career ambitions.

Thank you also to all the students and researchers that I met through the European COST Action DENORMs events. Being part of a research network is an invaluable learning experience that allowed me to develop new projects and improve existing ones. In particular, thanks to Dr. Vicent Romero-García and to Dr. Jean-Philippe Groby for hosting me at the University of Le Mans and for engaging in a fruitful collaboration.

My PhD would have not been the same without all the crew at the Centre for Ultrasonic Engineering. The hours spent in the lab together, the annual visit to Loch Lomond, and above all, those shared lunches and huge orders of coffee have been fun, cheerful, and will be a long-lasting memory.

During these years I was able to complete two internships at Apple Inc., and I would like to thank all the engineers, colleagues, fellow-interns, and foosball opponents I met in sunny California, who helped and encouraged me through this learning adventure.

Finally, this has been a long ride, that allowed me to travel around the world to attend conferences across Europe, to live in Scotland, California, and - due to a

global pandemic - Sicily. A heartfelt thanks goes to my closest friends and family in Italy and around the world for supporting me and for checking-in even when I was living far away.

To all of you: grazie. I hope you will enjoy reading this thesis. Slàinte mhath!

Contents

Declaration	i
Abstract	ii
Acknowledgements	iii
Contents	v
List of Figures	viii
List of Tables	xv
1 Introduction	1
1.1 Motivation	1
1.2 Novelty of Research & Objectives	4
1.3 Thesis Organization	4
1.4 List of Publications	6
2 Background and Theory	7
2.1 Introduction	7
2.2 Fundamentals of Acoustics	7
2.2.1 Acoustics of Waves	9
2.2.2 Helmholtz Resonator	17
2.2.3 Membranes and Plates	26
2.3 Review of Noise Control Techniques	33
2.3.1 Acoustic Materials	33

2.3.2	Insulators	34
2.3.3	Absorbers	35
2.3.4	Diffusers	37
2.3.5	Active Noise Cancellation	37
2.4	Review of Acoustic Metamaterials	38
2.4.1	General Introduction to Metamaterials	38
2.4.2	The Origin of Metamaterials	39
2.4.3	Acoustic Metamaterials	42
2.4.4	Acoustic Metamaterials Based on Local Resonances	50
2.4.5	Active Acoustic Metamaterials	52
2.4.6	Applications of Acoustic Metamaterials	55
3	Methods	63
3.1	Three-Dimensional Printing	63
3.2	Acoustic Booth Measurements	73
3.3	Laser Doppler Vibrometer Measurements	75
3.4	Impedance Tube Measurements	78
3.5	Transfer Matrix Modelling Method	78
3.6	Finite Element Modelling Method	83
4	3D Printed Acoustic Metamaterials Based on Tunable Helmholtz Resonators	89
4.1	Introduction	89
4.2	Methods	91
4.3	Model	97
4.4	Results	102
4.5	Conclusion and Future Work	107

5	Fabrication and Characterisation of Thin Plates for Acoustic Metamaterials Applications	110
5.1	Introduction	110
5.2	Methods	111
5.3	Model	114
5.4	Results	120
5.5	Conclusion and Future Work	126
6	Three-Dimensional Printed Acoustic Metamaterials Devices and Applications	128
6.1	Introduction	128
6.2	Three-Dimensional Printed Printed Active Acoustic Metamaterials	129
6.3	3D Printed Quiet Headphones Based on Acoustic Metamaterials .	133
6.4	Conclusion and Future Work	138
7	Conclusion and Future Work	140
A	APPENDIX	145
A.1	MATLAB Codes for Parametric Models of Helmholtz Resonators	145
A.2	MATLAB Codes for Parametric Models of Thin Plates	155
	Bibliography	173

List of Figures

2.1	Lindsay’s wheel of acoustics [1, 2] describing the different fields and subfields that deal with acoustics, source https://exploresound.org/what-is-new/fields-of-acoustics/ , accessed on 10 April 2021.	8
2.2	Helmholtz resonators made in 1870, Hunterian Museum and Art Gallery in Glasgow, source https://en.wikipedia.org	19
2.3	Representation of a Helmholtz resonator consisting of a cylindrical neck of length l , cross-sectional area S , and a cylindrical cavity of volume V and length h	20
2.4	Amplitude and phase lag of a driven damped Helmholtz resonator. The resonance frequency of the resonator is slightly higher than 5 kHz, its mass is 1 kg, damping is 1000. When the frequency of driving force is at 5 kHz, the mass of air in the neck oscillates in anti-phase with the impinging wave.	24
2.5	Amplitude and phase lag of a driven damped Helmholtz resonator. The frequency of the resonator with no damping is at 5 kHz, its mass is 1 kg, the damping value is swept between 1 and 10000 with an increment of 1000. The effect of the damping is noticeable in the detuned frequency and decreased Q factor.	25
2.6	Amplitude of vibration of a Helmholtz resonator decreases with increasing damping.	25
2.7	First twelve vibration modes of clamped membrane, obtained with MATLAB.	30
2.8	First twelve vibration modes of circular plates, obtained with MATLAB. Although the modes behaviour is the same as that of membranes, plates present higher and more distanced frequencies for corresponding modes.	32

2.9	Reflection, absorption and transmission of incident acoustic energy at a boundary including a material layer.	34
2.10	Visualisation of the refraction of a wave propagating between two different media as described by Snell’s law.	40
2.11	Visualisation of possible regions of wave refraction w_r when an incident wave w_i propagates between two different media. Quadrants 1 and 4 exhibit negative refractive index n and quadrants 2 and 3 positive refractive index n	41
2.12	First experimental realisation of acoustic metamaterials proposed by Liu et al. [3]. A three-dimensional structure made of periodically spaced lead spheres embedded in an epoxy matrix is capable of isolating low-frequency sound and to break the mass law.	43
2.13	Two-dimensional sonic crystal outdoor sculpture by Eusebio Sempere and resulting sound attenuation [4].	45
2.14	Two-dimensional sonic crystal slab based on aluminium rods embedded in air and resulting sound transmission [5].	46
2.15	Ultrasonic metamaterials based on Helmholtz resonators, proposed by Fang et al. [6] (a) Schematic of Helmholtz resonator, (b) chain of Helmholtz resonators, (c) effective modulus.	53
2.16	Acoustic metamaterials based on soda cans, introduced by Lemoult et al. [7]. (a) experimental setup, (b) sound transmission and band gap.	53
2.17	Transmission spectra and displacement amplitude of membrane-based acoustic metamaterials with attached mass as proposed by Yang et al. [8].	54
2.18	Single-sensor multispeaker based on acoustic metamaterials developed by Xie et al. [9].	56
2.19	Acoustic dispersive prism based on membrane-type acoustic metamaterials developed by Esfahlani [10].	57
2.20	Ultra-open acoustic metamaterial silencer proposed by Ghaffari-wardavagh [11].	58
2.21	Acoustic cloak [12].	59
2.22	Acoustic metasurface [13].	59

2.23	Single negative acoustic metamaterials producing a near-field subwavelength image [14].	60
2.24	Double negative acoustic metamaterials producing a subwavelength real image [14].	61
2.25	Energy harvesting metamaterial proposed by Wu et al.[15]. The PVDF film at the centre of a sonic crystal shows maximum output voltage near the resonance of the cavity created by the point defect in a 5 X 5 array of rods.	62
3.1	Illustration of SLA three-dimensional printer.	67
3.2	Illustration of FDM three-dimensional printer.	68
3.3	Illustration of the effect of adding Sudan I to the mix. Panel (a) shows an over-polymerisation when printing onto a void: a single layer expands to 10 layers, resulting in a thick membrane. Panel (b) shows how Sudan I absorbs the light and controls the exposure, resulting in a membrane of correct thickness.	70
3.4	Step by step illustration of customized three-dimensional printing process.	72
3.5	Experimental setup: a loudspeaker connected to a function generator emits a swept sine wave that impinges on the three-dimensional printed sample. A microphone, connected to a pre-amplifier and positioned right above the metamaterials, records the signal controlled by a data acquisition device and triggered by a software running on a laptop.	74
3.6	Illustration of Laser Doppler Vibrometer working principle, informed by http://www.polytec.com/us/company/technologies/	76
3.7	Schematic of setup used to measure objects vibration using a Polytec Laser Doppler Vibrometer.	77
3.8	Sketch of a four-microphone impedance tube and sample, used for transfer matrix method modelling as proposed by Song and Bolton [16, 17].	79
3.9	Geometry of Helmholtz resonators and impedance tube built with COMSOL Multiphysics.	85

3.10	Free tetrahedral meshed geometry of Helmholtz resonators and impedance tube built with COMSOL Multiphysics.	86
3.11	Transmission, reflection and absorption coefficients obtained by exporting acoustic pressure at microphones positions in COMSOL and plotted in MATLAB.	86
3.12	Sound Pressure Level at 700 Hz and 1500 Hz plotted in COMSOL Multiphysics.	88
4.1	Setup and measurements of acoustic metamaterials based on soda cans by Lemoult et al. [7].	90
4.2	Front view (a) and bottom view (b) of the small-scale acoustic metamaterials based on a 3 X 3 array of Helmholtz resonators. Equivalent CAD model (c) and wireframe view (d).	93
4.3	Thickness of the membranes against exposure time of UV light during the three-dimensional printing process. Longer exposure times will result in thicker membranes. The relation between these two parameters varies with the material used and the amount of absorber in the fluid.	94
4.4	Front view (a) and bottom view (b) of acoustic metamaterials based on thin plates and Helmholtz resonators. Equivalent CAD model with cut away section (c) and bottom view (d). The membranes have been highlighted in yellow for a better understanding of the design.	95
4.5	Experimental set-up: a speaker connected to a function generator emits a swept sine wave that impinges on the three-dimensional printed sample. A microphone, connected to a pre-amplifier and positioned right above the metamaterials, records the signal controlled by NI-DAQ hardware and MATLAB code running on a laptop.	96
4.6	Robotic arm configuration. To verify that the attenuation of sound in the band gap happens at any incident angle of the source a robotic arm holding a loudspeaker traces a quarter hemisphere around the sample. A reference microphone measures the sound transmission in air while a second microphone measures the transmission above the sample.	97

4.7	Plot of the sum of the response of N oscillators and an external sinusoidal driving force. The values of α (1%) and γ (2500) have been scaled to correlate with experimentally determined responses. Each curve represents the range of N from 1 to 10, with 10 being the darkest.	99
4.8	Variation of two parameters, while keeping the other two parameters at a fixed medium value, allows one to choose a desired value for f_0 and f_1	100
4.9	Variation of two parameters, while keeping the other two parameters at a fixed optimised value that maximises the difference between f_0 and f_1	101
4.10	Plot of normalised sound transmission as a function of frequency, showing an increase in sound attenuation with higher number of resonators. It can be noticed that the band gap is detuned with increased number of resonators. This is due to increased damping with higher number of resonators.	103
4.11	Sound transmission measured above the sample at 5000 Hz (left) and 6600 Hz (right) with respect to the source playing a swept sine wave and positioned along a quarter hemisphere with a radius of 100 ((a), (b)), 200 ((c), (d)), 300 ((e), (f)), and 400 ((g), (h)) mm.	104
4.12	Narrow stop bands 6.5 kHz apart, originated in acoustic metamaterials with unit cells having the dimensions of a soda can scaled down by a factor of 20 (a). Closer stop bands 2.5 kHz apart and hybridised by a band gap where the sound is still attenuated by 10 dB, generated by acoustic metamaterials with tuned overtones (b).	106
4.13	Sound transmission of the acoustic metamaterials based Helmholtz resonators (blue) and based on Helmholtz resonators with thin plates (red). The signal has been acquired above the resonator in the middle of a 3×3 array.	107
5.1	Three-dimensional printed thin plates front (left) and back (right).	113
5.2	Impedance tube used to measure the acoustic coefficients of the plate under test (a). Open sample holder with plate inserted (b) and closed sample holder with plate (c).	113

5.3	Scheme of the system modelled through the transfer matrix method. As in the experiments, the impedance tube contains a sample holder that supports the plate.	114
5.4	Variation of two parameters, while keeping the other two parameters at a fixed value, allows one to choose a desired value for f_0 and f_1 . The values of the fixed parameters are chosen to maximise f_0	116
5.5	Variation of two parameters, while keeping the other two parameters at a fixed value, allows one to choose a desired value for f_0 and f_1 . The values of the fixed parameters are chosen to obtain a mid-frequencies value for f_0	117
5.6	Variation of two parameters, while keeping the other two parameters at a fixed value, allows one to choose a desired value for f_0 and f_1 . The values of the fixed parameters are chosen to minimise f_0	118
5.7	Variation of two parameters, while keeping the other two parameters at a fixed value, allows one to choose a desired value for f_0 and f_1 . The values of the fixed parameters are chosen to obtain a value for f_0 within the speech frequencies range.	119
5.8	Modes (0,1), (1,1), (0,2), (0,3) for the PEGDA 250 sample (a). Modes (0,1), (1,1), (0,2), (1,2) for the PEGDA 700 sample (b). . .	121
5.9	Transmission, reflection and absorption coefficients represented by the dotted lines correspond to the parameters retrieved with the optimised transfer matrix model. The solid lines show reflection and transmission coefficients measured through the impedance tube and normalised to the input signal. PEGDA 250 values are shown in graph (a) and PEGDA 700 in graph (b).	123
5.10	Cross-section of the PEGDA 250 sample used for nanoindentation and obtained with scanning electron microscope. It can be noticed that the top and bottom side contain different amounts of BaTiO ₃ and PEGDA.	125
6.1	Setup used to measure the response of the Helmholtz resonator and to drive the piezoelectric transducer in phase with the signal.	131
6.2	User Interface developed to measure the signal and control the phase and frequency of piezoelectric transducer in real-time. . . .	131

6.3	Front (left) and bottom (right) picture of a three-dimensional printed piezoelectric thin-plate with silver paint sprayed on top.	132
6.4	Measured transmission for simple passive Helmholtz resonator (blue) and active metamaterial (red) composed of a Helmholtz resonator and an active piezoelectric stack. The active metamaterial has a 4 dB deeper band gap, i.e. enhanced noise attenuation.	133
6.5	Headphones based on acoustic metamaterials.	135
6.6	Cut-through view of headphones based on acoustic metamaterials.	135
6.7	Free-field measurement of noise attenuation properties of headphones based on acoustic metamaterials.	136
6.8	Head and torso simulator measurement of noise attenuation properties of headphones based on acoustic metamaterials.	136
6.9	Free-field sound transmission of headphones based on acoustic metamaterials measured in acoustic booth. A frequency band around the speech frequencies shows that it is possible to attenuate noise up to 4 dB in this region (a). Higher frequency bands are also attenuated due to overtones of the resonant meta-atoms (b).	137
6.10	Sound transmission of headphones based on acoustic metamaterials placed on a B&K Head & Torso Simulator inside an acoustic booth. A frequency band around the speech frequencies shows that it is possible to attenuate noise up to 10 dB in this region (a). Higher frequency bands are also attenuated up to 20 dB due to overtones of the resonant meta-atoms (b).	138

List of Tables

2.1	Zeros of Circular Membrane Equation of Motion	29
2.2	Coefficients for Vibration of Circular Plates Clamped at Edge . .	31
2.3	Absorption coefficients of commonly used absorbing materials. . .	35
3.1	Material properties of materials used in this thesis, estimated before printing from vendors specifications and preliminary tests.	69
5.1	Values of fundamental frequency and first circular and radial modes for samples of PEGDA 250 and PEGDA 700 having a 15 mm diameter, measured using a 3D laser vibrometer.	121
5.2	Properties of the materials used to 3D print the plates as retrieved by using the transfer matrix approach and optimisation with the impedance tube measurements.	124
5.3	Young's modulus of PEGDA 250 and PEGDA 700 obtained through nanoindentation measurements. Both top and bottom of the samples have been measured because of non-homogeneous distribution of BaTiO ₃ in the sample, as highlighted by scanning electron microscopy.	125

Chapter 1

Introduction

1.1 Motivation

The pervasiveness of acoustic noise has become a significant problem that can negatively affect the health and well-being of the world's population. According to the World Health Organization (WHO), noise can seriously harm human health and has a long-term effect on hearing, school and work performance, sleep, and cardiovascular health. The WHO estimates that every year a total of one million healthy years of life are lost in Western Europe due to traffic-related noise pollution [18–22]. To better understand the sources and distribution of noise pollution, various studies have generated noise maps by positioning sensors at key locations around cities and by developing machine listening algorithms that can identify the main types of noise sources [23–27]. Similarly, sensors placed in forests and other habitats and hydrophones used for underwater sound detection have shown how environmental noise represents a risk for the health of animals and how it drastically changes their behaviour [28–31].

As a consequence of the growing concerns related to the impact of noise in our everyday experience, our ability to control the propagation of acoustic waves is of fundamental importance. Traditional ways to reduce noise include absorbers such as porous-fibrous materials and panels, reflecting surfaces like noise barriers, and enclosures. These solutions are usually applied inside and outside buildings or near roads, allowing to efficiently enclose and isolate noise sources such as engines

and to dampen mechanical vibrations [32, 33]. Nevertheless, the efficacy of these materials is constrained by the mass-law [34], which states that the frequency of the acoustic wave attenuated by any traditional noise mitigation material is inversely proportional to its density and thickness. In general, absorbers like foams are effective at frequencies above 1000 Hz, while noise reduction below this frequency is usually achieved through thick barriers or dense coating materials [35, 36]. For small-scale audio devices, such as headphones, noise attenuation solutions rely mostly on traditional absorbers and sometimes on active noise cancellation. However, the latter approach works well only at frequencies below 500 Hz and it is limited by the necessity of using electricity to charge batteries and to power signal processing computations [36–38]. Therefore, noise reduction and the development of materials with new attenuation properties are ongoing and important engineering challenges.

Acoustic metamaterials are artificial structures made of building blocks, also called meta-atoms. When resonant building blocks are assembled to form an acoustic metamaterial, stop bands where the sound is deeply attenuated - usually named band gaps - are generated near the meta-atoms individual resonance frequencies. Acoustic metamaterials have been extensively studied in the last decade because of their ability to control sound waves in new ways. Their peculiar properties - such as negative effective mass density and bulk modulus - had not been previously found in nature and have led to advancements in the fields of noise control, wave steering and sound focusing [39–41]. Similar results had been obtained in the past by using phononic and sonic crystals. These are periodic materials capable of controlling frequencies with a wavelength of the same order of the lattice parameter, defined as the distance between the building blocks. In comparison, the unusual attenuating properties of resonant acoustic metamaterials represent a more effective approach to noise reduction. In fact, as these properties originate from the resonances of the meta-atoms, acoustic metamaterials are capable of breaking the mass-law and can control acoustic waves in the subwavelength regime [3, 6, 7, 42–44].

Until recently, the majority of research related to acoustic metamaterials had been confined in the laboratory environment and was applied mainly to noise

control for large-scale applications, such as panels and metadiffusers for room and buildings acoustics [8, 13]. Some recent papers have shown that the properties of metamaterials can be used to create innovative devices that can function as frequency and sound directionality analysers [9, 10] or as ultra-open silencers that attenuate noise while allowing air flow [11]. These latter examples suggest that it would be possible to include metamaterials in small-scale devices such as headphones or hearing aids or other applications that have space limits and require lightweight solutions. To do so, it is necessary to develop reliable techniques for the fabrication of resonant unit-cells tuned at the desired frequency and at the same time to design these unit-cells in a way that can accommodate the required space constraints.

In this thesis, unit-cells for acoustic metamaterials are designed and fabricated with the aim to present new noise control materials for applications that require lightweight subwavelength-attenuating solutions. Parametric models are built to adapt the unit-cells designs to specific frequency and space constraints. A new technique based on additive manufacturing technology is also developed to fabricate Helmholtz resonators, membranes, and thin plates, which are often used as unit-cells or meta-atoms in acoustic metamaterials. As highlighted in [45], many commercial three-dimensional printers are not able to fabricate thin and accurate membranes, but recent advances in digital light processing, stereolithography, and multi-material fabrication have shown promising results for three-dimensional printing passive thin plates and membranes as well as active piezoelectric membranes [46–48].

The development of these novel fabrication techniques together with the research on optimisation algorithms can pave the way for the integration of acoustic metamaterials into products. This new field has the potential to change the approach to noise control not only in large-scale scenarios such as noise attenuation in buildings and cities, but also for small-scale audio devices like hearing aids, headphones, and smart speakers or in the automotive and aerospace industries.

1.2 Novelty of Research & Objectives

The principal work of this thesis involved the design and fabrication of new resonant unit-cells for acoustic metamaterials. The novelty of these unit-cells was found both in the design aimed at tuning the band gaps to the sought frequency range as well as in the novel three-dimensional printing techniques that allowed to obtain small-scale and subwavelength noise reduction solutions. The research objectives of this work are summarised below.

- i. To study the possible designs of Helmholtz resonators and to broaden their band gap by including multiple sources of resonance such as overtones and thin plates inside one resonator. This would allow to obtain broadband noise attenuation in small-scale applications by exploiting multiple resonances within one unit-cell rather than alternating unit-cells with different resonances.
- ii. To investigate the use of membranes or thin plates as unit-cells for resonant acoustic metamaterials. Special attention is given to the development of a novel three-dimensional printing technique that allows to customise the choice of materials and hence to tune the band gaps according to specific material properties.
- iii. To apply the concepts and techniques detailed above to real-world devices. Specifically, the first prototype explores the possibility to 3D printing piezoelectric thin plates for active and reconfigurable acoustic metamaterials applications such as real-time noise attenuation. The second prototype consists of 3D printed headphones capable of attenuating external noise by integrating acoustic metamaterials in the ear cups.

1.3 Thesis Organization

The remaining part of this thesis is organised as follows:

Chapter 2 introduces the background and theory necessary to understand the content of this thesis. Firstly, basic theory on fundamentals of acoustics and

wave propagation is discussed. Secondly, reviews of noise control techniques and the origin and development of acoustic metamaterials are presented.

The methods used for modelling, fabricating and measuring acoustic metamaterials are presented in Chapter 3. Modelling methods include the transfer matrix approach and finite element methods. Fabricating methods describe the main new techniques developed in this thesis for three-dimensional printing. Measurement techniques include experimental measurement in the acoustic booth using microphone, function generators, and loudspeakers, and the description of instruments such as impedance tube, and laser Doppler vibrometer.

The main work conducted for this thesis was experimental and consisted in designing and fabricating resonant building blocks for acoustic metamaterials. Chapter 4 presents the design and fabrication of acoustic metamaterials based on small-scale Helmholtz resonators. A study of the design of Helmholtz resonators allowed to carefully tune the first overtone at a frequency close to the frequency of the first mode of vibration. By doing so, it was possible to obtain a broad band gap which was the result of hybridisation of the band gap of the first resonance and the band gap of the overtone. This band gap was subsequently further broadened by fabricating thin plates inside Helmholtz resonators. A parametric model of Helmholtz resonators is presented, along with the fabrication and measurement procedures, and a discussion of the results.

Chapter 5 presents the fabrication and characterisation of thin plates unit-cells for acoustic metamaterials. A parametric model of thin plates allows to predict the resonance of the plate according to its geometry and material properties. Special attention is given to three-dimensional printing procedures and to the choice of materials. Measurements using impedance tube, laser vibrometer and nanoindentation are presented and compared with transfer-matrix models and finite-element models.

Chapter 6 introduces two prototypes: the first is an active acoustic metamaterial based on three-dimensional printed resonators and piezoelectric plates, and the second consists of noise cancelling headphones integrating acoustic metamaterials

in their design.

Finally, Chapter 7 presents a conclusion on the research presented in this thesis as well as discussions on future work.

1.4 List of Publications

The work discussed in this thesis has been published in journal papers, conference proceedings, and presented through talks and posters, as follows.

Journal Papers

C. Casarini, V. Romero-García, J.P Groby, B. Tiller, J. F. C. Windmill, J. C. Jackson, “Fabrication and Characterization of 3D Printed Thin Plates for Acoustic Metamaterials Applications”, in *IEEE Sensors Journal*, vol. 19, no. 22, pp. 10365 - 10372, Nov.15, 2019.

C. Casarini, B. Tiller, C. Mineo, C.N. Macleod, J.F.C. Windmill and J.C. Jackson, ”Enhancing the Sound Absorption of Small-Scale 3-D Printed Acoustic Metamaterials Based on Helmholtz Resonators,” in *IEEE Sensors Journal*, vol. 18, no. 19, pp. 7949-7955, Oct.1, 2018.

Conference Proceedings

C. Casarini, B. Tiller, J.F.C. Windmill and J.C. Jackson, “3D Printed Membrane-Type Acoustic Metamaterials for Small-Scale Applications”, *Proceedings of SAPEM International Conference*, Le Mans 2017 (Slides for Oral Presentation).

C. Casarini, J. F. C. Windmill and J. C. Jackson, ”3D printed small-scale acoustic metamaterials based on Helmholtz resonators with tuned overtones,” *2017 IEEE Sensors Conference*, Glasgow, 2017, pp. 1-3.

Chapter 2

Background and Theory

2.1 Introduction

This chapter presents the theory and background knowledge necessary to understand the research presented in this thesis. Firstly, some fundamental concepts of general acoustics are introduced, with particular focus on acoustic waves propagation in air and on acoustic systems studied in this thesis, namely Helmholtz resonators and thin plates. Secondly, traditional noise attenuation techniques such as acoustic insulation, absorption, and active noise cancellation are reviewed. Thirdly, acoustic metamaterials are discussed through a literature review investigating their origin, development, and the state-of-the-art.

2.2 Fundamentals of Acoustics

Acoustics is a branch of science that studies the vibration of waves and propagation of sound [49, 50]. In its broader definition, acoustics is an interdisciplinary field encompassing various disciplines such as physics, engineering, psychology, neuroscience, physiology, audiology, architecture, music, and others, as represented in Lindsay's wheel of acoustics [1, 2] (See Fig. 2.1). This section aims to provide some introductory notes on acoustics concepts that are fundamental to understanding the research presented in this thesis. It can be utilised as a glossary, and a reference to each notion will be added where appropriate in the remaining chapters.

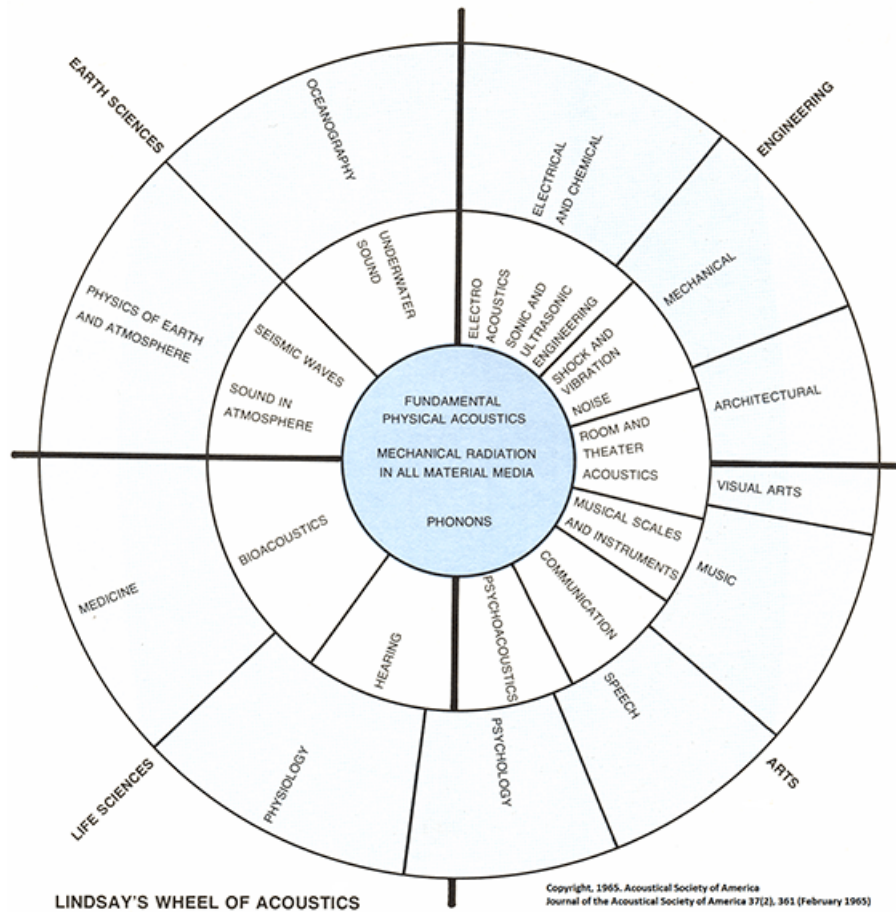


Figure 2.1: Lindsay’s wheel of acoustics [1, 2] describing the different fields and subfields that deal with acoustics, source <https://exploresound.org/what-is-new/fields-of-acoustics/>, accessed on 10 April 2021.

2.2.1 Acoustics of Waves

What is a Wave?

A wave is a traveling disturbance that transmits energy from one point to another in a medium, without transmitting matter [49, 51]. Mechanical waves can propagate in any medium that possesses a mass density and an elastic modulus [52]. In this thesis, we mainly encounter two types of waves: acoustic waves, which are longitudinal waves that travel through a fluid such as air parallel to the direction of propagation and waves on a membrane or thin plate, that are transverse waves where the disturbance travels perpendicular to the direction of propagation.

Acoustic Waves

Acoustic waves generally refer to the longitudinal propagation of vibrations in a fluid, such as gas or water. In this thesis, the medium in which the acoustic waves propagate is air. Sound transmission is generated by a change in pressure that results in compression and rarefaction of air particles. Air is considered an adiabatic medium, as the energy propagation due to pressure change is much faster than energy propagation generated by heat flow [53]. The acoustic wave's motion mainly depends on the interaction between inertial and elastic physical properties of air: density and bulk modulus.

Density

Density - or more specifically mass density - ρ is defined as mass m per unit volume V :

$$\rho = \frac{m}{V}. \quad (2.1)$$

The SI unit of density is m/kg^3 . The density of air is $1.29 \text{ kg}/\text{m}^3$ [35], which can be calculated by knowing the volume of an air particle and the atomic mass and percentage of each gas that composes the air molecule. It is worth noting that density represents the inertial property of air, and a wave propagating through a denser medium is slower, as the same applied force will result in a lower acceleration, hence a slower disturbance. However, in the vast majority of

materials, this effect is massively compensated for by the usual increase in bulk modulus.

Bulk Modulus

Bulk modulus B is a measure of resistance to compressibility of a fluid, and describes the decrease in volume V with an increase of pressure p [52]:

$$B = -V \frac{dp}{dV}. \quad (2.2)$$

A higher bulk modulus results in a gas that compresses less easily. As stiffer materials speed up the displacement of force between two neighboring molecules, a high bulk modulus produces a faster wave propagation. It has units of Pascals.

Speed of Sound

Given the mass density ρ and the bulk modulus B of a medium, it is possible to define the speed of sound of acoustic waves through that particular medium. The speed of sound in a fluid medium describes the speed at which a wave can transport energy:

$$c = \sqrt{\frac{B}{\rho}}. \quad (2.3)$$

As explained in 2.2.1, the adiabatic bulk modulus is dependent on static pressure of gas, which in turn is dependent on temperature T , hence the speed of sound varies as \sqrt{T} . A generally accepted value for the speed of sound in air at 20°C is 343 ms⁻¹ [52]. It is worth noting that a higher Bulk modulus, results in a higher speed of sound. Conversely, the larger the mass density, the slower the speed of sound.

Wavelength

The wavelength λ of a wave is the distance in meters over which the phase of the wave repeats. It has units of metres [51].

Frequency

Frequency determines the number of repetitions of a particular event in time. In acoustics, frequency is measured as cycles per seconds (Hz) and quantifies the repetition of the phase of a wave in time. A sine wave with a period T of 1 s, which means that the phase repeats every 1 s, has a frequency $f = 1/T = 1/(1\text{s}) = 1$ Hz. Angular frequency ω is defined as:

$$\omega = 2\pi f, \quad (2.4)$$

and has units of rad/s. A sine wave with a frequency of 1 Hz repeats once per second, which means that in 1 s it will complete 2π radians, the full rotation of a circle [51].

Wavenumber

Wavenumber k depends on the wavelength λ and is defined as:

$$k = \frac{2\pi}{\lambda}. \quad (2.5)$$

While frequency quantifies the repetition of the phase of a wave in time, the wave number can be interpreted as a spatial frequency, with units of m^{-1} , and quantifies the number of repetitions per meter of the phase of a wave [51].

Universal Wave Equation

The universal wave equation is a well known physical relation that links the speed of a wave c to its wavelength and frequency [51]:

$$c = f\lambda. \quad (2.6)$$

An example of the utility of this equation throughout this thesis is the prediction of the properties of phononic crystals and acoustic metamaterials. In phononic crystals, the distance between two unit cells is of the same order of the wavelength of the wave to be attenuated due to Bragg scattering [54]. For example, two pillars positioned at 3 cm distance in air will attenuate a wave with frequency $f = c/\lambda = c/0.03\text{m}$. If we assume $c = 343 \text{ ms}^{-1}$, the frequency attenuated

is $f = (343 \text{ m/s})/(0.03\text{m}) = 11433 \text{ Hz}$. Acoustic metamaterials are considered subwavelength, because the same frequency can be attenuated with unit cells at a distance that is at least one order of magnitude less than the wavelength, resulting in more compact structures.

Dispersion Relation

The dispersion relation describes how the speed of sound changes with the frequency of a wave. In many simple vibrating systems existing in nature, the wave frequency and the wavenumber scale linearly; hence, the speed of sound remains constant at every frequency. In this case, the dispersion relation is obtained by rewriting equation 2.6:

$$\omega(k) = ck, \quad (2.7)$$

where c is the speed of sound, k is the wavenumber, and $\omega(k)$ is the angular frequency. When a sound wave travels through air and reaches the listener, all the frequencies arrive at the same moment in time, since air is a non-dispersive medium. If a medium is dispersive, the speed of sound changes with frequency, and each frequency reaches the listener at a different moment, which is what happens in the typical example of light passing through a prism. The dispersion relation is fundamental in the study of acoustic metamaterials and phononic crystals, as they are often modelled using the wave band theory, where the dispersion relation is usually called dispersion diagram or band diagram. In such systems, not only the dispersion relation shows a nonlinear relation between frequency and wavenumber, but also presents some frequency bands - namely band gaps - where sound energy does not propagate [55].

Sound Fields

A sound field can be divided into two regions - near field and far field - defined by the distance from the sound source [33].

Near Field

The near field is the region situated in the proximity of the sound source; it extends for less than a wavelength in the outward direction. In this region, the

particle velocity is not in phase with the sound pressure and sound waves behave as evanescent waves (2.2.1).

Far Field

The far field extends from the near field outwards. An object is located in the far field with respect to the sound source with dimension l if its distance r from the source satisfies the conditions:

$$r \gg \frac{\lambda}{2\pi}, \quad (2.8)$$

$$r \gg l, \quad (2.9)$$

$$r \gg \frac{\pi l^2}{2\lambda} \quad (2.10)$$

In the far field, sound waves propagating from the approximately point-source behave as acoustic plane waves (2.2.1) and the particle velocity is in phase with the sound pressure.

Propagation of Acoustic Plane Waves

The pressure of a plane acoustic wave propagating in the direction x is:

$$p(t, x) = Ae^{i(\omega t - kx)}, \quad (2.11)$$

where p is the pressure, t is time, A is the amplitude of the wave, $\omega = 2\pi f = kc$ is the angular frequency of the wave, f its frequency, k its wave number and c the speed of sound. The pressure p and particle velocity u are:

$$p = Ae^{i(\omega t - kx)}, \quad (2.12)$$

$$u = \frac{A}{\rho c} e^{i(\omega t - kx)}, \quad (2.13)$$

where ρ is the density of the medium in the far field.

Evanescent Waves

In the near field, sound waves are characterised by a complex behaviour not directly associated with sound propagation. The sound energy never really

propagates from the sound source, rather circulates back and forth. These waves that do not propagate but are generated and decay exponentially are called evanescent waves. For evanescent waves, the equation of wave propagation introduced in 2.2.1 holds:

$$p(t, x) = Ae^{i(\omega t - kx)}. \quad (2.14)$$

However, the propagation vector k for evanescent waves is imaginary, hence ik is real:

$$p(t, x) = Ae^{i\omega t} e^{-k_{real}x}. \quad (2.15)$$

Therefore, evanescent waves are sinusoidally varying over time and exponentially decaying in space.

Characteristic Impedance of a Medium

The characteristic impedance z_c of a medium is the product of density ρ and speed of sound c of the medium:

$$z_c = \rho c. \quad (2.16)$$

The characteristic impedance is an important quantity in the field of sound control, as when the acoustic wave propagates between two media having a different characteristic impedance, the acoustic wave can be reflected, absorbed, diffused according to the physical characteristics of the two media. Given Eq. (2.3) for the speed of sound, the characteristic impedance can also be defined by:

$$z_c = \sqrt{B\rho}, \quad (2.17)$$

where B is the Bulk modulus, and ρ is the density of the medium.

Sound Transmission Loss

Transmission loss TL of an acoustic material can be defined as the difference between the incident sound intensity level I_{in} and the transmitted sound intensity

level I_{tr} given the reference sound intensity I_{ref} :

$$TL = 10 \log_{10} \left(\frac{I_{in}}{I_{ref}} \right) - 10 \log_{10} \left(\frac{I_{tr}}{I_{ref}} \right) = 10 \log_{10} \left(\frac{I_{in}}{I_{tr}} \right). \quad (2.18)$$

If $\tau = \left(\frac{I_{in}}{I_{tr}} \right)$ is defined as the intensity transmission coefficient,

$$TL = 10 \log_{10} \left(\frac{1}{\tau} \right). \quad (2.19)$$

In composite materials, the effective transmission loss of the composite is:

$$TL_{eff} = 10 \log_{10} \left(\frac{1}{\bar{\tau}} \right), \quad (2.20)$$

where:

$$\bar{\tau} = \frac{\sum_{i=1}^n S_i \tau_i}{\sum_{i=1}^n S_i}, \quad (2.21)$$

S_i is the surface area of the material i , and n is the number of materials in the composite.

Absorption Coefficient

When an incident sound wave passes through a material layer, part of the energy is dissipated by the material and transformed into heat. The energy lost in the process of reflection from the material is considered to be absorbed. The absorption coefficient α is defined as the ratio of the sound intensity absorbed by the material I_{ab} to the sound intensity incident on the material I_{in} :

$$\alpha = \frac{I_{ab}}{I_{in}}; \quad (2.22)$$

the sound intensity absorbed by the material is the sum of the dissipated I_{dis} and transmitted I_{tr} sound intensity:

$$I_{ab} = I_{dis} + I_{tr}. \quad (2.23)$$

Hence, the sound intensity absorbed by the material I_{ab} is also the difference between the incident sound wave I_{in} and the reflected sound waven I_r . Therefore,

$$\alpha = \frac{I_{in} - I_r}{I_{in}} = 1 - R^2, \quad (2.24)$$

where $R = \frac{p_r}{p_i}$ is the pressure reflection coefficient. The sound absorption coefficient α is a function of frequency, it is also defined as the ratio between the absorbed and incident sound intensity, and it is $0 \leq \alpha \leq 1$. In composite materials, the effective absorption coefficient $\bar{\alpha}$ of the composite is:

$$\bar{\alpha} = \frac{\sum_{i=1}^n S_i \alpha_i}{\sum_{i=1}^n S_i}, \quad (2.25)$$

where S_i is the surface area of the material i and n is the number of materials in the composite. The total absorption by a surface follows Sabine definition:

$$\text{Total absorption by a surface} = S\bar{\alpha} \quad (2.26)$$

1 Sabine, a unit of measurement named after one of the founders of the field of architectural acoustics Wallace Clement Sabine, is defined as the sound absorption unit of a 1 m^2 surface with total absorption [51].

The Mass-Law

The mass-law relates the transmission of airborne sound across a wall with its mass. It is considered of particular importance when introducing acoustic metamaterials, as - differently from traditional materials - they can break this law. The mass-law states that the transmission T of a sound wave through a material immersed in a fluid is described by [34]:

$$T \approx \left(\frac{2\rho c}{m''\omega} \right)^2, \quad (2.27)$$

where ρ is the density of the fluid, c is the speed of sound in the fluid, $m'' = \rho_m h$ is the mass per unit area of the material, ρ_m is the density of the material, h its thickness and ω is the angular frequency of the sound wave. Therefore, by doubling the mass, density, or thickness of a material or by doubling the frequency of the incident sound wave, the sound transmission across a wall is halved. A halved sound transmission corresponds to an attenuation of 6 dB SPL. For example, given a sound transmission T_1 Pa measured across a wall, by doubling

its thickness (or mass, density, incident frequency) the transmission T_2 Pa is:

$$T_2 = \frac{1}{4} T_1. \quad (2.28)$$

The corresponding transmission in dB SPL of T_1 is given by \tilde{T}_1 :

$$\tilde{T}_1 = 10 \log_{10} (T_1). \quad (2.29)$$

Therefore, the transmission in Decibels across T_2 is given by;

$$\begin{aligned} \tilde{T}_2 &= 10 \log_{10} (1/4) \\ &= \tilde{T}_1 + 10 \log_{10} \left(\frac{1}{4} \right) \\ &= \tilde{T}_1 - 6 \text{dB SPL}. \end{aligned} \quad (2.30)$$

As will see later, acoustic metamaterials can break the mass-law, because they are capable of deep sound attenuation well above 6 dB for a doubling of thickness in specific frequency bands, without an increase in mass, density or frequency.

Interference of Acoustic Waves

When two plane waves in a linear medium encounter, the superposition law tells us that a resulting wave is formed from their sum. If the waves have the same phase and periodicity, a constructive interference is formed. If they have opposite phase, a destructive interference is formed, where the amplitude of the wave is 0 [51]. The destructive interference of acoustic waves is at the base of active noise cancellation methods and, as we will see later, also happens in sonic crystals and acoustic metamaterials.

2.2.2 Helmholtz Resonator

Definition and Origin

The Helmholtz resonator consists of a rigid cavity with an open neck immersed in a fluid, usually air. It was invented in 1850 by Herman von Helmholtz (1821-

1894), a physicist, physiologist, and pioneer of acoustics theory [56]. Helmholtz engineered resonators having different cavities and with a neck that could fit into a human ear (see Fig. 2.2). Every resonator was characterised by a different resonance, covering various frequencies within the human audible spectrum. By inserting one resonator in the ear, it was possible to amplify a particular frequency corresponding to the resonance frequency of the Helmholtz resonator and attenuate any other sound. This way, a complex sound could be analysed to obtain its frequency components: a primitive spectrum analyser was invented. As shown in the next paragraph, a Helmholtz resonator's advantage with respect to a simple pipe is that a similar volume corresponds to a lower frequency. In a pipe, the air inside the cavity acts as a mass. Conversely, the cavity of the Helmholtz resonator acts as a spring and the air inside the neck as a mass, resulting in a different system that produces a lower frequency [52]. Numerous acoustics systems can be modelled as Helmholtz resonators. For example, empty bottles and cans are cavities filled air having an open neck. In musical instruments, the body of the guitar, ocarinas and other types of flutes, act as Helmholtz resonators. Often, the enclosure of a loudspeaker includes a port, since the membrane of the loudspeaker has a natural low-frequency resonance that modifies or 'colours' the sound and makes it 'boomy': by adding a port to the enclosure, the enclosure becomes a Helmholtz resonator with a lower resonance that matches the resonance of the membrane and compensates for the coloration by resonating in anti-phase with respect to the loudspeaker's membrane [51]. In the field of room acoustics, Helmholtz resonators are usually placed in corners of rooms to attenuate low frequencies, otherwise difficult to tackle due to the mass-law Section 2.2.1, requiring thick and dense walls for low-frequencies attenuation. In biology, Helmholtz resonators constitute the body of insects such as cicadas and have the function of amplifying the buckling of ribbed tymbals [52]. Finally, and of interest for this thesis, Helmholtz resonators are extensively used as unit cells for acoustic metamaterials [6, 7].

Vibration of Helmholtz Resonator

To study the behaviour of Helmholtz resonators when inserted in acoustic systems, it is useful to model and measure their vibration and specifically



Figure 2.2: Helmholtz resonators made in 1870, Hunterian Museum and Art Gallery in Glasgow, source <https://en.wikipedia.org>.

their resonance frequency. A standard formula for the resonance frequency of Helmholtz resonators is reported below. It is worth noting that this standard formula is valid when the dimensions of the resonator do not exceed $1/10$ of the wavelength of the incident wave. When this assumption is not valid, the geometry of Helmholtz resonators has to be taken into account in the model. A Helmholtz resonator (see Fig. 2.3) can be approximated to a mass-spring system: the air in the cavity acts as a spring, and the air inside the neck vibrates like a mass. It can be shown that - when damping is not considered - its resonance frequency f_0 is given by:

$$f_0 = \frac{c}{2\pi} \sqrt{\frac{S}{L'V}}, \quad (2.31)$$

where c is the speed of sound in the gas filling the cavity, S is the cross-sectional area of the neck, $L' = l + 1.7a$ is the effective length of the neck, l is the length of the neck, a is the radius (for cylindrical Helmholtz resonators) or surface length (for non cylindrical Helmholtz resonators) of the neck and V is the volume of the cavity. The effective length of a pipe is a quantity that takes into account

both the length of the pipe and its end correction, i.e. a short distance applied to the actual length whose value depends on the type of end (open/flanged, or closed) and geometry of the pipe. When the Helmholtz resonator is vibrating at its resonance frequency, the neck behaves as an open/flanged pipe, and its end correction parameter is usually approximated as 1.7. As shown later in this Section, when the Helmholtz resonator vibrates at one of its overtones' frequencies the cavity acts as a pipe, which is closed at one end and almost closed at the end facing the neck, hence its end correction parameter is usually approximated as 0.6 [57].

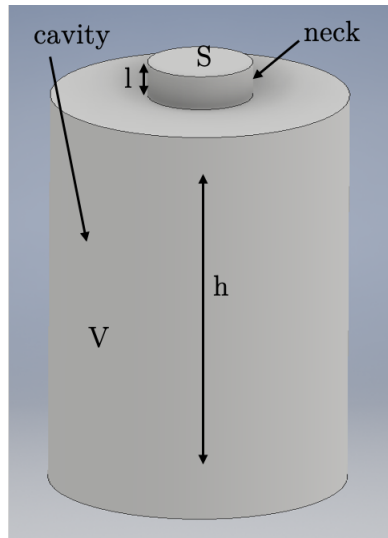


Figure 2.3: Representation of a Helmholtz resonator consisting of a cylindrical neck of length l , cross-sectional area S , and a cylindrical cavity of volume V and length h .

Eq. (2.31) has been obtained by assuming that the cavity behaves as a mass, the neck as a spring, and can be derived as follows. The angular resonance frequency of the resonator depends on mass m of the neck and spring constant k of the cavity (2.2.2):

$$\omega = \sqrt{\frac{k}{m}}, \quad (2.32)$$

where the mass m ($m = \text{volume} \times \text{density}$, see Eq. (2.1)) is given by the density of air ρ , the effective length of the neck L' and its cross-sectional area S :

$$m = \rho L' S. \quad (2.33)$$

When the mass of air in the neck oscillates it is displaced by a distance dx into the cavity, reducing the volume of the cavity by Sdx . The change in the cavity volume dV is:

$$dV = -Sdx. \quad (2.34)$$

Recalling from Eq. (2.2) that the bulk modulus is defined as $B = dp/(-dV/V)$, the pressure inside the cavity varies by:

$$dp = B(-dV/V) = BSdx/V. \quad (2.35)$$

The force acting on the mass of air in the neck is:

$$dF = -dpS = -dx\left(\frac{BS^2}{V}\right), \quad (2.36)$$

where the negative sign represents the outward movement of the mass. From Hooke's law, $F = -kx$, hence the spring constant k is:

$$k = \frac{-dF}{dx} = \frac{BS^2}{V}. \quad (2.37)$$

By substituting Eq. (2.33) and Eq. (2.37) into equation Eq. (2.32) and by recalling from Section 2.2.1 the speed of sound $c = \sqrt{B/\rho}$, we obtain the angular resonance frequency of the Helmholtz resonator:

$$\omega = \sqrt{\frac{k}{m}} = \sqrt{\frac{BS^2}{V\rho L'S}} = c\sqrt{\frac{S}{VL'}}, \quad (2.38)$$

which gives Eq. (2.31), since - after Eq. (2.4) - $f = \omega/2\pi$.

Sinusoidally Driven Damped Helmholtz Resonator

Since the Helmholtz resonator acts as a mass-spring system, it can be modelled as the well-known harmonic oscillator. A simple harmonic oscillator consists of a mass m and a spring k . By equating Newton's second law $F = m\ddot{x}$ and Hooke's law $F = -kx$ we obtain:

$$m\ddot{x} + kx = 0, \quad (2.39)$$

where x is the displacement of the mass over time and \ddot{x} is its acceleration. To model a forced, sinusoidally driven, Helmholtz resonator, it is necessary to add damping to equation Eq. (2.39), which is conservative and - without damping - would lead to exponentially increasing solutions. Damping models the energy losses of the system, as for example the viscous losses in the neck of the resonator where the mass of air is moving or the imperfections of the cavity, that acts as the spring of the resonator. This kind of damping is proportional to the velocity of the oscillator.

In particular, in this thesis Helmholtz resonators are used to attenuate an incoming sound wave, hence a sinusoidal driving force needs to be added to the model. The equation of motion of the driven damped harmonic oscillator is represented by [52]:

$$m\ddot{x} + \gamma\dot{x} + kx = Fe^{i\omega t}, \quad (2.40)$$

where m is the mass, γ is the damping parameter, k is the stiffness, F is the amplitude of the driving force, ω is its angular frequency, ω_0 is the angular resonance frequency of the oscillator, and t is time. Dividing by m we obtain:

$$\ddot{x} + 2\alpha\dot{x} + \omega_0^2x = (F/m)e^{i\omega t}, \quad (2.41)$$

where $\alpha = \gamma/2m$ is the damping factor and $\omega_0 = \sqrt{k/m}$ is the resonance of the oscillator. By assuming as solution $x = ae^{i(\omega t + \Theta)}$ and substituting this solution into Eq. (2.41), we obtain:

$$ae^{i\Theta} = \frac{(F/m)}{(\omega_0^2 - \omega^2) + 2j\omega\alpha}. \quad (2.42)$$

This equation of motion is formulated in the complex domain, and to observe the motion of the resonator we need to compute amplitude and phase in the real domain. The absolute value of Eq. (2.42) gives the amplitude of the motion of the resonator with respect to the driving force. Since $|e^{i\Theta}| = 1$ and for complex numbers of the kind $z = x + iy$ the magnitude is $\sqrt{x^2 + y^2}$, the amplitude a of the driven damped resonator is:

$$a = \frac{(F/m)}{\sqrt{(\omega_0^2 - \omega^2)^2 + 4\omega^2\alpha^2}}. \quad (2.43)$$

By looking at Eq. (2.43), it is possible to notice that when the denominator is at its minimum, the amplitude of oscillation is at its maximum, i.e. at resonance. To find the minimum, the derivative of the denominator is calculated and equated to zero. By solving this equation, it can be shown that when the frequency ω of the driving force is equal to $\sqrt{\omega_0^2 - 2\alpha^2}$, the denominator is at its minimum value; hence, the amplitude of the oscillation of the mass of air inside the neck is maximum. To approximate even further, given $\alpha \ll \omega_0$, it can be stated that amplitude is at its peak when the driving force has a frequency slightly lower than the resonance frequency of the resonator. The phase-lag of the motion of the resonator with respect to the impinging wave is given by:

$$\Theta = \tan^{-1}\left(\frac{-2\omega\alpha}{\omega_0^2 - \omega^2}\right). \quad (2.44)$$

At low frequencies, $\Theta \approx 0$. When $\omega = \omega_0$, $\Theta = -\pi/2$. In other words, in the frequency band near resonance, the mass of air inside the neck begins to oscillate with an amplitude which is high in value (near the peak) and 90° out of phase with respect to the impinging wave. In the frequency band after the resonance, $\Theta = -\pi$ it oscillates in anti-phase (i.e. 180° out of phase) with the impinging wave.

This is a key point for the study of acoustic metamaterials, as this behaviour is leveraged to create a band gap where the sound is deeply attenuated. When the response of the resonator is out of phase with the incoming wave, a frequency band is generated where the energy is still amplified by the resonance effect, that oscillates in anti-phase with the impinging wave. A destructive interference (see Section 2.2.1) is created, where the sound is attenuated. The extent of the band gap is determined by the Q factor: a very high Q factor will result in a narrow frequency band where there is still enough energy in the anti-phase zone and a low Q factor will see a larger band gap, but at a lower energy that might not be enough to cancel the amplitude of the driving force. This trade-off should be taken into consideration when designing a system, based on the constraints of a particular application and objectives of the experiment. This response based on Eq. (2.43) and Eq. (2.44) is shown in Fig. 2.4. It is worth noting that, by increasing the amount of damping, the frequency of the resonator is detuned and the Q factor

decreases. This effect can be observed in Fig. 2.5, where the damping value is swept between 1 and 10000 with 1000 increments. The amplitude of vibration of Helmholtz resonators decreases with damping, as shown in Fig. 2.6.

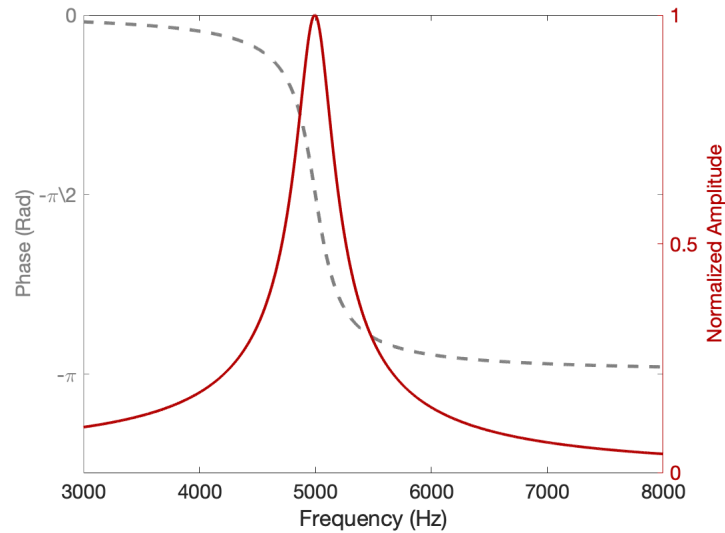


Figure 2.4: Amplitude and phase lag of a driven damped Helmholtz resonator. The resonance frequency of the resonator is slightly higher than 5 kHz, its mass is 1 kg, damping is 1000. When the frequency of driving force is at 5 kHz, the mass of air in the neck oscillates in anti-phase with the impinging wave.

Overtone of Helmholtz Resonators

As shown in the previous section, the first mode of vibration of Helmholtz resonators is the result of the volume of air in the neck acting as a mass and the volume of air in the cavity acting as a spring. There are however higher modes of vibrations due to the oscillation of air in the cavity. As a consequence, higher resonances are not integer multiples of the fundamental frequency and are classified as overtones instead of harmonics [57]. The ocarina is a musical instrument that leverages the different origins of higher mode of vibration, emitting almost a pure tone containing very few overtones, as the higher modes of vibration are considerably higher in frequency and lower in amplitude than the fundamental resonance. According to Fletcher [52], cylindrical Helmholtz resonators with a large cavity behave - at higher modes of vibration - as pipes closed at both ends. On the other hand, when volumes are smaller, the cavity

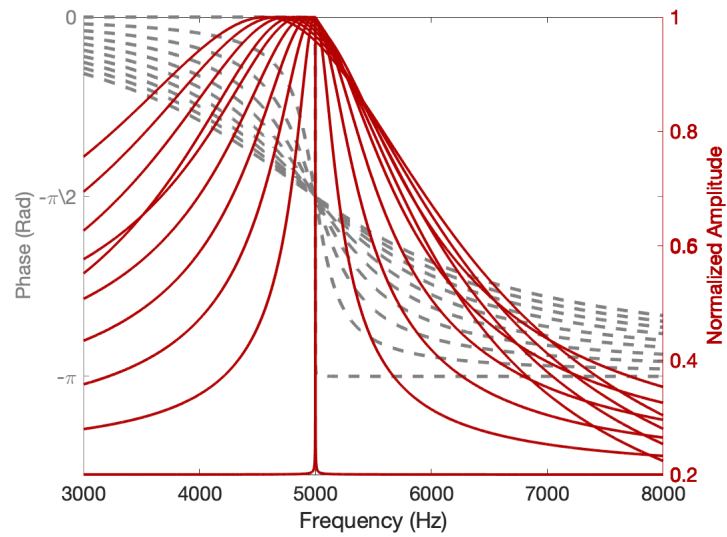


Figure 2.5: Amplitude and phase lag of a driven damped Helmholtz resonator. The frequency of the resonator with no damping is at 5 kHz, its mass is 1 kg, the damping value is swept between 1 and 10000 with an increment of 1000. The effect of the damping is noticeable in the detuned frequency and decreased Q factor.

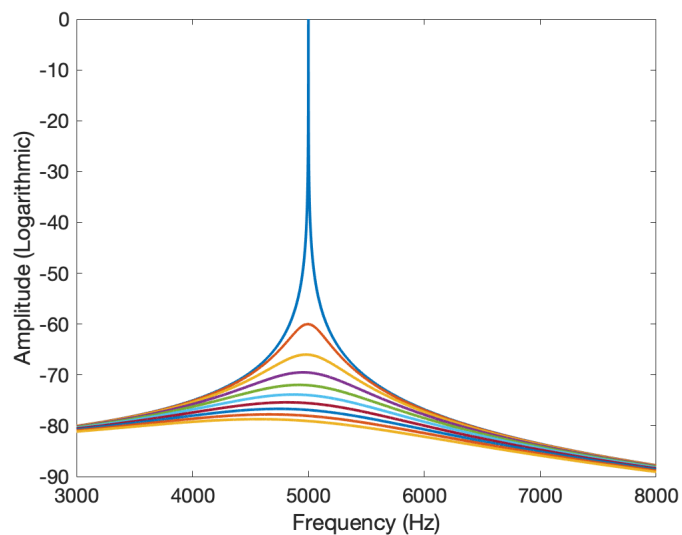


Figure 2.6: Amplitude of vibration of a Helmholtz resonator decreases with increasing damping.

acts as a pipe closed at one end and open at the other end. In the first case, the overtones will be:

$$f_n = (n - 1) \frac{c}{2h'}, \quad (2.45)$$

with $n = 2, 3, 4, \dots, \text{etc.}$ In the second case, the overtones will be:

$$f_n = (2n - 1) \frac{c}{4h'}, \quad (2.46)$$

with $n = 1, 2, 3, \dots, \text{etc.}$,

where c is the speed of sound in the host medium, $h' = h + 0.6r$ is the effective length of the cavity and r is its radius. Finally, it is worth noting that in many cases these idealised models do not reflect the behaviour of resonators, and factors like the geometry of cavity and neck and the constituting materials can greatly influence the vibration of Helmholtz resonators.

2.2.3 Membranes and Plates

Introduction and Definition

Membranes and plates are two-dimensional representations of common acoustic surfaces. In membranes, the restoring force depends on tension and are assumed to be infinitely thin and with no stiffness. Examples of membranes include drums, resonators found in banjos, as well as the tympanic membrane or eardrum. In plates, the restoring force depends on stiffness and material properties. The sounding board of a piano can be modelled as a plate. Other two-dimensional models of surfaces include shells, in which the thickness of the material is small compared to its lateral extent. In general, many two-dimensional surfaces existing in nature or that are part of musical instruments can be modelled as membranes, plates, or shells [52]. Membranes, plates with or without loaded masses have become popular as unit cells in acoustic metamaterials, because of their potential lightweight and small size. In some cases - particularly when these surfaces are fabricated via additive manufacturing techniques - these surfaces could exhibit a behaviour in-between the three main models outlined above. The three-dimensional printed layers presented in Chapter 5 of this thesis can be modelled

as thin plates; hence they are dominated by stiffness, and they have no tension. However, some small discrepancies between experiments and models suggests that some tension is applied in the three-dimensional printing process. In the next sections, general models of both membranes and plates will be introduced. Since the vibration of thin plates depends on their material properties, the concepts of Young's modulus, Poisson's ratio and molecular weight will also be defined.

Young's Modulus

Young's modulus is defined as the amount of elastic stress (force/area) to strain (extension/length) of a material [52]. It is measured in Pascals, and defined as force per unit area, or N/m^2 . In general, Young's modulus can vary from sample to sample according to purity of material. Some common values for polyethylene are $2 - 7$ GPa, for aluminium $6.9 - 7.9 \times 10^2$ GPa, steel has values around $1.9 - 2.1 \times 10^3$ GPa [51].

Poisson's Ratio

The Poisson's ratio of a material under stress is defined as the ratio of the fractional decrease in diameter to the fractional increase in length [52]. When a sample of material is compressed in the transverse direction, it becomes thicker in the longitudinal direction, and vice versa. When the sample is elongated in the transverse direction, it becomes thinner in the longitudinal direction and vice versa. Most materials have values between 0 and 0.5, the typical value of Poisson's ratio for most materials is ~ 0.3 [53].

Molecular Weight

Molecular weight is defined as the sum of the atomic weight values of the atoms in a molecule.

Vibration of Membranes

Membranes need to be stretched on a frame in order to vibrate. The amount of tension resulting from the attachment to a support plays a significant role in determining their vibration behaviour. The most commonly modelled membranes

- as well as those presented in this thesis - have a circular geometry. The equation of motion of rectangular membranes is [52]:

$$\frac{\partial^2 z}{\partial x^2} + \frac{\partial^2 z}{\partial y^2} = \frac{\sigma}{\rho_M} \frac{\partial^2 z}{\partial t^2}, \quad (2.47)$$

where σ is the elastic stress of the membrane, and ρ_M is the density of the membrane. For circular membranes, the transformation using polar coordinates (r, ϕ) yields:

$$\frac{1}{r} \frac{\partial z}{\partial r} + \frac{1}{r^2} \frac{\partial^2 z}{\partial \phi^2} = \frac{\sigma}{\rho_M} \frac{\partial^2 z}{\partial t^2}. \quad (2.48)$$

If we define c_M as the wave speed in the membrane, we can rewrite Eq. (2.48) as:

$$\frac{1}{r} \frac{\partial z}{\partial r} + \frac{1}{r^2} \frac{\partial^2 z}{\partial \phi^2} = \frac{1}{c_M^2} \frac{\partial^2 z}{\partial t^2}. \quad (2.49)$$

If an oscillatory behaviour along the z axis is assumed with angular frequency ω and following the convention $e^{i\omega t}$, we obtain:

$$z(r, \phi, t) = \Psi_{mn}(r, \phi) e^{i\omega t}, \quad (2.50)$$

where Ψ are the eigenfunctions of the form:

$$\Psi_{mn}(r, \phi) = M_{mn} J_m(k_{mn} r) \cos m\phi, \quad m = 0, 1, 2, \dots \quad n = 1, 2, 3, \dots \quad (2.51)$$

with:

$$M_{0n} = [J_1(k_{0n} a)]^2 \quad M_{mn} = [J_{m-1}(k_{mn} a)]^2. \quad (2.52)$$

The above result is obtained by fitting the boundary condition of a membrane clamped ($z = 0$) at $r = a$, J is a Bessel function. The main zeros of the Bessel functions are given in Table 2.1.

The angular resonance frequency at each mode is obtained as follows:

$$\omega_{mn} = k_{mn} c_M, \quad (2.53)$$

and values for membranes of different radiuses a can be obtained by substituting the values in Table 2.1 and value of radius:

Table 2.1: Zeros of Circular Membrane Equation of Motion

$m = 0$	$k_{01}a = 2.405$	$k_{02}a = 5.520$	$k_{03}a = 8.654$
$m = 1$	$k_{11}a = 3.832$	$k_{12}a = 7.016$	$k_{13}a = 10.173$
$m = 2$	$k_{21}a = 5.136$	$k_{22}a = 8.417$	$k_{23}a = 11.620$
$m = 3$	$k_{31}a = 6.380$	$k_{32}a = 9.761$	$k_{33}a = 13.015$
$m = 4$	$k_{41}a = 7.588$	$k_{42}a = 11.065$	$k_{43}a = 14.373$
$m = 5$	$k_{51}a = 8.772$	$k_{52}a = 12.339$	$k_{53}a = 15.700$
$m = 6$	$k_{61}a = 9.936$	$k_{62}a = 13.589$	$k_{63}a = 17.004$

$$\omega_{mn} = \frac{k_{mn}}{a} c_M. \quad (2.54)$$

By substituting values from Table 2.1 into Eq. (2.51) and in Eq. (2.53), it is possible to show the main modes of vibration of circular clamped membranes and their resonance frequencies with respect to the fundamental resonance f_0 , as illustrated in Fig. 2.7.

Vibration of Plates

Plates are dominated by stiffness with no tension. They can also be referred to as stiff membranes or panels and they are the two-dimensional equivalent of bar. Plates can be clamped to a frame or can also vibrate freely without being attached to any support. The material properties of plates play a major role in determining their vibration behaviour. With respect to membranes, the overtones of plates are increased in frequencies due to the effect of stiffness, which makes the fundamental frequency much lower than the frequency of other modes of vibration. The equation of motion of a plate clamped at its edges without tension is [53]:

$$\nabla^4 z + \frac{3\rho_M(1-\nu^2)}{E(h/2)^2} \frac{\partial^2 z}{\partial t^2} = 0, \quad (2.55)$$

where ρ_M is the density of the material, ν its Poisson's ratio, E its Young's modulus and h is the thickness of the plate. It is worth noting that the equation of motion of the plates presents a higher order with respect to the equation of

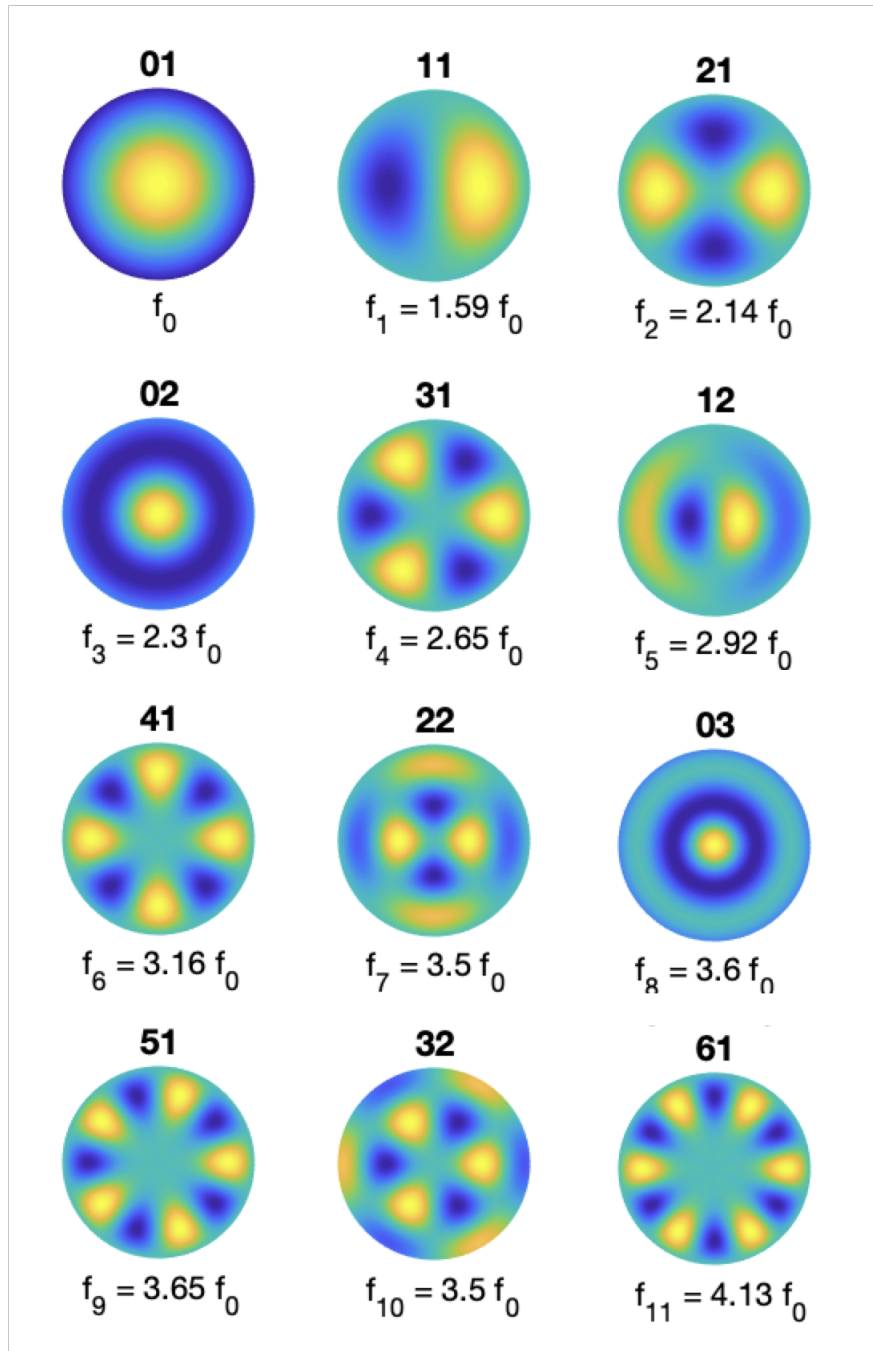


Figure 2.7: First twelve vibration modes of clamped membrane, obtained with MATLAB.

2.2. Fundamentals of Acoustics

motion of membranes; while membranes stretch only in the xy plane and are considered to have no thickness, plates stretch over the xyz plane. It can be shown that frequencies of vibration for a circular plate of radius a clamped at its edges are [53]:

$$f_{mn} = \frac{\pi h}{4a^2} \sqrt{\frac{E}{3\rho_M(1-\nu^2)}} (\beta_{mn}^2), \quad (2.56)$$

where the first nine coefficients β_{mn} are [53]:

Table 2.2: Coefficients for Vibration of Circular Plates Clamped at Edge

$m = 0$	$\beta_{01} = 1.015$	$\beta_{02} = 2.007$	$\beta_{03} = 3.000$
$m = 1$	$\beta_{11} = 1.468$	$\beta_{12} = 2.483$	$\beta_{13} = 3.490$
$m = 2$	$\beta_{21} = 1.879$	$\beta_{22} = 2.992$	$\beta_{23} = 4.000$
$m = 3$	$\beta_{31} = 2.274$	$\beta_{32} = 3.354$	$\beta_{33} = 4.391$
$m = 4$	$\beta_{41} = 2.657$	$\beta_{42} = 3.768$	$\beta_{43} = 4.822$
$m = 5$	$\beta_{51} = 3.032$	$\beta_{52} = 4.172$	$\beta_{53} = 5.244$
$m = 6$	$\beta_{61} = 3.402$	$\beta_{62} = 4.569$	$\beta_{63} = 5.658$

By substituting values from Table 2.2 into Eq. (2.56), it is possible to show the main modes of vibration of circular clamped plates and their resonance frequencies with respect to the fundamental resonance f_0 , as shown in Fig. 2.8.

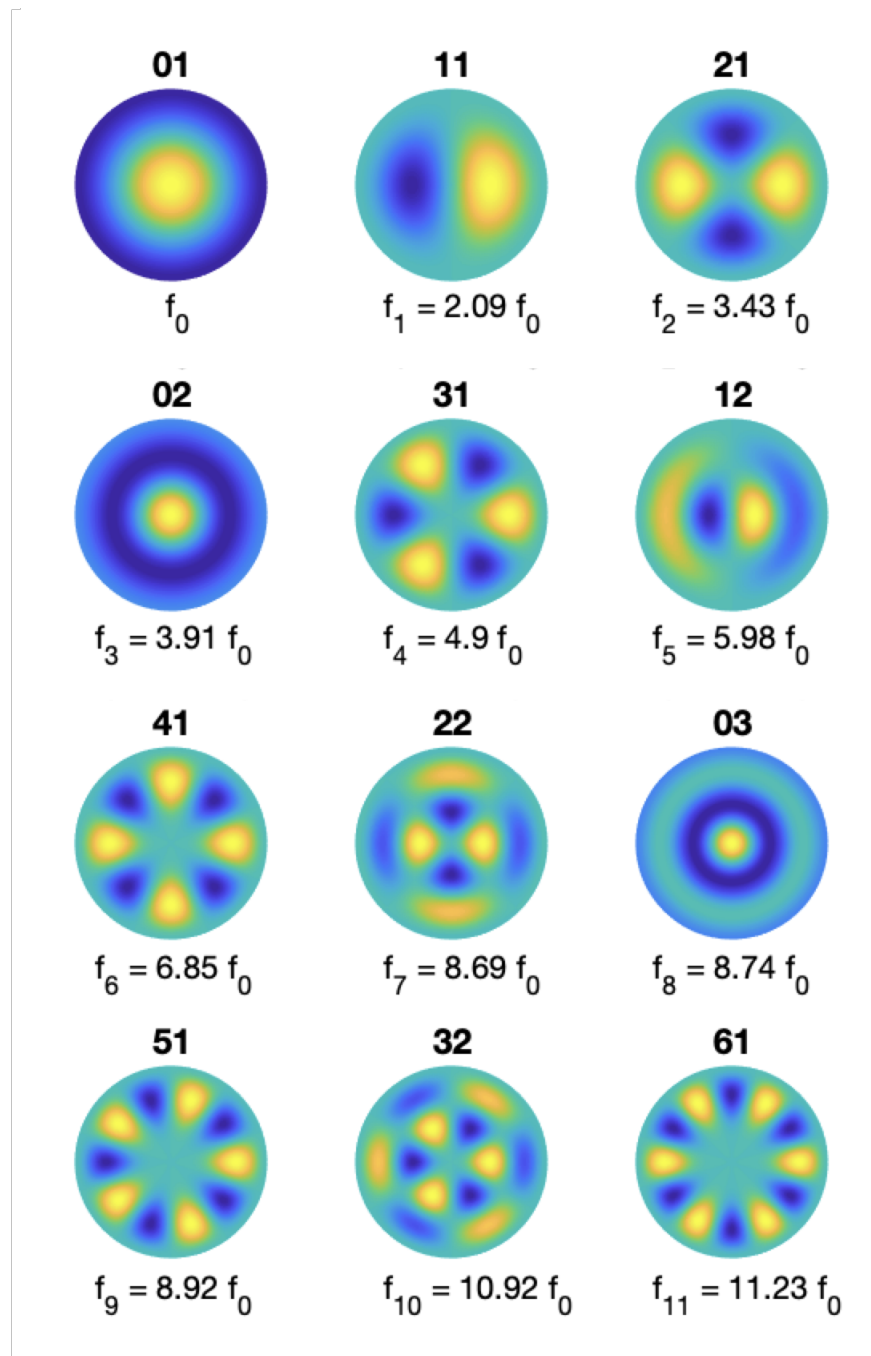


Figure 2.8: First twelve vibration modes of circular plates, obtained with MATLAB. Although the modes behaviour is the same as that of membranes, plates present higher and more distanced frequencies for corresponding modes.

2.3 Review of Noise Control Techniques

Noise can be defined as a part of acoustic energy that is unwanted and needs to be controlled. Depending on the context, some sound energy needs to be enhanced, and other sound energy needs to be attenuated. For example, in a classroom, the voice of a teacher should be enhanced, while the speech of other students or the noise coming from other neighbouring rooms and from the external environment should be attenuated. Noise has negative consequences on health, causing hearing loss, difficulty in sleeping and concentration, headache, fatigue [18–22]. Noise control techniques can be applied at the source, in the acoustic path separating source and receiver, or directly at the receiver location. At the source, a better design of the mechanics that introduce vibration can lead, for example, to quieter motors or compressors and reduce electric noise. Barriers can be placed in the acoustic path between highways and houses to isolate communities from traffic noise; absorbers and isolators can be built outside or inside buildings. At the receiver end, earmuffs, earplugs, and headphones with active noise cancellation can be used to reduce external noise and protect the hearing health of individuals [36]. To better understand the advantages of acoustic metamaterials in noise control applications, it is essential to identify traditional noise control techniques that have been successfully used in various contexts in the past decades. In this section, traditional noise control techniques such as absorption, isolation, diffusion, and active noise cancellation will be reviewed.

2.3.1 Acoustic Materials

Acoustic materials are designed to attenuate noise by controlling, steering, and manipulating sound waves. When an acoustic wave encounters a boundary, it is partly reflected, transmitted, and absorbed (see Fig. 2.9). Noise control techniques use materials and structures, including insulators, diffusers, and absorbers, to manipulate the transmission, reflection, and absorption needed for a specific application. Metrics to evaluate the performance of acoustic materials are transmission loss and absorption coefficient (Section 2.2.1).

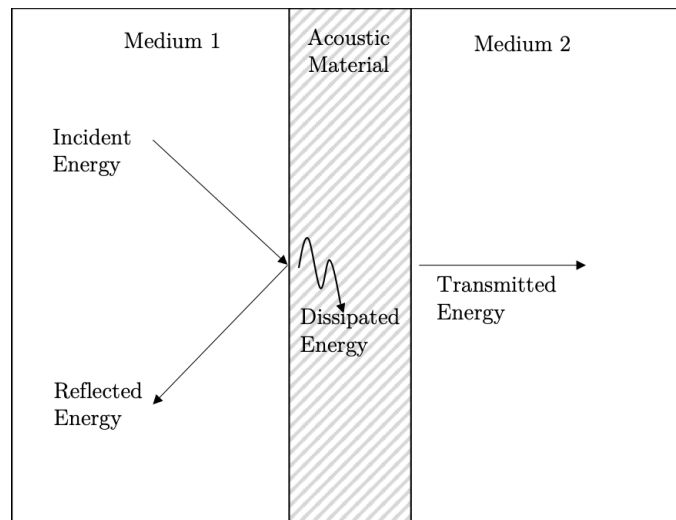


Figure 2.9: Reflection, absorption and transmission of incident acoustic energy at a boundary including a material layer.

2.3.2 Insulators

Acoustic insulation leverages impedance mismatch between two different mediums to reflect the incident sound wave. When the density or elasticity - hence the speed of sound - of a medium changes, an impedance mismatch is created, and the sound wave is partially or totally reflected. In this type of mirror-like or specular reflection, the angle of incidence and reflection from the surface are equal. Acoustic insulation is a type of noise control used, for example, to prevent sound from penetrating a neighbour wall, a barrier, or from entering a building or a theatre. Typical materials used for insulation are hard materials that reflect and block the propagation of waves. In the case of headphones, the hard plastic cover that surrounds the foam and the electronics in circumaural and supra-aural headphones functions as a flat reflecting surface. In order to maximise the impedance mismatch with air, dense and thick materials are needed, as modelled by the mass-law (Section 2.2.1). It is worth noting that insulators are effective for reflecting sound, but do not necessarily absorb it. An insulating barrier placed between source and receiver will result in a quieter environment on the receiver side, but not on the source side. Concrete, wood, and metal are good acoustic insulators [36].

2.3.3 Absorbers

Absorption happens when acoustic energy is transformed into another kind of energy, for example, heat. In room acoustics, we can define maximum absorption as that of an open window, where no reflections are present and there is no impedance mismatch between two materials [51]. Table 2.3 reports the absorption coefficient of commonly used absorbers [51, 58].

Table 2.3: Absorption coefficients of commonly used absorbing materials.

Materials	125 Hz	250 Hz	500 Hz	1000 Hz	2000 Hz
Acoustic tile	.80	.90	.90	.95	.90
Brick	.03	.03	.03	.04	.05
Carpet over concrete	.08	.25	.60	.70	.72
Heavy curtains	.15	.35	.55	.75	.70
Wood floor	.15	.11	.10	.07	.06
Fiberglass	.22	.82	.99	.99	.99
Marble	.01	.01	.01	.01	.02

Absorption is commonly used in reverberant spaces such as gyms, swimming pools, restaurants and stations. In headphones, absorbers have multiple functions: they seal the headphone to the ear to avoid sound leakage, absorb part of the external noise and absorb the reflections coming from the eardrum. However, the absorption provided with respect to the external noise does not impede sound to pass through - as with an open window, sound is completely absorbed as no reflections are present, but it will still pass through and be heard outside the window - hence the use of active noise cancellation or the potential use of acoustic metamaterials. Common absorbers reflect less, transmit less, and dissipate more energy. Most part of absorbed energy is dissipated as heat, and the remaining is transmitted. There are three main types of absorbers: porous-fibrous absorbers, panel absorbers, and resonant absorbers.

Porous-Fibrous Absorbers

Common porous-fibrous absorbers are polyurethane foam and fibreglass. Porous-fibrous absorbers are materials constituted both by a solid-phase frame, like foam

or fibres, and by a fluid phase, for example, air, situated in the pores of the material. Sound waves can enter these materials through the numerous pores and gaps on their surface. The interconnecting fluid tunnels within the materials minimise the reflection and maximise the absorption of sound energy. Dissipation happens through the friction of fibres. When the Young Modulus of the solid-phase frame is high, dissipation can also be achieved through scattering, thanks to the tortuosity of material or through the structural vibration. A smooth surface will not allow a sound wave to enter the pores and will result in larger reflection and, therefore, less absorption. A common porous-fibrous material is usually protected by a thin, lightweight membrane that allows the sound wave to pass through and avoids pores blockage over time by contaminating agents such as dust. A rigid backing material can also be added on one side of the porous layer to reflect the sound wave towards the pores, and increase absorption. A small air gap can optionally be introduced between the porous material and the backing layer: the air gap will help low-frequency absorption, and slightly decrease the high-frequency average absorption coefficient (see Section 2.2.1)[36]. Advantages of porous-fibrous materials are good absorption at high frequencies, availability of natural recyclable materials, and low costs of production. Limitations of porous-fibrous absorbers are their low durability, easy obstruction by dust, difficulty to clean, and poor performance at low frequencies below 1000 Hz [59].

Panel Absorbers

Panel absorbers consist of non porous thin sheets of metal or plywood that absorb low frequencies thanks to their vibrations. They can be fixed or freely suspended. They can be painted, and are considered aesthetically pleasing and commonly used for indoor applications. These panels are usually designed and modelled to vibrate at the natural frequencies of the room to compensate for room modes. One of the main limitations is the narrow frequency of absorption and the need for multiple panels to attenuate different frequencies [59].

Resonant Absorbers

Helmholtz resonators are an example of resonant absorbers. They are commonly used as low frequencies absorbers and individual resonators are placed in

recording studios near corners between walls to cancel low frequency room modes, or in noisy environments such as electrical power stations [32]. Only recently, their absorption functionality has been extended to acoustic metamaterials, where they form the base of unit-cells. In some cases, Helmholtz resonators are inserted in panel absorbers, to enhance their properties, and to obtain perforated panel absorbers.

2.3.4 Diffusers

When the surface used to reflect a sound wave is not flat, the sound is not reflected according to the incidence angle, but multiple angles of incidence are formed, producing a diffused scattering. This effect is used above all in theatres, to avoid echoes and coloration and to provide a more homogeneous listening experience to the entire audience regardless of position. Otherwise, the audience would receive an enhanced or attenuated signal according to the position of their seat with respect to the source position and the angle of incidence on the walls and acoustics of the space. Differently from absorbers, diffusers placed on a wall will not affect the acoustic energy, dispersing the reflections without altering the reverberation time of the room [32].

2.3.5 Active Noise Cancellation

As explained in the sections above, attenuating low-frequency sound waves is a challenging endeavour, as long wavelengths necessitate thick absorbers, or very dense and thick acoustic insulation structures. Active Noise Cancellation (ANC) leverages the destructive interference of waves (see Section 2.2.1) by creating an 'anti-noise' signal: a microphone measures the noise to be minimised, and a wave with opposite phase to the measured one is built to cancel or reduce noise. ANC is often used in headphones to protect the user from external noise and to prevent listeners from playing a louder signal than necessary and damaging their hearing. In a feed-forward ANC system, a reference microphone positioned on the external cover of the headphones measures the noise. A loudspeaker positioned in the internal side of the headphones generates an anti-noise signal that inverts the reference signal. A feed-back ANC system is usually based on an internal microphone close to the loudspeaker that measures the noise and feeds it back to

the loudspeaker. Feed-back systems are cheaper, as they use just one microphone, but they are hard to tune and present stability problems. In hybrid systems, external microphones perform the main function of measuring noise as done by feed-forward systems. However, they also use an error microphone positioned close to the loudspeaker to measure the residual noise: the signal measured by the error microphone is then fed into adaptive algorithms such as the Least Mean Square method that minimise the residual noise [38]. Today, feed-forward and hybrid systems are usually preferred.

2.4 Review of Acoustic Metamaterials

2.4.1 General Introduction to Metamaterials

Creating new materials from the ones readily available in nature is a process that has challenged and attracted human civilisation for centuries. Today, the most common way to create new materials consists in mixing atoms of chemical elements that exist in nature and that are listed in the periodic table. The invention of metamaterials - from the Greek word *μετά*, meaning 'beyond' - goes beyond this approach by using macroscopic structures as new 'atoms' that, when joined together in space, create a new material that acts as a continuous medium [60]. These 'atoms', also called 'unit cells', are in most cases disposed in a periodic way, but in some cases a different order is also possible [40]. The unit cells can be shaped and chosen according to the purposes of a specific experiment, they might be passive or active, and they should be subwavelength with respect to the incident wave in order to act as an effective medium. One of the first definitions of the term 'metamaterials', described them as "Macroscopic composites having a manmade, three-dimensional, periodic cellular architecture designed to produce an optimised combination, not available in nature, of two or more responses to a specific excitation" [61]. Despite the fact that the purpose of using metamaterials is indeed their unusual properties, as pointed out by Lapine [60] and Shvoda [62], other materials could have properties not previously found in nature and it is hence important to also highlight their structural organisation. Therefore, a more complete definition would be "Metamaterials are artificial structures, typically periodic (but not necessarily so), composed of small meta-atoms that, in the

bulk, behave like a continuous material with unconventional effective properties” [40].

2.4.2 The Origin of Metamaterials

Before presenting the first examples of acoustic metamaterials, it is important to take a step back in history to the search for negative index materials and the first realisations of electromagnetic metamaterials. The possibility of manufacturing electromagnetic materials with negative parameters was first predicted by Veselago [63] in 1968. Veselago noted that the only material properties that govern the propagation of an electromagnetic wave through a medium are electric permittivity and magnetic permeability. The refractive index n of a material is described by permittivity ϵ - a measure of the polarisability of a material - and permeability μ - a measure of the resistance of a material against the formation of a magnetic field - as follows [64]:

$$n = \sqrt{\mu\epsilon}. \quad (2.57)$$

In optics, the refractive index n of a material describes the propagation of light in the material:

$$n = \frac{c}{v}, \quad (2.58)$$

where c is the speed of light in vacuum and v is the phase velocity of light in the material. A higher refractive index describes a slower propagation of light in a medium. Snell’s law (Fig. 2.10) describes the relationship between the refractive indices of two media as the ratio of sines of angle of incidence and angle of transmission (more commonly known as angle of refraction) of a wave propagating between two different media [64]:

$$\frac{n_1}{n_2} = \frac{\sin \theta_2}{\sin \theta_1}, \quad (2.59)$$

where θ is the angle measured from the normal to the boundary of the two media. Veselago predicted through mathematical proof that a negative refractive index where waves could bend ”backward” could be obtained at particular frequencies if either ϵ or μ were negative:

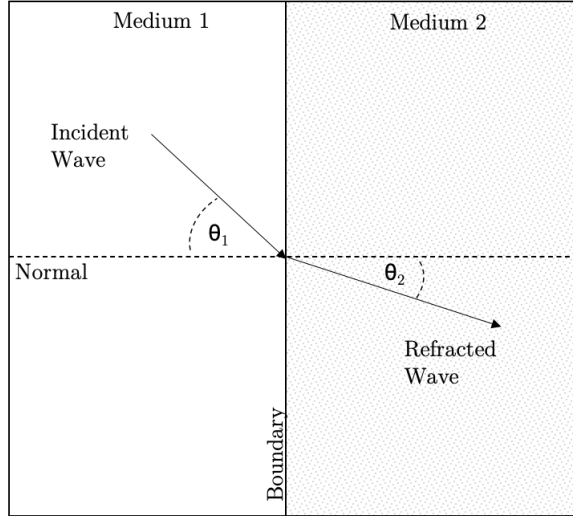


Figure 2.10: Visualisation of the refraction of a wave propagating between two different media as described by Snell's law.

$$\mu = -|\mu| \quad (2.60)$$

$$\epsilon = -|\epsilon| \quad (2.61)$$

$$\begin{aligned} n &= \sqrt{\mu\epsilon} & (2.62) \\ &= \sqrt{-1} \times \sqrt{-1} \times \sqrt{|\mu||\epsilon|} \\ &= j^2 \sqrt{|\mu||\epsilon|} \\ &= -\sqrt{|\mu||\epsilon|} \\ &\implies n < 0. \end{aligned}$$

He also predicted that if both ϵ and μ were negative, the wave would propagate forward and would be characterised by an effective negative refractive index. As shown in Fig. 2.11, a negative refractive index could cause a wave to bend backward in quadrants 1 and 4, while a positive index would transmit the wave in quadrants 2 and 3.

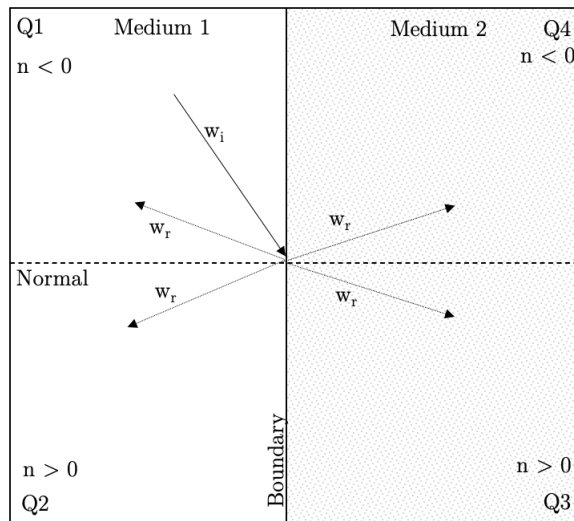


Figure 2.11: Visualisation of possible regions of wave refraction w_r when an incident wave w_i propagates between two different media. Quadrants 1 and 4 exhibit negative refractive index n and quadrants 2 and 3 positive refractive index n .

From an experimental point of view, some successful results were obtained in the late '80s and early '90s by Yablonovitch who built a periodic dielectric structure that created a band gap to attenuate spontaneous electromagnetic emissions [65, 66]. Similarly, Genack and Garcia leveraged destructive interference to attenuate electromagnetic waves traveling through periodic metallic spheres [67]. These devices that could control electromagnetic waves were referred to as 'photonic crystals'. In fact, it was noted that the distance between the microstructures of these periodic devices determined the wavelength of the incoming wave that was attenuated.

In 1999, 31 years after Veselago's prediction, Pendry was able for the first time to fabricate a device that exhibited negative permeability [68]. This device consisted in a copper split-ring structure with a resonance frequency characterised by a wavelength which is much larger than the diameter of the ring. This type of structure was referred to as 'metamaterial'. Pendry also extended the work of Veselago by proposing a new method create a lens having a theoretically perfect focus [69].

Following this discovery, negative index metamaterials and other metamaterials with negative parameters were experimentally obtained [70, 71]. Today, negative index metamaterials can be applied to the study of lenses, subwavelength imaging and invisibility cloaks [72–75].

2.4.3 Acoustic Metamaterials

In acoustics, the quest for new materials is driven by the possibility to control sound waves in new ways. For example, acoustic metamaterials could substitute traditional materials by attenuating sound with small-scale and light-weight structures, or they could bend sound in different directions, control vibrations, realise acoustic cloaks, and energy harvesting devices.

In parallel to the field of photonic crystals, in the early '90s researchers started to apply similar concepts to the realm of elastic and acoustic waves, giving origin to the field of phononic crystals. Sigalas and Economou noted that in acoustics the two material parameters that characterised wave properties are density and bulk modulus [76]. Phononic crystals were periodic composites made of two alternating materials with different elastic properties, that, thanks to Bragg scattering and wave interferences, could bend or attenuate vibrations and sound waves with a wavelength of the same order of the distance between the materials [77–79].

About 11 years after Pendry's realisation of electromagnetic materials prediction, the concept of metamaterials was extended to acoustic materials as well, through the work of Liu et al. [3] who modelled and fabricated a locally resonant acoustic metamaterial to achieve wave attenuation. Liu built a three-dimensional structure made of heavy resonators - specifically lead spheres - embedded in an epoxy matrix (Fig. 2.12). Differently from phononic crystals, the phase shift and wave attenuation were caused by the resonance of inclusions, that due to a difference in phase speed with the coating material could oscillate and generate a 180° phase shift. Since these materials could attenuate waves having a wavelength much larger than their dimensions and because this was considered a breakthrough with respect to the properties of phononic crystals, they were named acoustic metamaterials. Today, the definition of acoustic metamaterials

sometimes includes phononic crystals and defines as 'locally resonant acoustic metamaterials' the types of materials that leverage resonance instead of Bragg scattering to control waves. According to other taxonomies, phononic and sonic crystals are not considered to be acoustic metamaterials. Finally, it is worth noting that many publications propose the use of unit cells that are both resonant and periodically spaced, leveraging both types of band gaps. The main focus of this thesis is on resonant acoustic metamaterials, hence sometimes the structures here presented are simply referred to as acoustic metamaterials. In the next sections, some basic theory and literature review of phononic crystals, sonic crystals and locally resonant acoustic metamaterials will be presented.

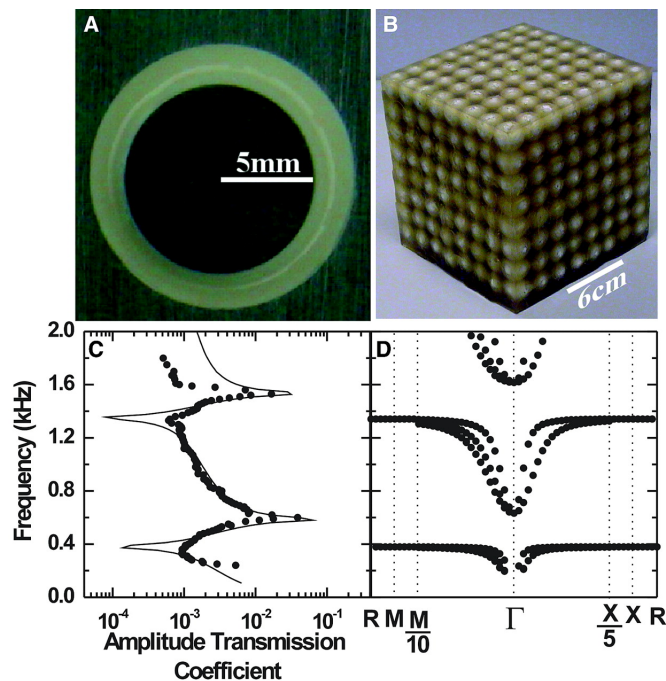


Figure 2.12: First experimental realisation of acoustic metamaterials proposed by Liu et al. [3]. A three-dimensional structure made of periodically spaced lead spheres embedded in an epoxy matrix is capable of isolating low-frequency sound and to break the mass law.

Crystals

Crystals are solid materials that can be found in nature. A crystal is characterised by components or units, such as atoms and ions, that are arranged in a periodic

or ordered structure to form a lattice [80]. In a lattice, units are organised in regularly repeating patterns. Examples of natural crystals are table salt, sugar, snowflakes, quartz and diamonds.

Sonic and Phononic Crystals

Following from the definition of a natural crystal, sonic crystals can be defined as artificial crystals whose units (or unit cells) are scatterers (also called sonic scatterers) made of reflective materials such as wood or metal, usually embedded in a fluid homogeneous host material. When the host material is a solid, these types of metamaterials are called phononic crystals [81]. The periodicity of the crystals can be in one, two, or three dimensions. One-dimensional sonic crystals are a series of scatterers positioned at an equal distance along the direction of periodicity and separated by a fluid such as air; they are characterised by periodic variation of bulk modulus and density (or in other words characteristic impedance) in one direction. Two-dimensional sonic crystals are arranged in two directions and the distance between scatterers can be equal or different in the two chosen directions; bulk modulus and density vary periodically in the two independent directions. The drawback of sonic crystals is that, following from Bloch's Theorem, the wavelength of the attenuated sound waves must be of the same order of the lattice constant, i.e. the distance between the unit-cells. Considering that the audio frequencies between 100 Hz and 20000 Hz have wavelengths in air in the range of 17 cm to 3.4 m, sonic crystals are large structures and cannot be used to attenuate noise in small-scale devices or machinery. The first example of two-dimensional sonic crystal was realised by Martinez [4], who proposed an outdoor structure that could shield environmental noise (see Fig. 2.13). The sculpture had a diameter of 4 meters and was composed of a cylindrical base filled with hollow stainless steel cylinders that acted as scatterers, having a 2.9 cm diameter. Sound attenuation up to 20 dB was obtained at frequencies around 1.5, 2.5, 3.5 and 4 kHz. Miyashita [5] proposed a two-dimensional sonic crystal where a panel of rods was embedded in air and arranged at equal distances along two directions. Similarly, three-dimensional sonic crystals are characterised by independently periodic variation of bulk modulus and density in three directions. As shown in the previous paragraph (Fig. 2.12), Liu et al.

[3] were the first to propose a three-dimensional sonic crystal that was made of locally-resonant unit cells. In their publication, they presented a cubic structure made of lead balls embedded in a matrix of epoxy. According to the definition and terminology used, this first example of three-dimensional sonic crystal can also be considered the first metamaterial or simply a locally-resonant sonic crystal.

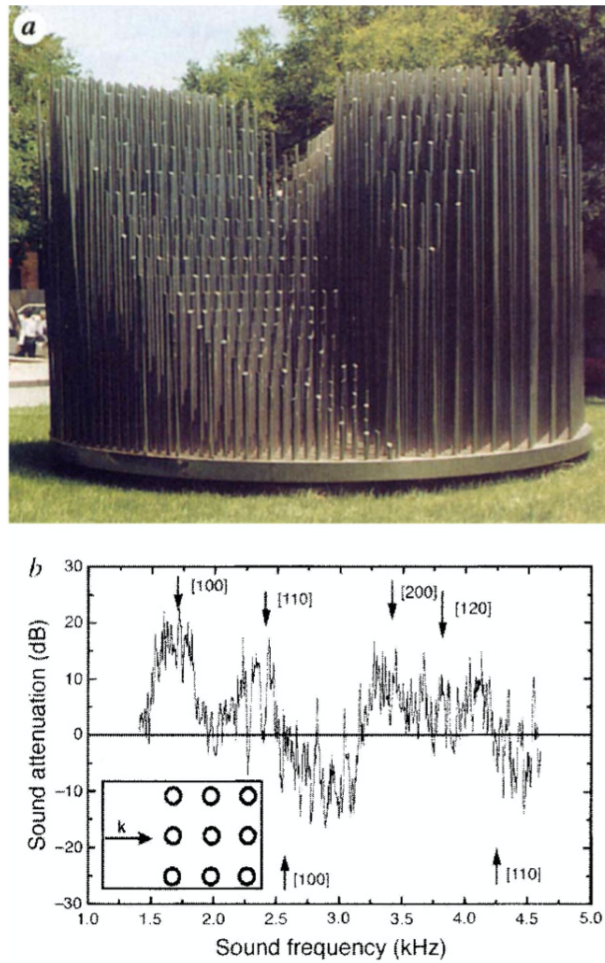


Figure 2.13: Two-dimensional sonic crystal outdoor sculpture by Eusebio Sempere and resulting sound attenuation [4].

To study acoustic wave propagation in crystals, models rely on their symmetry. This allows to investigate wave propagation in a reduced area of a unit cell and to then extend it to the entire crystal. To do so, concepts such as Bravais lattice, direct and reciprocal lattice, irreducible Brillouin zone and Bloch's Theorem are

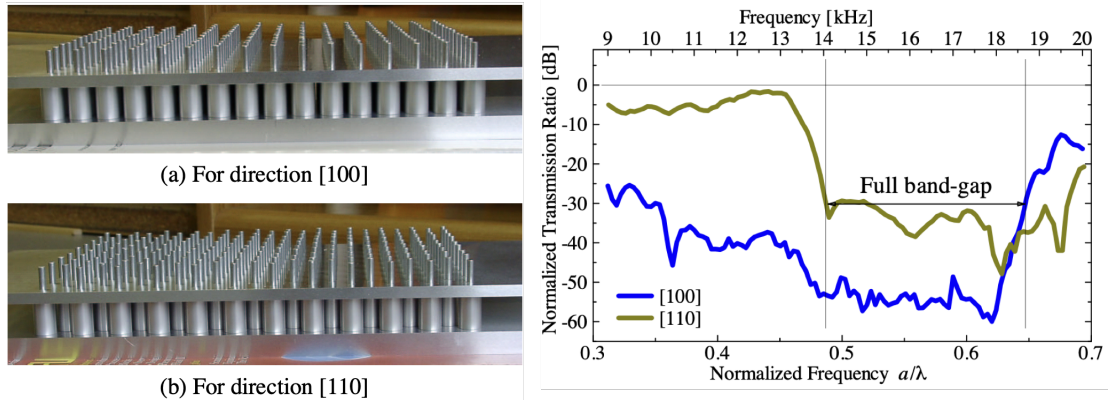


Figure 2.14: Two-dimensional sonic crystal slab based on aluminium rods embedded in air and resulting sound transmission [5].

briefly introduced.

Band Gaps

Band gaps are frequency bands where the sound does not propagate or is greatly attenuated. In periodic structures, band gaps are the result of periodic modulation of density or bulk modulus of the materials alternating in the unit cell. The band gaps can be interpreted as the result of destructive Bragg interferences and are modelled by Bloch's Theorem. Hence, the wavelength of the attenuated sound waves are of the same order of the lattice constant, which is the minimum distance between two unit cells. By analogy, the attenuation band resulting from destructive interference in acoustic metamaterials is also called band gap. In this thesis we use the term 'band gap' to refer to frequency bands where the sound is deeply attenuated as a result of the effect of acoustic metamaterials. Although a better terminology would be 'attenuation band' or 'stop band', the term 'band gap' is used as is commonly found in the literature. It is also important to reflect on the definition of the limits of the band gap. In absence of an official standard to define the limits of band gaps in acoustic metamaterials, we propose to use a similar rule of thumb to the one used for transition bands in filters. The proposed definition would define the start of the band at the point where the attenuation is 1 dB with respect to reference and the end the point where the notch is again 1 dB from the reference.

Bravais Lattice

In crystallography, a Bravais lattice is an infinite array of unit cells whose orientation appears to be the same regardless of the unit cell the array is observed from. In one dimension, there exists only one possible Bravais lattice. In two dimensions, there are five possible categories of Bravais lattices, for example rectangular or oblique; in three dimensions there exist fourteen different arrangements of unit cells, such as cubic, hexagonal, tetragonal, etc. [80]. A three dimensional Bravais lattice can be described in mathematical terms as a collection of points with position vector \vec{R} :

$$\vec{R} = n\vec{a}_1 + m\vec{a}_2 + l\vec{a}_3, \quad (2.63)$$

where \vec{a}_1 , \vec{a}_2 and \vec{a}_3 are the three primitive vectors lying in three different planes and n , m and l are integers [55].

Primitive Cell

The primitive cell of a lattice is the space that contains one unit cell and can be translated in all the lattice dimensions without overlapping itself or leaving voids [55].

Filling Fraction

The filling fraction or packing density in a sonic crystal is the ratio between the volume occupied by the primitive cell and the total volume occupied by the sonic crystal. Typical arrangement in sonic crystals are cubic lattices - because they are easy to build - and hexagonal lattices [59]. The metamaterials presented in the next Chapter of this thesis present a circular geometry in order to replicate previous work on soda cans, as well as to facilitate the fabrication at the prototyping stage. Nevertheless, filling fraction is important to consider in the research area of metamaterials optimisation and in order to scale production.

Direct Lattice

The direct lattice is a Bravais lattice, it represents the geometrical arrangement of the crystal and it is studied in the real space.

Wigner-Seitz Cell

The Wigner-Seitz cell is a primitive cell in the direct lattice constructed by drawing lines that connect a lattice point to all the neighbouring lattice points. Given these connecting lines, by adding new lines that pass through their mid point and normal to them, the smallest volume enclosed by these lines or planes is defined as the Wigner-Seitz cell. This cell respects the symmetry of the underlying Bravais Lattice [55].

Reciprocal Lattice

The reciprocal space can be described as the Fourier Transform of the real space. For any function $f(\vec{r})$ which is periodic in the direct lattice, there exists a set of vectors \vec{G} , such as:

$$f(\vec{r}) = \sum_{\vec{G}} f(\vec{G})e^{i\vec{G}\vec{r}}. \quad (2.64)$$

A periodic function in the Bravais lattice satisfies:

$$f(\vec{r}) = f(\vec{r} + \vec{R}), \quad (2.65)$$

where $\vec{R} = n\vec{a}_1 + m\vec{a}_2 + l\vec{a}_3$. Therefore,

$$f(\vec{r} + \vec{R}) = \sum_{\vec{G}} f(\vec{G})e^{i\vec{G}(\vec{r} + \vec{R})} = f(\vec{r}) = \sum_{\vec{G}} f(\vec{G})e^{i\vec{G}\vec{r}}. \quad (2.66)$$

Hence,

$$e^{i\vec{G}\vec{R}} = 1, \quad (2.67)$$

and

$$\vec{G}\vec{R} = 2\pi N, \quad (2.68)$$

where N is an integer. The reciprocal lattice is a set of unit cells or points whose positions are given by the vectors \vec{G} , that satisfy the condition $\vec{G}\vec{R} = 2\pi N$, where N is an integer, for all \vec{R} in the Bravais lattice. It can be shown that, if \vec{a}_1 , \vec{a}_2 and \vec{a}_3 are the primitive vectors of the three dimensional direct lattice, the primitive vectors of the reciprocal lattice \vec{b}_1 , \vec{b}_2 and \vec{b}_3 are given by:

$$\begin{cases} \vec{b}_1 = 2\pi \frac{\vec{a}_2 \times \vec{a}_3}{\vec{a}_1 \cdot (\vec{a}_2 \times \vec{a}_3)} \\ \vec{b}_2 = 2\pi \frac{\vec{a}_3 \times \vec{a}_1}{\vec{a}_2 \cdot (\vec{a}_3 \times \vec{a}_1)} \\ \vec{b}_3 = 2\pi \frac{\vec{a}_1 \times \vec{a}_2}{\vec{a}_3 \cdot (\vec{a}_1 \times \vec{a}_2)} \end{cases} \quad (2.69)$$

and:

$$\vec{G} = n'\vec{b}_1 + m'\vec{b}_2 + l'\vec{b}_3, \quad (2.70)$$

where n' , m' and l' are integers [55]. The reciprocal lattice is also a Bravais lattice and it corresponds to the direct lattice in the reciprocal space. If for example a simple cubic direct lattice is created in the real space, having a distance a between each unit cell, the reciprocal lattice will be a cubic Bravais lattice with distance $2\pi/a$ between unit cells.

Irreducible Brillouin Zone

The Brillouin zone can be found in the reciprocal lattice following the same rules defined to find the Wigner-Seitz cell in the direct lattice. Given the symmetries in the Brillouin zone, it is possible to limit the study to the irreducible Brillouin zone, which is the space limited by the points of high symmetry. Usually the points of highest symmetry in a two dimensional lattices are represented with the letters Γ , X and M . Studying the wave propagation along the perimeter of the irreducible Brillouin zone is sufficient to understand the propagation of waves throughout the entire crystal.

Bloch's Theorem

Bloch's Theorem states that the acoustic field inside a periodic structure takes on the same symmetry and periodicity of the structures [59]. The waves created inside a periodic structures are denominated Bloch Waves and can be represented as:

$$p(\vec{r}) = A(\vec{r})e^{j\vec{k}\vec{r}}, \quad (2.71)$$

where A is the amplitude envelope that reflects the same periodicity and symmetry of the crystal and satisfies $A(\vec{r} + \vec{a}) = A(\vec{r})$, $e^{j\vec{k}\vec{r}}$ is the plane-wave-like term and \vec{a} represents the primitive lattice vectors. Bloch waves exist just at discrete frequencies, which must have the same periodicity of the crystal. Since the allowed frequencies are discrete, there must be some frequencies at which wave propagation is not allowed in the material.

Bragg Scattering

From a physics point of view, Bragg's law predicts the angles of reflection of a wave passing through two different media and describes the resulting constructive and destructive interferences. In phononic crystals, the impedance contrast between the matrix material and the inclusion (scattering) material, results in waves being scattered at an angle described by Bragg's law. The main effect, as modelled by multiple scattering theory, is destructive interference [82, 83]. This makes phononic crystals a good candidate for applications such as noise attenuation. However, waves attenuated by phononic crystals have a wavelength of the same order of the lattice constant (or distance between two unit cells). For this reason, applications in the audio domain would be quite large and therefore, phononic crystals are more often used in ultrasound applications.

2.4.4 Acoustic Metamaterials Based on Local Resonances

When an oscillator is driven by a wave slightly higher than its resonance frequency, there is a delay in the oscillator with respect to the driving force that results in a 180 degrees phase shift. Since the behaviour of an oscillator near resonance is characterised by a larger displacement than at other frequencies, the phase shift has an amplitude large enough to interfere constructively or destructively with the incoming wave. Given the size limitation of sonic and phononic crystals, the realisation that metamaterials-based local resonances could not only achieve negative effective parameters, but also attenuate noise using subwavelength structures gave origin to the new field of locally resonant acoustic metamaterials.

Acoustic metamaterials based on local resonances are at least two orders of magnitude smaller than the wavelength of the attenuated wave. Typical unit cells consist of Helmholtz resonators (which are more subwavelength than pipes) for negative effective bulk modulus and membranes and thin plates for negative effective density [40]. The standard way to fabricate locally resonant acoustic metamaterials is to include resonant objects inside a matrix material characterised by a higher phase speed. The first three-dimensional acoustic metamaterial based on resonances was introduced by Liu et al. in 2000 [3]: an $8 \times 8 \times 8$ array of unit cells, where each unit cell consisted of an epoxy matrix embedding a lead sphere. These acoustic metamaterials had wave attenuating properties at narrow frequency bands near the resonances of the lead spheres (around 300 Hz and 1500 Hz). Following Liu et al. work, many researchers presented ways to maximise the attenuation, optimise unit cells, obtain larger band gaps and create hybridisation band gaps using both phononic crystals and resonant acoustic metamaterials [84–87].

Physical Interpretation of Negative Effective Properties

In acoustic metamaterials, when the effective bulk modulus B_{eff} and the effective mass density ρ_{eff} are negative, the refractive index becomes negative, and the acoustic wave can be bent very sharply towards the source direction or at other unusual angles. When either effective bulk modulus or density become negative, the speed of sound becomes imaginary, and the wave decays exponentially; hence the sound wave is deeply attenuated. The physical meaning of negative effective density can be interpreted as an acceleration to the left when a medium is pushed towards the right direction and vice versa. The negative effective bulk modulus implies an expansion of the medium when experiencing compression and vice versa. In other words, due to the 180 degrees phase shift at resonance, the average momentum or expansion of the unit cells moves in the opposite direction to the wave propagating in towards the metamaterial.

Acoustic Metamaterials Based on Helmholtz Resonators

As shown in Section 2.2.2, Helmholtz resonators have lower resonances with respect to pipes of similar dimension; hence they are good candidates for

low-frequency subwavelength attenuation in acoustic metamaterials. Another advantage of Helmholtz resonators is that, for sound applications, they do not produce impedance mismatch and maximise the wave control effect of metamaterials: the medium of wave propagation is the same as the medium that causes them to resonate. Acoustic metamaterials based on Helmholtz resonators can achieve a negative effective bulk modulus. One of the first publications using Helmholtz resonators as unit-cells was a paper by Fang et al. [6] (see Fig. 2.15). Fang obtained ultrasonic wave attenuation near 30 kHz. Another notable publication by Lemoult et al. used arrays of soda cans acting as Helmholtz resonators to steer and focus sound waves [7] (see Fig. 4.1). Recently, Helmholtz resonators have become a common and popular way to attenuate sound and control acoustic waves [88–91]. A promising development is the investigation of active Helmholtz resonators that can change shape in real-time or be driven by piezoelectric actuators in order to tune the frequency to be controlled [92, 93].

Acoustic Metamaterials Based on Membranes and Thin Plates

The first paper to introduce the idea of membrane-based acoustic metamaterials was published by Yang et al. [94]. These metamaterials are characterised by membranes as unit-cells and have a negative effective mass density: $\rho_{eff} \leq 0$ [95, 96]. In the literature, it is common to find two types of membranes and thin plates: with no mass attached [43] and with a small masses attached to the centre of the membrane or thin plate [97, 98]. The membranes are usually inserted inside waveguides or sometimes attached to other resonators. Yang et al. proposed a membrane-based metamaterial panel for sound attenuation in the 50-1000 Hz regime[8] (see Fig. 2.17). The advantage of this type of metamaterials is the very thin nature of membranes and thin plates and their lightweight and small-scale characteristics.

2.4.5 Active Acoustic Metamaterials

The acoustic metamaterials described above use resonance to passively control sound. Passive acoustic metamaterials are capable of going beyond narrowband attenuation and of controlling sound in extended frequency bands. Nevertheless, once the metamaterials are designed and built, the band gap where the sound

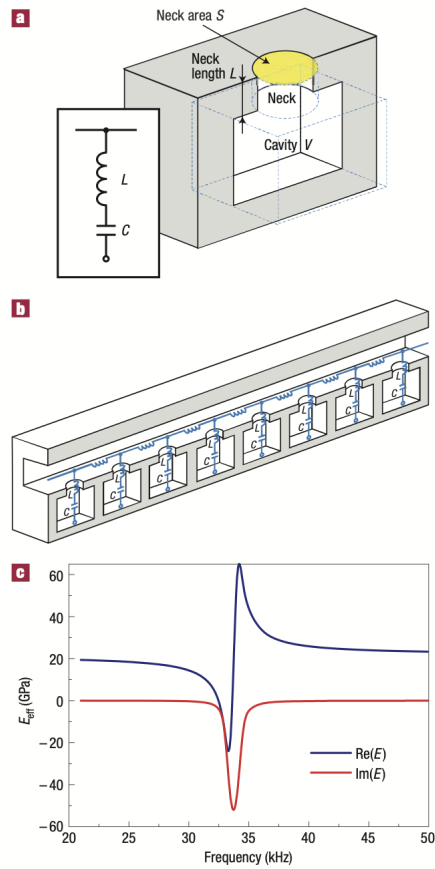


Figure 2.15: Ultrasonic metamaterials based on Helmholtz resonators, proposed by Fang et al. [6] (a) Schematic of Helmholtz resonator, (b) chain of Helmholtz resonators, (c) effective modulus.

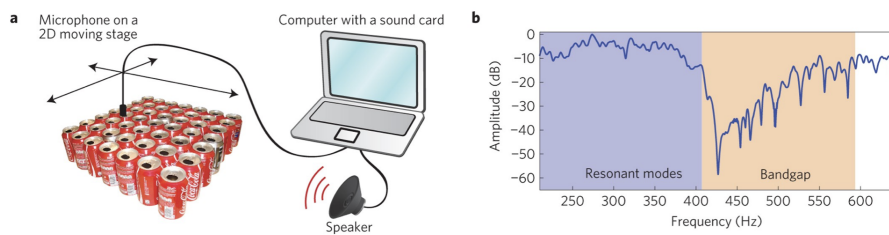


Figure 2.16: Acoustic metamaterials based on soda cans, introduced by Lemoult et al. [7]. (a) experimental setup, (b) sound transmission and band gap.

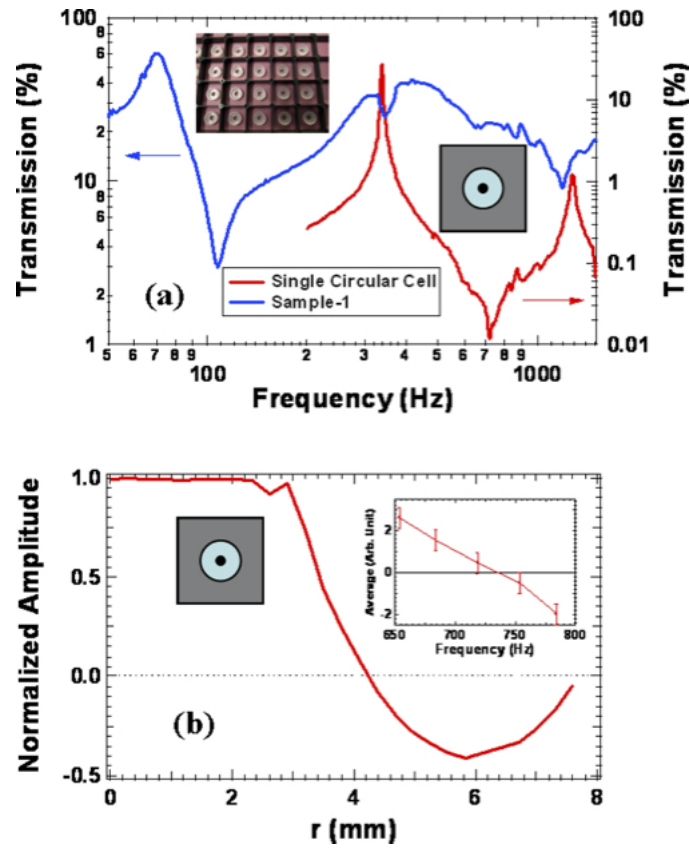


Figure 2.17: Transmission spectra and displacement amplitude of membrane-based acoustic metamaterials with attached mass as proposed by Yang et al. [8].

is controlled cannot be modified. Active acoustic metamaterials can offer reconfigurable and tunable solutions that respond in real-time to changes in the acoustic field. This is possible for example by integrating transducers in the metamaterials, by fabricating unit-cells made of piezoelectric materials or by mechanically reconfiguring the elasticity, mass or shape of unit cells [40, 99–107].

2.4.6 Applications of Acoustic Metamaterials

In the past decade, the field of acoustic metamaterials has obtained outstanding achievements in research labs. However, thus far, there has been limited progress from the lab environment to industrial fabrication. Nevertheless, this field is rapidly growing, and new developments and real-world products are expected in the coming years. The main applications that have been proposed include noise attenuation in automotive and aerospace industries, sound control in audio devices, acoustic cloaks, acoustic superlenses, and energy harvesting devices.

Noise Attenuation

One of the most sought-after applications of acoustic materials is noise reduction, which is also the primary purpose of the work presented in this thesis. The advantages of using acoustic metamaterials for noise attenuation are, of course, the ability to break the mass-law and to fabricate thin and lightweight materials that can attenuate low frequencies. Acoustic metamaterials have been successfully used for low-frequency noise reduction of traffic and transportation noise and as filters in sensors and transducers [8, 11, 108, 109]. In this type of application, acoustic metamaterials have either negative effective bulk modulus or density. When these properties become negative, the speed of sound is just composed by the imaginary part, and therefore the sound propagation stops inside the material and noise is filtered out.

Applications to Audio Devices

Applications to audio devices are one of the main objectives of this thesis. Designing small-scale acoustic metamaterials that could fit into audio devices such as headphones, hearing aids, and loudspeakers would have the advantage of

2.4. Review of Acoustic Metamaterials

reducing noise, localising, and enhancing sounds without using power-consuming complex signal processing computations. Xie et al. [9], see Fig. 2.18, developed a device to tackle the problem of 'cocktail party problem' [110] and mimic the auditory system ability to focus on one speaker when multiple speakers are talking in a noisy environment. This device consisted of a single microphone surrounded by fan-like waveguides holding Helmholtz resonators of random heights. The wave modulating properties of Helmholtz resonators allowed to filter the incoming waves in unique ways depending on the source location and, consequently, to amplify signals coming from a specific direction. A similar application was developed by Esfahlani [10], who proposed an acoustic dispersive prism consisting of a fluid-filled waveguide with vibrating thin plates and attached ducts. Recently, Ghaffarivardavagh [11] (see Fig. 2.20) presented a small-scale circular device that cancels sounds and, at the same time, allows air to flow by using acoustic metamaterials based on pipes elliptically shaped around the air gap.

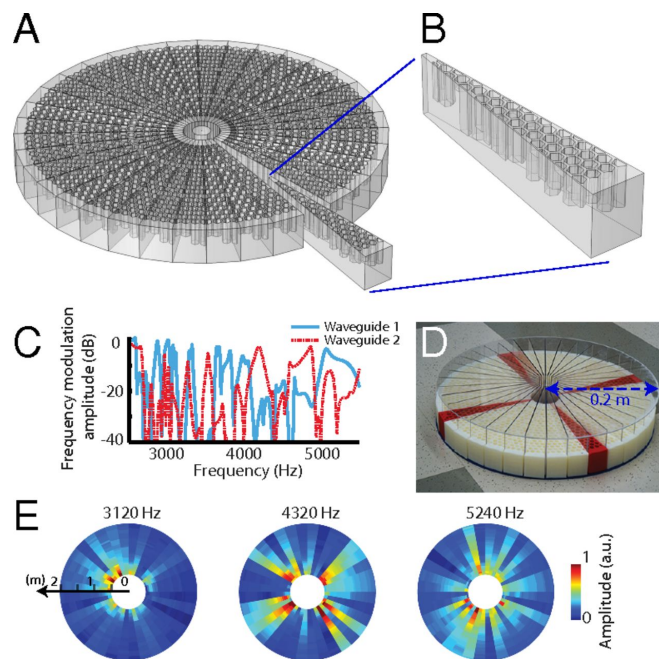


Figure 2.18: Single-sensor multispeaker based on acoustic metamaterials developed by Xie et al. [9].

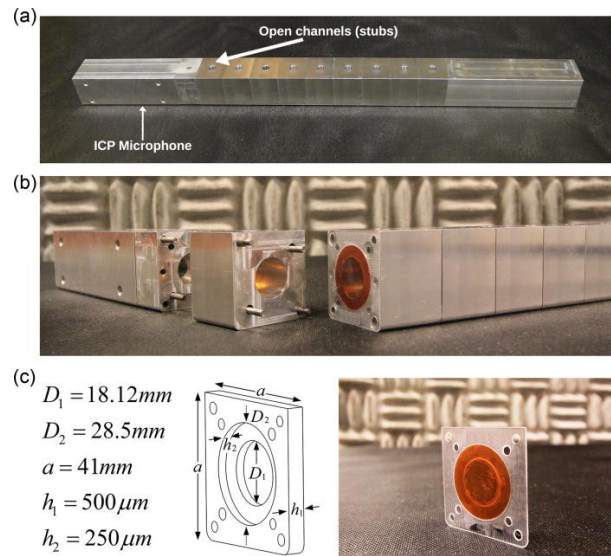


Figure 2.19: Acoustic dispersive prism based on membrane-type acoustic metamaterials developed by Esfahlani [10].

Acoustic Cloaks and Metasurfaces

Acoustic cloaks are devices that enclose objects and bend the acoustic waves around them to avoid reflections from the target [12, 111–114]. Acoustic cloaks (see Fig. 2.21) could be used, for example, to soundproof buildings, concert halls, rooms: by coating walls with acoustic cloaks, the incident sound waves coming from external sources would bend around the building and realise acoustic insulation. Another application of acoustic cloaking is in defence, for example, in sonar. To identify the location of an object, sonar underwater systems use a transducer to transmit acoustic waves towards the desired direction and then measure - through a hydrophone - the acoustic waves reflected from the object back to the sonar. The time delay between the incident and reflected waves permits to calculate the distance from the object to the sonar system. By coating an object - such a submarine or water vessel - with acoustic cloaks, it is possible to bend the waves around it and to prevent reflections from being sent to sonar systems. A variation of acoustic cloaks consists of metasurfaces and metadiffusers. By coating the internal side of walls in concert halls, it would be possible to control the reflections and spread them more uniformly across the concert hall for better control of reverberation (see Fig. 2.22) [13, 115].

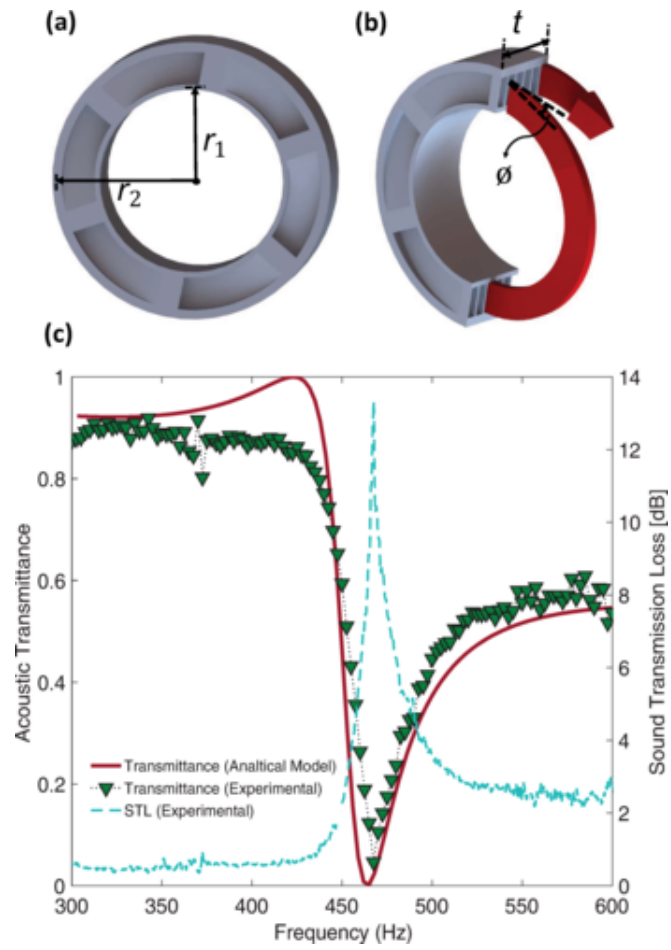


Figure 2.20: Ultra-open acoustic metamaterial silencer proposed by Ghaffarivardavagh [11].

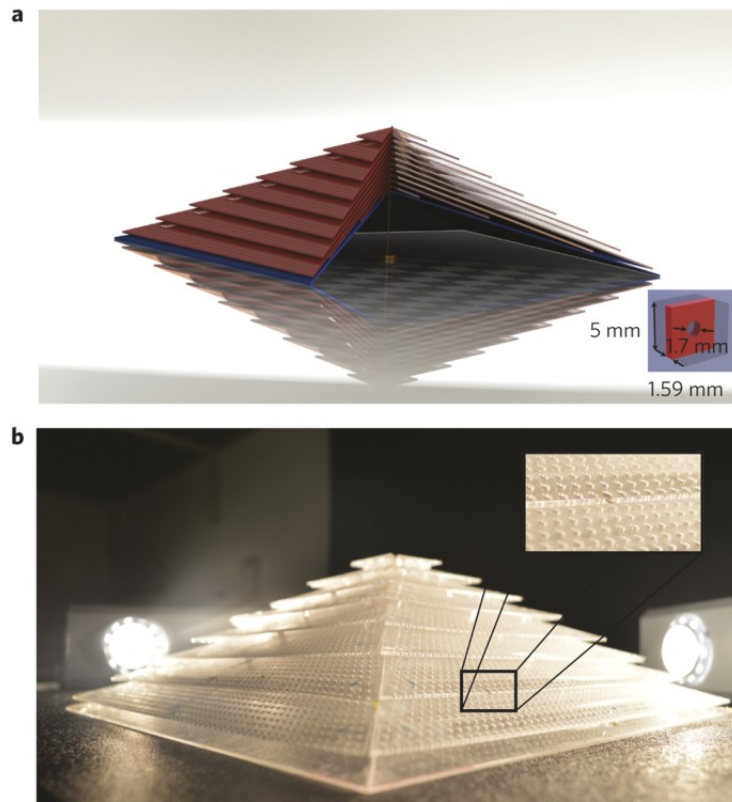


Figure 2.21: Acoustic cloak [12].

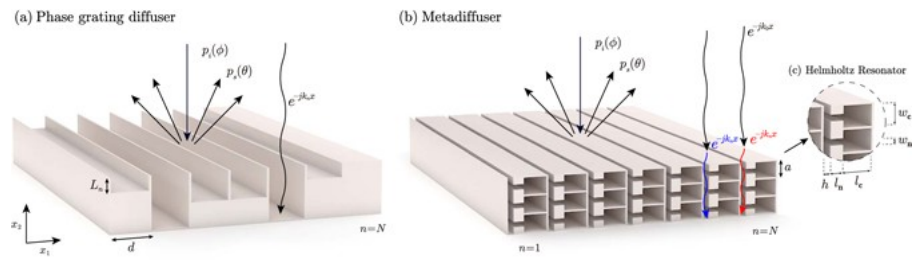


Figure 2.22: Acoustic metasurface [13].

Acoustic Superlenses

Traditionally, acoustic lenses are capable of focusing waves propagating in the far field. They do so by designing the reflecting material in a way that bends - following Snell's Law - the waves and makes them converge in the same point. Far fields extend from a distance λ from the source to infinity (Section 2.2.1): this limitation on spatial resolution is called the diffraction limit. Acoustic superlenses can be defined as devices that are capable of creating acoustic images of subwavelength objects or materials, i.e., materials that have a dimension that is less than the wavelength of the wave propagating through the lens. Double negative acoustic metamaterials have a negative refractive index and can bend waves at angles not possible with traditional materials. By reverse-bending the refracted waves, it is possible to amplify not only propagating waves, but also evanescent decaying waves situated in the near field. Acoustic superlenses can be used to increase the resolution of ultrasounds and non-destructive testing or decrease the frequency of waves used for medical imaging [14, 116, 117]. For example, Deng et al [14] theoretically investigate subwavelength imaging obtained by immersing acoustic metamaterial slabs in a liquid matrix (see Fig. 2.23 and Fig. 2.24).

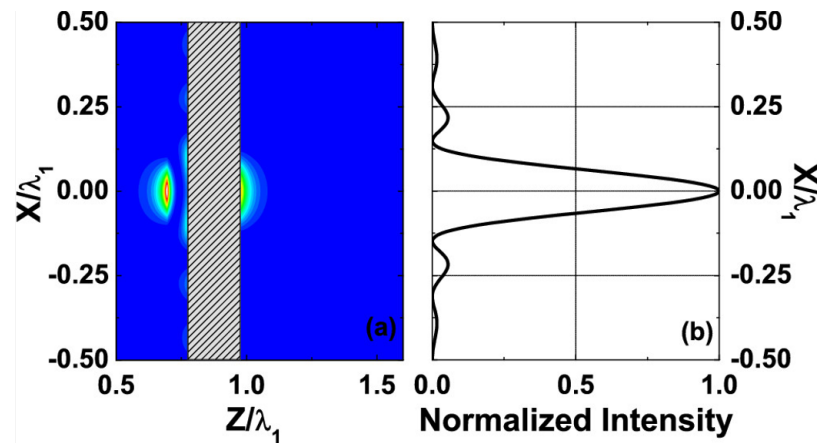


Figure 2.23: Single negative acoustic metamaterials producing a near-field subwavelength image [14].

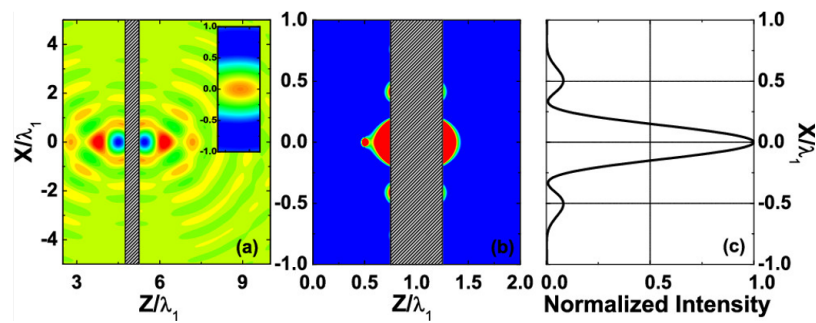


Figure 2.24: Double negative acoustic metamaterials producing a subwavelength real image [14].

Energy Harvesting

An exciting application of acoustic metamaterials is the development of energy harvesting devices [15, 108, 118, 119]. Energy harvesting devices take energy from the environment - such as acoustic energy - and convert it to a different type of energy, for example, electrical. A common way to harvest energy in acoustic systems is to make piezoelectric membranes vibrate and to store the resulting electrical energy. Other ways to harvest acoustic energy include converting mechanical waves into electromagnetic or electrostatic energy. Wu et al. [15] (see Fig. 2.25) were able to harvest energy by removing a unit-cell at the centre of a sonic crystal made of rods and substituting it with a piezoelectric piezoelectric material. Hu et al. [119] proposed a multifunctional acoustical metamaterial capable of simultaneously create a band gap and harvest energy.

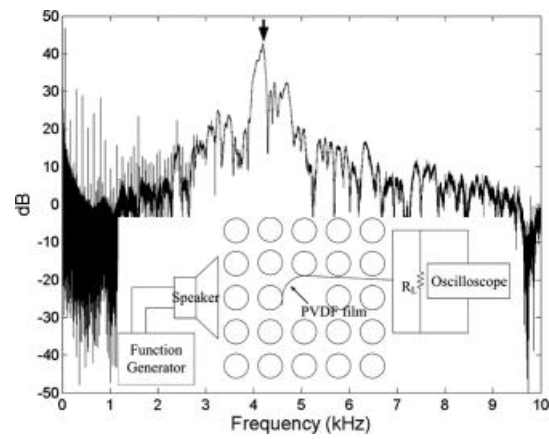


Figure 2.25: Energy harvesting metamaterial proposed by Wu et al.[15]. The PVDF film at the centre of a sonic crystal shows maximum output voltage near the resonance of the cavity created by the point defect in a 5 X 5 array of rods.

Chapter 3

Methods

Chapter 3 outlines the methods used in this dissertation to model, fabricate metamaterials, measure, and analyse their performance. An overview of three-dimensional printing is provided, focusing on stereolithography and the manufacturing techniques developed in this research. The laboratory free-field set-up used to measure the response of Helmholtz resonators is illustrated in detail. Next, the impedance tube used to measure thin plates is described. An introduction to laser Doppler vibrometry and its use for thin plates vibration analysis is provided. Finally, the two modelling methods used in this thesis are presented. The transfer-matrix approach is used to model the impedance tube system. The finite element analysis software COMSOL Multiphysics is used throughout this work in conjunction with analytical models to predict the behaviour of acoustic metamaterials.

3.1 Three-Dimensional Printing

Introduction

Three-dimensional printing - also known as additive manufacturing - is a method to fabricate a physical object, layer by layer. The object is first designed using Computer-Aided Design (CAD) software or by three-dimensional scanning an existing shape, and it is then converted into STL format. The three-dimensional printed software slices the STL file in layers of specified thickness, determined by the printer's highest resolution. Next, various three-dimensional

printing techniques can be deployed to fabricate the object layer by layer. The most common techniques will be described below and include extruding heated materials from a nozzle, solidifying liquid polymers, and melting powders. Lastly, the printed object is cleaned and polished. Three-dimensional printing has become increasingly popular in the last decade, both in industry and academia, as a rapid prototyping method. As these techniques are refined, additive manufacturing is also starting to find its place in final products. The following sections will review the history and development of three-dimensional printing, the principal additive manufacturing techniques, and the role these methods play in the world of acoustics and acoustic metamaterials.

Origin of Three-Dimensional Printing

Three-Dimensional Printing originated in 1981 when the Japanese inventor Hideo Kodama used ultraviolet light to harden polymers and obtain a solid object. Three years later, in 1984, Stereolithography (SLA) and the ‘.STL’ file format were invented and patented by Charles Hull [120]. In 1986 Carl Deckard patented Selective Laser Sintering (SLS) [121], and in 1989, Scott Crump invented Fusion Deposition Modelling (FDM) [122].

In the 30 years following the invention of the principal three-dimensional printing methods, these fabrication techniques were gradually improved. It became possible to fabricate objects with complex shapes and various materials. Today the list of three-dimensional printable parts includes human tissue, food, clothes, musical instruments, replacement parts for electronic appliances, entire houses, and machines that can three-dimensionally print other similar machines [123–130]. While some of these applications require expensive machines, a market has developed for cheaper desktop three-dimensional printers that have become popular for rapid prototyping in Universities, Fab Labs, maker spaces, and sometimes for home use [131–133].

Three-Dimensional Printing in Acoustics

The field of acoustics could greatly benefit from the advances of three-dimensional printing technology. The use of additive manufacturing in the fabrication of musical instruments has already produced examples of three-dimensional printed violins made of plastic, flutes, ukuleles, and other small instruments [129, 134–136]. For now, these early examples have mostly produced cheap musical instruments made in plastic that do not compete with traditionally hand-crafted instruments produced using wood and traditional materials. As these techniques advance and more materials can be used, it might become possible to quickly produce good quality musical instruments and to witness new inventions in the music technology field. Rapid and reliable fabrication of three-dimensional printed transducers is also desirable and has been investigated in research publications [47, 137]. Acoustic metamaterials could greatly benefit from using three-dimensional printers, as suggested by Cummer et al. [40]. The study of acoustic metamaterials has seen the publication of many models, but in comparison, few laboratories have produced samples, and even fewer have realised fully-functional products. The lack of experimental research might be due to the difficulty of fabricating several identical unit cells. Membranes and thin plates are usually stretched by hand on supports and might result in units having different resonance frequencies. Thus, the research presented in this dissertation aims to present new examples of acoustic metamaterials and methods to rapidly prototype these unit cells using additive manufacturing technology.

Three-dimensional Printing Techniques

The main three-dimensional printing techniques are briefly presented in the following paragraphs, with particular attention to stereolithography - which is the principal technique used in this research.

Stereolithography

A stereolithography apparatus (SLA) is a three-dimensional printer that uses a light source to cure a liquid photopolymer into hardened plastic, layer by layer, following a specified geometry [138]. Resins usually consist of one or more monomer materials, a photoinitiator, and an absorber, used to control

3.1. Three-Dimensional Printing

light's penetration depth. The penetration depth can be predicted by Beer's law [139], that relates the quantity of light absorbed by a material to its thickness. As described in [139] it is possible to describe the critical dose at which polymerisation of the resin travels at a distance through the material sufficient to result in a solid material. The critical dose necessary to reach a certain depth in the material depends on time. Therefore, once the material properties are known, it is possible to predict the exposure time necessary to reach the desired polymerisation depth. A step by step process of this three-dimensional printing technique is illustrated in Fig. 3.1 and explained below:

- i. Design a three-dimensional object in a CAD program and save it as STL format. Common CAD software offers basic shapes and helpful tools to develop a design quickly. Some advanced software allows to automatically obtain a drawing from an imported photo.
- ii. Send the STL file to the printer software (most printers offer proprietary software) to slice the design in layers along the z-axis. The specifications of the printer determine the minimum layer. Today, most printers can achieve a 10 μm -100 μm layer, while cheaper printers might offer a thicker minimum layer of 0.4 mm.
- iii. Choose the liquid polymer (also referred to as resin) and pour it into the resin tank. While most printers only allow using proprietary materials, in some cases, it is possible to customise the resin by mixing it directly in the laboratory using off-the-shelf chemicals.
- iv. Start the printer. Today, most SLA printers use an upside-down printing process, starting with the last layer of the CAD file and ending the print with the first layer.
- v. A laser or projector will focus the UV light at a specific wavelength on the resin through the transparent film at the bottom of the tank and trace the first layer's geometry.
- vi. Thanks to the polymerisation process, molecular chains of monomers will join together, harden into plastic, and attach to the build platform.

3.1. Three-Dimensional Printing

- vii. The build platform will then move upwards of one step to allow the second layer to be printed. This process will continue until the last layer has been fabricated. In order to obtain an object made of multiple materials, some printers allow the user to pause this process and substitute the tank with a different material. Some supports might also be printed around and inside the object to keep it in place and maintain a correct calibration.
- viii. The three-dimensional printed object is then manually detached. The post-processing involves eliminating the supports and cleaning the printed object from the viscous fluids that might remain attached to the object using isopropyl alcohol (IPA) or machines such as ultrasonic cleaners.

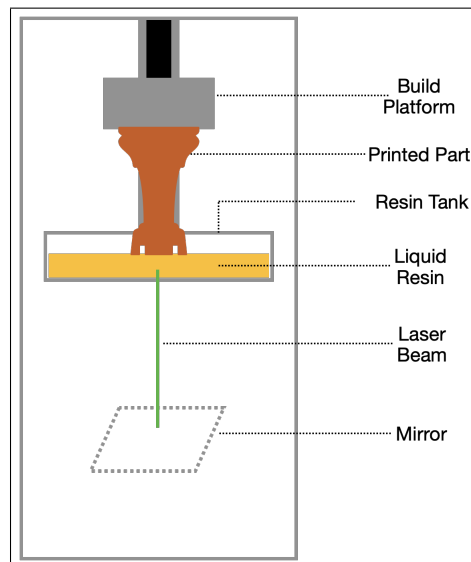


Figure 3.1: Illustration of SLA three-dimensional printer.

Fusion Deposition Modelling

Fusion Deposition Modelling (FDM) is a three-dimensional printing technique based on the extrusion of heated material Fig. 3.2. A wire of polymer is heated and extruded through a nozzle and deposited to the build platform. When deposited, the extruded material cools down and hardens into a solid object. FDM works layer by layer, moving the nozzle upwards at each step of the process. Usually, the minimum layer is thicker than SLA; its lower resolution and average

3.1. Three-Dimensional Printing

lower price make FDM printing an excellent investment for Fab Labs, maker spaces, rapid prototyping in universities and industries.

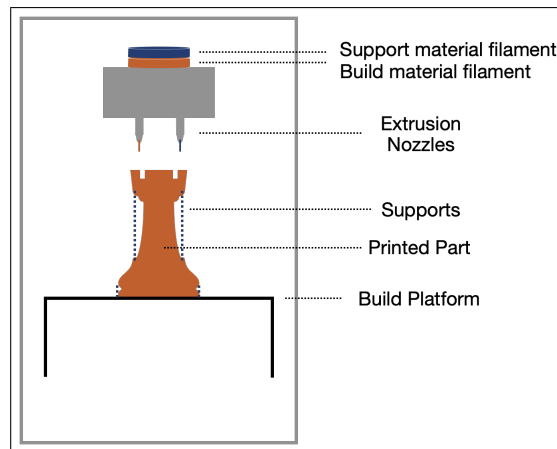


Figure 3.2: Illustration of FDM three-dimensional printer.

Selective Laser Sintering

Similarly to SLA, Selective Laser Sintering (SLS) directs a light source through the tank which contains powder. The powder will melt according to the specified geometry and solidify to form an object.

Digital Light Processing

Digital Light Processing (DLP) printers are based on a mechanism very similar to SLA. The resin is poured into a tank with a transparent bottom, and the part is printed layer by layer and upside-down. While SLA projects the laser point-by-point onto the resin, DLP uses a digital projector screen to cure all the points in a layer simultaneously.

Inkjet Printing

Like FDM, three-dimensional inkjet printing uses a nozzle to extrude material, layer by layer, on a build platform. While FDM extrudes hot material that cools and hardens once released, inkjet printing extrudes liquid polymers cured through exposure to a light source, similarly to SLA.

Development of Customised Stereolithography Technique

In this dissertation, acoustic metamaterials have been fabricated using SLA printing. The printer chosen for fabrication is Asiga Pico Plus 27 (Sydney, Australia) with a pixel image resolution of 27 by 27 μm , a minimum build layer thickness of 1 μm , and a build area of 20.58 mm \times 32.86 mm \times 76 mm. The advantages of this printer are the possibility of using non proprietary materials during the fabrication process and its resolution, originally intended for small-scale fabrication such as dentistry or jewellery and applicable to small-scale acoustic metamaterials. The main idea developed here in order to customise the printing process consisted in mixing polymers with other materials using off-the-shelf chemicals, instead of purchasing resins ready to be used. In particular, the base polymer was chosen paying attention to the material properties, such as Young's modulus and density. Table 3.1 shows the values of Young's modulus, density and Poisson's ratio that were estimated before the printing process began, and used to determine which polymer to use based on the desired application. For example, if one were to print thin plates, then a lower Young's modulus would result in a lower resonance frequency. During the printing process, the physical properties of materials change, hence some characterisation processes were developed and are reported in the next sections.

Table 3.1: Material properties of materials used in this thesis, estimated before printing from vendors specifications and preliminary tests.

Material	Density	Young's Modulus	Poisson's Ratio
PEGDA 250	1.11 g/mL	250 MPa	0.35 – 0.4
PEGDA 700	2 g/mL	10 MPa	0.35 – 0.4
PMMA	1.11 g/mL	1800 – 3100 MPa	0.35 – 0.4
BEMA	1.09 g/ML	12 MPa	0.35 – 0.4

After choosing the base polymer, the photo-initiator I819 is added to initiate the photo-polymerisation reactions. Photo-initiators are compounds that, when exposed to UV light, generate free radicals. These free radicals then react with monomers, such as PEGDA, and initiate polymer chain growth.

3.1. Three-Dimensional Printing

It is worth noting that, even if in the Asiga Pico Plus 27 software it is possible to select a layer 1 μm thick, when printing on a void the resin will keep expanding and produce a layer 100 μm thick. This phenomenon is predicted by Beer's law and modelled by [139] as explained in the sections above. To avoid this behaviour and to finely control the thickness of membranes and thin plates that are usually printed on hollow cylinders, the absorber Sudan I was added to the mix. Fig. 3.3 illustrates the difference between printing on a void with and without the use of absorbers.

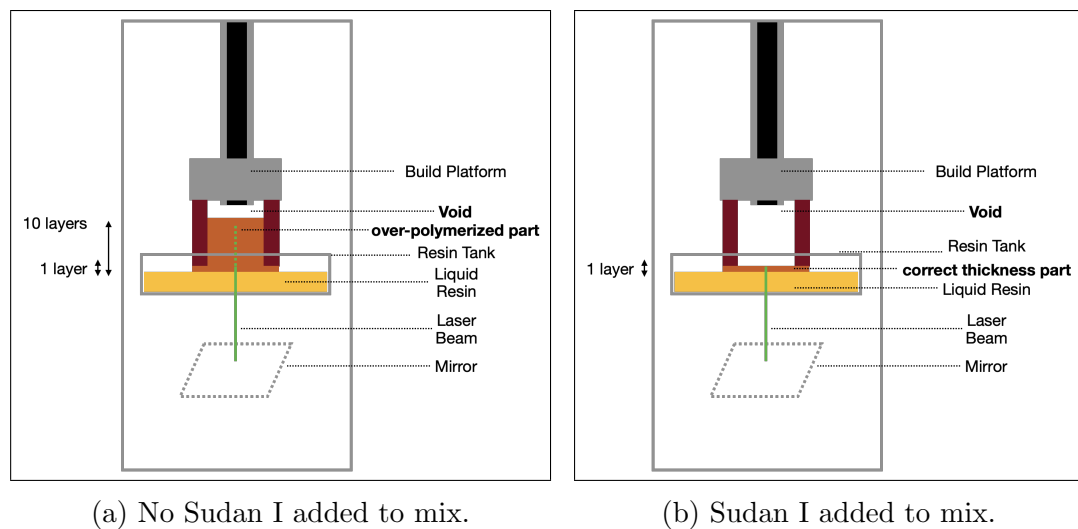


Figure 3.3: Illustration of the effect of adding Sudan I to the mix. Panel (a) shows an over-polymerisation when printing onto a void: a single layer expands to 10 layers, resulting in a thick membrane. Panel (b) shows how Sudan I absorbs the light and controls the exposure, resulting in a membrane of correct thickness.

Optionally, other chemicals can be added to the mix. For example, Barium Titanate (BaTiO_3) was used to scatter the light more uniformly along the horizontal plane and was also chosen for its piezoelectric properties, useful for active metamaterials applications. If printing a multi-material sample, where for example a structure such a cylinder is printed with one material and the membrane stretching above it is printed with a different material, it is possible to pause the printer, clean the sample without detaching it from the build platform, change the resin tank, and start the printer again. To combine all the chemicals and obtain a uniform resin, they were first mixed using Thinky ARE 250 planetary

3.1. Three-Dimensional Printing

mixer (INTERTRONICS) and then sonicated for 15 minutes. Finally, the post-processing step consisted of cleaning the part with isopropyl alcohol (IPA) within an ultrasonic cleaner or applied directly to the part if too fragile. A general scheme of the customised SLA three-dimensional printing process is reported in Fig. 3.4 below. This scheme was adapted to each application, and details for each experiment will be described in the corresponding chapters.

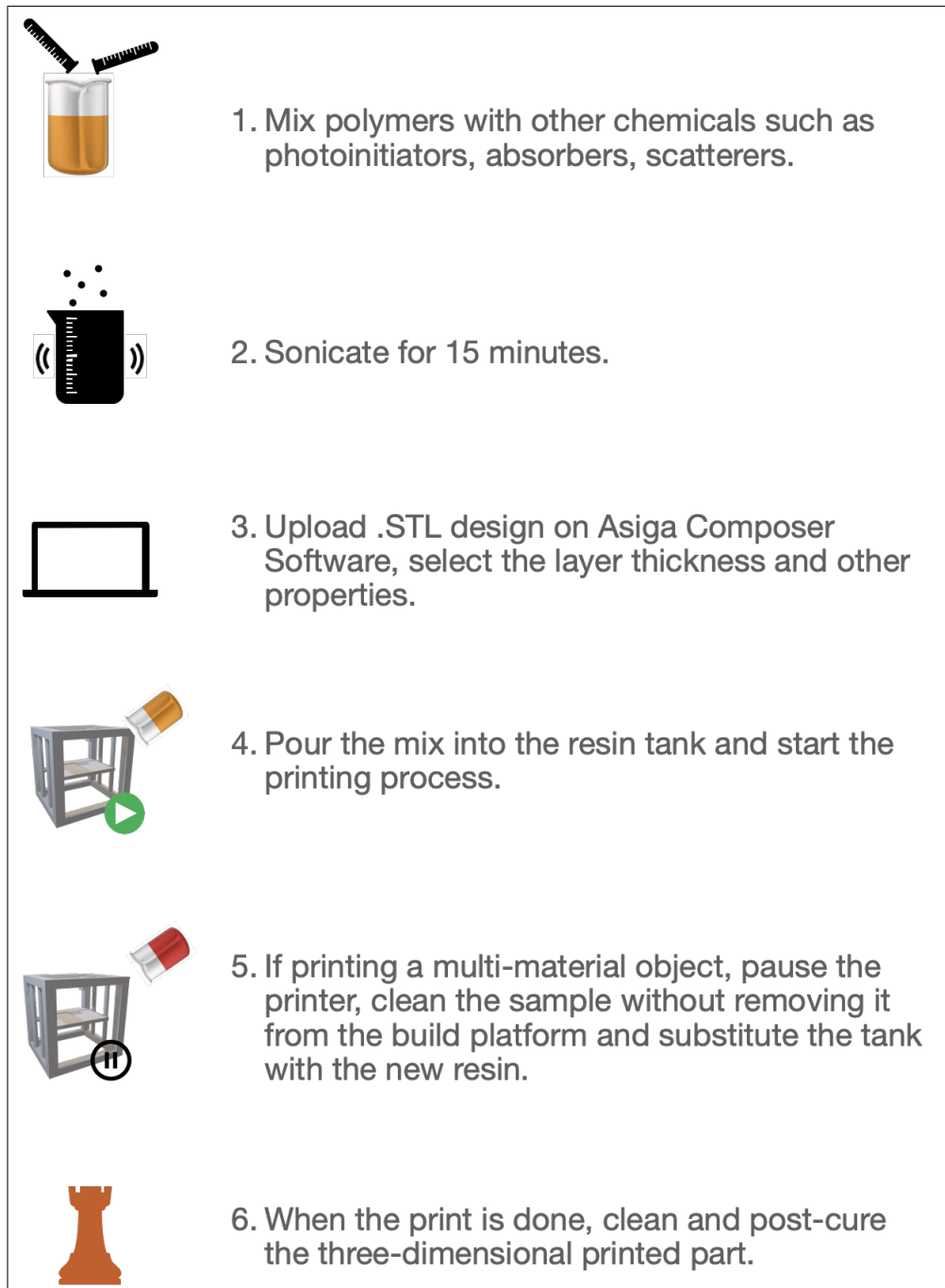


Figure 3.4: Step by step illustration of customized three-dimensional printing process.

3.2 Acoustic Booth Measurements

The experiments described in Chapter 4 and Chapter 6 have been conducted inside an acoustic booth, using a setup which can be classified as free-field measurement. Free-field measurements are defined as measurements conducted inside anechoic chambers, where all the reflections from surfaces have been eliminated. This type of measurement is different from a diffuse field measurement, where walls are highly reflective and positioned at oblique angles. In diffuse-fields experiments, the sound does not appear to have a single source; conversely, free-field measurements are ideal when it is crucial to consider the source and receiver location. Fig. 3.5 shows the typical setup used throughout this dissertation in experiments that evaluated the noise attenuation performance of acoustic metamaterials.

Data Acquisition and Post-Processing Software

A MATLAB (Natick, Massachusetts, USA) code was written to trigger the National Instruments (NI) Data Acquisition System and post-processes data. The code uses proprietary NI libraries to trigger both the function generator and loudspeaker, and at the same time to record through the microphone and pre-amplifier. In this type of setup, the sound field is measured first with and then without the sample to obtain the noise attenuation performance of acoustic metamaterials. Since the acoustic booth provides partial isolation from external noise, the measurements are repeated multiple times and averaged to eliminate sudden changes in the sound field. Final results are plotted on logarithmic scale, to present and analyse information using an appropriate scale that reflects human hearing perception characteristics.

Data Acquisition Hardware

A National Instruments (Austin, Texas, U.S.) Data Acquisition System (DAQ) was used to communicate with the microphone. This system was required in order to trigger data acquisition and it is preferred to a standard sound card, as it provides input/output synchronisation, lower noise floor, and high sampling rate.

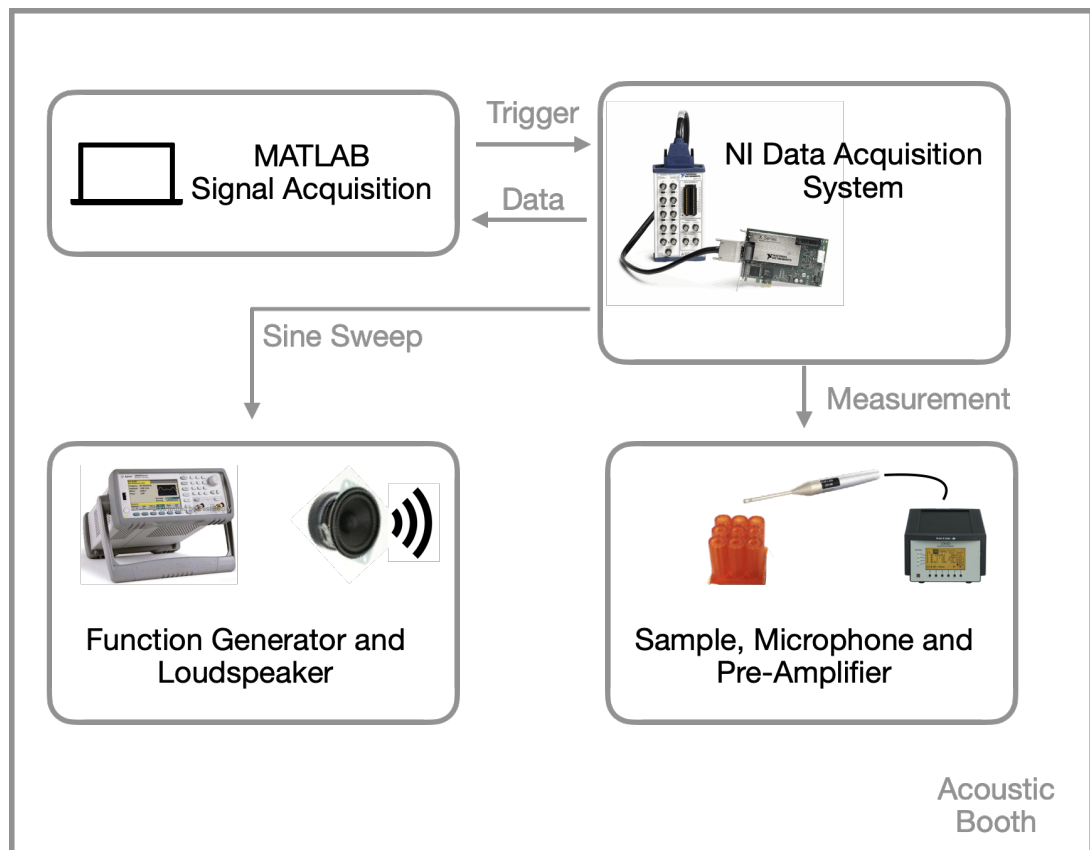


Figure 3.5: Experimental setup: a loudspeaker connected to a function generator emits a swept sine wave that impinges on the three-dimensional printed sample. A microphone, connected to a pre-amplifier and positioned right above the metamaterials, records the signal controlled by a data acquisition device and triggered by a software running on a laptop.

Loudspeaker and Function Generator

A periodic chirp extending along the human frequency range (20 Hz - 20 kHz) is a standard way to measure the performance of an acoustic system [140]. The chirp used in this dissertation was generated by a function generator (Keysight Technologies, Santa Rosa CA, USA) and emitted by a $8\ \Omega$, 2" loudspeaker (Visaton, Haan, Germany).

Microphone and Pre-Amplifier

To measure sound pressure, a Bruel & Kjaer (B&K, Nærum, Denmark) 1/8" pressure-field microphone connected to a pre-amplifier (B&K Nexus Microphone Conditioner) was positioned above the metamaterials. The same setup was used to measure the sound field in the absence of acoustic metamaterials. Because of its small size with comparison to wavelength of frequencies used in this dissertation, this microphone could be positioned as shown in Fig. 3.5 without any change in response between waves incident on the front or on the side of the microphone head.

Oscilloscope

Although the setup illustrated in Fig. 3.5 was preferred to allow a better control of parameters and a quick conversion of data for post-processing, an oscilloscope was also used in some experiments described in chapter 6. An oscilloscope is an electronic test device that displays the variation of signal voltages over time. It allows one to easily trigger function generator and measurement system and to observe the time domain and frequency domain response in real-time.

3.3 Laser Doppler Vibrometer Measurements

A Laser Doppler Vibrometer (LDV) uses the Doppler Effect to measure vibrations of an object under test. The Doppler Effect describes the change in frequency of a wave, measured by a receiver that is moving with respect to the position of the source. In a LDV measurement, a laser beam is pointed towards an object that is set into vibration. The measured Doppler shift allows one to retrieve the velocity,

3.3. Laser Doppler Vibrometer Measurements

displacement, phase and frequency of vibration of the object. Principles of wave superpositions are used to analyse the signal received by the photodetector and to retrieve displacement and velocity of the sample, its resonance modes and phase changes. Fig. 3.6 illustrates the working principle of a LDV.

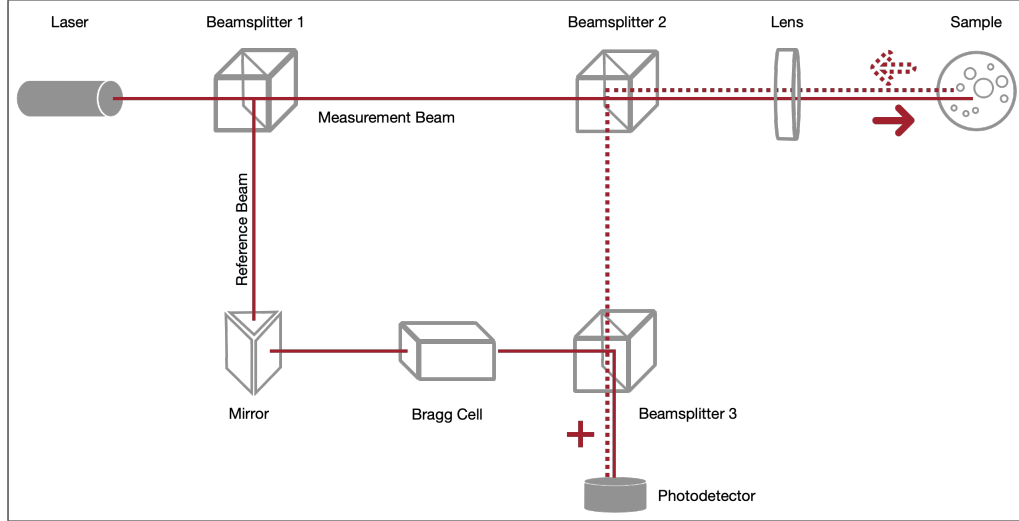


Figure 3.6: Illustration of Laser Doppler Vibrometer working principle, informed by <http://www.polytec.com/us/company/technologies/>.

Firstly, the laser beam with a frequency $f_{reference} = f_0$ is split by a beamsplitter into reference beam and test beam. The reference beam is directed by a mirror through a Bragg cell towards the photodetector. The test beam is focused towards the sample under test using an adjustable lens. While the sample vibrates, the reflected beam having a frequency $f_{test} = f_0 + \delta f$ is redirected through a beam splitter where it is added to the reference beam and reaches the photodetector. Therefore, the Doppler-shifted signal s_d captured by the photodetector would be:

$$\begin{aligned}
 s_d &= \sin(f_0) + \sin(f_0 + \delta f) \\
 &\approx \sin\left(\frac{2f_0 + \delta f}{2}\right) \sin\left(\frac{\delta f}{2}\right).
 \end{aligned} \tag{3.1}$$

Since the initial frequency of the reference signal emitted by the laser is very high, the Bragg cell acts as modulator and adds a frequency shift f_1 to the test signal.

3.3. Laser Doppler Vibrometer Measurements

Therefore, the test signal s_t measured at the photodetector is:

$$\begin{aligned} s_t &= \sin(f_0 + \delta f) + \sin(f_0 + f_1) \\ &\approx \sin\left(\frac{2f_0 + f_1 + \delta f}{2}\right) \sin\left(\frac{f_1 + \delta f}{2}\right). \end{aligned} \quad (3.2)$$

The 'beat' frequency $f_1 + \delta f$ is in a range that can be measured by the photodetector. This method is called heterodyne.

Fig. 3.7 shows the typical setup used in Chapter 5 and 6 of this dissertation. A loudspeaker emits a sound wave that causes the sample under test to vibrate, while the Polytec three-dimensional Laser Doppler Vibrometer measures the Doppler shift caused by the sample vibration. A reference microphone is also used to measure the sound level near the sample. The Polytec PSV-300-F used during this research offers 1D, 2D or 3D modes; when measuring membranes and plates displacements in Chapter 5 and 6, the 2D mode is preferred. Polytec software is also used to trigger the loudspeaker, select the type of sine sweep and post-process data, to analyse frequencies of vibration, obtain animations of the modes of vibration and phase shifts.

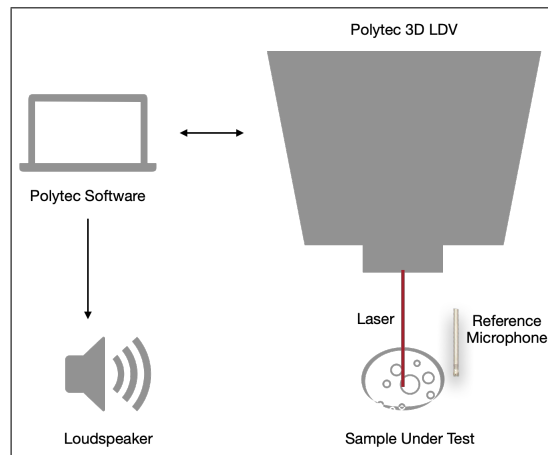


Figure 3.7: Schematic of setup used to measure objects vibration using a Polytec Laser Doppler Vibrometer.

3.4 Impedance Tube Measurements

An impedance tube, also known as a standing wave apparatus or standing wave tube, is a device commonly used to measure the sound absorbing properties of acoustic materials. A standing wave tube with two microphones allows one to obtain absorption and reflection coefficients and normally incident acoustic impedance. With four microphones, it is possible to also obtain transmission coefficients. An illustration of a typical four microphone standing wave tube is presented in Fig. 3.8. A loudspeaker is inserted at one end of the tube and continuously produces a swept sine wave. The sound pressure from the loudspeaker travels through the tube towards the material sample, positioned in the middle of the tube, where it is partly reflected, absorbed and transmitted. The forward acoustic waves transmitted by the loudspeaker and the reverse acoustic waves reflected by the material under test combine to form a standing wave. When the sample material completely reflects the incident sound wave, forward and reverse wave will have the same amplitude; antinodes will have twice the initial pressure and nodes will have zero pressure. When the sample material absorbs or transmits the incident sound wave, the microphones positioned alongside the tube will measure the amplitude values of nodes and antinodes. The standing wave ratio, defined as the ratio between pressure at antinode and node, determines absorption, reflection, transmission coefficients and impedance of material sample. The impedance tube used in Chapter 5 of this dissertation was fabricated by the Centre de Transfert de Technologie du Mans at the University of Le Mans, France. The work conducted using this impedance tube was completed at the Laboratoire d'Acoustique of the University of Le Mans (France) during a Short Term Scientific Mission founded by the DENORMS COST Action 15125, with the help of Dr. Vicente Romero García and Dr. Jean-Philippe Groby. Details on how to obtain the coefficients are reported in Section 3.5.

3.5 Transfer Matrix Modelling Method

The transfer matrix method can be used to model the propagation of acoustic waves travelling inside an impedance tube containing the material under test and to retrieve the acoustic properties of the material. Fig. 3.8 illustrates the

3.5. Transfer Matrix Modelling Method

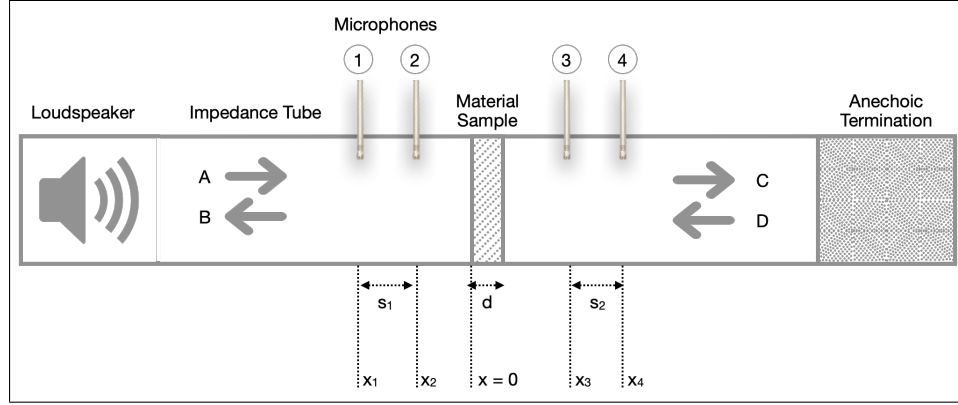


Figure 3.8: Sketch of a four-microphone impedance tube and sample, used for transfer matrix method modelling as proposed by Song and Bolton [16, 17].

impedance tube modelled below, as proposed by Song and Bolton [16, 17]. A loudspeaker placed at one end of the impedance tube generates a plane wave measured by microphones at positions x_1 , x_2 , x_3 and x_4 , with pressure P_1 , P_2 , P_3 and P_4 :

$$P_1 = (Ae^{-jkx_1} + Be^{jkx_1})e^{j\omega t}, \quad (3.3a)$$

$$P_2 = (Ae^{-jkx_2} + Be^{jkx_2})e^{j\omega t}, \quad (3.3b)$$

$$P_3 = (Ce^{-jkx_3} + De^{jkx_3})e^{j\omega t}, \quad (3.3c)$$

$$P_4 = (Ce^{-jkx_4} + De^{jkx_4})e^{j\omega t}. \quad (3.3d)$$

In Eq. (3.4a) k is the wave number in air, A and C are the complex amplitudes of the forward wave in the first and second section of the tube, while B and D are the complex amplitudes of backward waves in the first and second section of the tube. The plane wave is represented using a $e^{+j\omega t}$ convention. It is possible

3.5. Transfer Matrix Modelling Method

to rewrite Eq. (3.4a) in terms of the coefficients A, B, C, D:

$$A = \frac{j(P_1 e^{jkx_2} - P_2 e^{jkx_1})}{2 \sin k(x_1 - x_2)}, \quad (3.4a)$$

$$B = \frac{j(P_2 e^{-jkx_1} - P_1 e^{-jkx_2})}{2 \sin k(x_1 - x_2)}, \quad (3.4b)$$

$$C = \frac{j(P_3 e^{jkx_4} - P_4 e^{jkx_3})}{2 \sin k(x_3 - x_4)}, \quad (3.4c)$$

$$D = \frac{j(P_4 e^{-jkx_3} - P_3 e^{-jkx_4})}{2 \sin k(x_3 - x_4)}. \quad (3.4d)$$

The transfer matrix method is used to relate the pressure P_0 and particle velocity V_0 at the incident end of the material sample and the pressure P_d and particle velocity V_d at the transmission end:

$$\begin{bmatrix} P \\ V \end{bmatrix}_{x=0} = \begin{bmatrix} T_{11} & T_{12} \\ T_{21} & T_{22} \end{bmatrix} \begin{bmatrix} P \\ V \end{bmatrix}_{x=d}. \quad (3.5)$$

By rewriting Eq. (3.5) in terms of the plane acoustic waves, we obtain:

$$P_0 = A + B, \quad (3.6a)$$

$$V_0 = \frac{(A - B)}{\rho_0 c}, \quad (3.6b)$$

$$P_d = C e^{-jkd} + D e^{jkd}, \quad (3.6c)$$

$$V_d = \frac{C e^{-jkd} - D e^{jkd}}{\rho_0 c}, \quad (3.6d)$$

where ρ_0 represents air density and c is the speed of sound in air. After obtaining ρ and c based on ambient temperature and humidity, pressures P_1 , P_2 , P_3 , P_4 through microphones measurements, it is possible to retrieve the coefficients A, B, C, D from Eq. (3.4a) and thus to obtain P_0 , P_d , V_0 and V_d from Eq. (3.6). Assuming reciprocity and symmetry, the following conditions are set in order to

3.5. Transfer Matrix Modelling Method

simplify Eq. (3.5) and obtain only two unknown for two equations:

$$T_{11} = T_{22}, \quad (3.7a)$$

$$T_{11}T_{22} - T_{12}T_{21} = 1. \quad (3.7b)$$

It is then possible to obtain the transfer matrix elements in terms of pressure and particle velocity:

$$T_{11} = \frac{P_d V_d + P_0 V_0}{P_0 V_d + P_d V_0}, \quad (3.8a)$$

$$T_{12} = \frac{P_0^2 - P_d^2}{P_0 V_d + P_d V_0}, \quad (3.8b)$$

$$T_{21} = \frac{V_0^2 - V_d^2}{P_0 V_d + P_d V_0}, \quad (3.8c)$$

$$T_{22} = \frac{P_d V_d + P_0 V_0}{P_0 V_d + P_d V_0}. \quad (3.8d)$$

If the incident plane wave has unit amplitude, Eq. (3.6) reduce to:

$$P_0 = 1 + R, \quad (3.9a)$$

$$V_0 = \frac{(1 - R)}{\rho_0 c}, \quad (3.9b)$$

$$P_d = T e^{-jkd}, \quad (3.9c)$$

$$V_d = \frac{T e^{-jkd}}{\rho_0 c}, \quad (3.9d)$$

where $R = B/A$ is the reflection coefficient and $T = C/A$ is the transmission coefficient. By substituting Eq. (3.9) into Eq. (3.8) we obtain transmission (T), reflection (R), and absorption (α) coefficients of a sample inserted in an impedance tube with anechoic termination:

$$T = \frac{2e^{jkd}}{T_{11} + (T_{12}/\rho_0c) + \rho_0cT_{21} + T_{22}}, \quad (3.10a)$$

$$R = \frac{T_{11} + (T_{12}/\rho_0c) - \rho_0cT_{21} - T_{22}}{T_{11} + (T_{12}/\rho_0c) + \rho_0cT_{21} + T_{22}}, \quad (3.10b)$$

$$\alpha = 1 - |T|^2 - |R|^2. \quad (3.10c)$$

The method described above allows one to retrieve transmission and reflection coefficients of any sample by measuring pressure at four points in the impedance tube as illustrated in Fig. 3.8. To obtain the characteristic impedance of the sample under test, it is necessary to know or analytically model the transfer matrix of that sample and to solve for the characteristic impedance. For example, the transfer matrix of a homogeneous, isotropic porous material of thickness d is [17]:

$$\begin{bmatrix} T_{11} & T_{12} \\ T_{21} & T_{22} \end{bmatrix} = \begin{bmatrix} \cos k_p d & j\rho_p c_p \sin k_p d \\ j \sin k_p d / \rho_p c_p & \cos k_p d \end{bmatrix}. \quad (3.11)$$

The wave number k_p is retrieved as:

$$k_p = \frac{1}{d} \sin^{-1} 1 \sqrt{-T_{12}T_{21}}, \quad (3.12)$$

and the characteristic impedance Z_p is:

$$Z_p = \rho_p c_p = \sqrt{\frac{T_{12}}{T_{21}}}. \quad (3.13)$$

In general, the method to retrieve material parameters, as for example reported in Chapter 5, is as follows:

- i. measure the material sample in the impedance tube,
- ii. obtain the transfer matrix,
- iii. calculate the reflection, transmission and absorption coefficients,
- iv. model the transfer matrix analytically,

- v. compare the coefficients obtained with impedance tube to those obtained through a model,
- vi. change the material parameters in the model until reflection, transmission and absorption coefficients overlap in model and measurements.

3.6 Finite Element Modelling Method

When studying the acoustic behaviour of systems based on simple geometrical objects - like circles and rectangles - or of well known acoustic systems - such as musical instruments, pipes, and Helmholtz resonators - it is common to rely on mathematical and analytical models, as in the case of the transfer matrix described in the previous section. The analytical approach models the physics of the acoustic systems under test and obtains the equation of motion of such an object, relating Newton's laws of motions to conservation of energy laws, thermodynamics, and other physics laws that describe it. However, analytical models and resulting differential equations can become very hard to solve or rely on simplified assumptions when the system under test is characterised by a complex geometry, different boundary conditions, or multiple materials. An alternative to analytic models is represented by Finite Element Modelling (FEM). FEM methods use meshes to subdivide complex geometries into simple shapes, such as triangular, quadrilateral, or tetrahedral elements. The nodes at the intersection between meshes or elements vertices are assigned a number of degrees of freedom, depending on the specific application or physics domain's parameters. Next, a set of differential equations are formed and solved at each node. Software packages like COMSOL Multiphysics, used for research throughout this dissertation, conveniently allow the user to create or import a CAD design, choose one or multiple domains (such as acoustics, structural mechanics, heat transfer, optics), set material parameters and boundary conditions either manually or by selecting predefined models and materials. The user can then select a mesh and a type of analysis, and results can be analysed through COMSOL or exported for analysis with a different package. The choice of mesh resolution determines the computation power and accuracy of results; hence careful trade-off considerations need to be addressed when using FEM methods. An example of acoustic

metamaterial model using COMSOL is reported below.

Modelling impedance tube and Helmholtz resonators with COMSOL Multiphysics

A typical unit cell used for acoustic metamaterials is the Helmholtz resonator. This paragraph gives an example of how to model several Helmholtz resonators placed into an impedance tube. A similar method can be followed if modelling the resonators in the free-field, as done in Chapter 4.

- i. The first step when opening COMSOL Multiphysics is to select the 'Model Wizard' icon, that allows to load pre-defined models. The selected geometry in this example is a three-dimensional geometry. The physics domain is the Pressure Acoustics, Frequency Domain. If modelling also the walls of Helmholtz resonators, the module Acoustic-Solid Interaction should be selected instead. The frequency domain study allows to evaluate the response of metamaterials in the frequency domain, and to find the frequencies at which Helmholtz resonator attenuate incoming sound waves.
- ii. Firstly, the geometry of the model is imported or built directly in COMSOL. A solid cylinder is selected to model the waveguide part of impedance tube. To build Helmholtz resonators, two cylinders are joined to form the neck and cavity. Microphones are modelled as four points inside the tube. Fig. 3.10 shows the geometry including waveguide, microphones and three Helmholtz resonators.
- iii. Materials are then assigned to tube and air. In the case of a Helmholtz resonator embedded in a tube, it is usually sufficient to assign the material properties of air to the fluid domain. The tube material will just act as a rigid wall. It is also possible to assign a specific material to the tube walls. For example, in case the resonator material is PEGDA or PMMA, modelling the material properties can help to determine the minimum thickness needed to avoid coupling between the vibration modes of walls and volume of air inside the mass and cavity. Typical properties of air

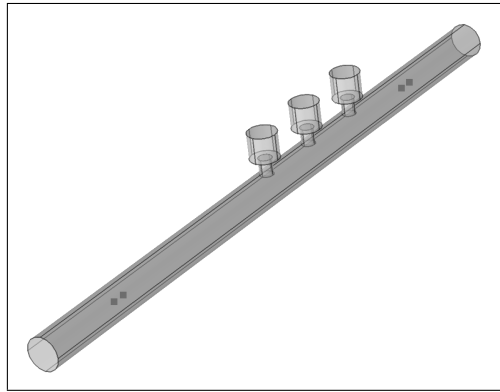


Figure 3.9: Geometry of Helmholtz resonators and impedance tube built with COMSOL Multiphysics.

are available in COMSOL material properties and can be adjusted if room temperature and humidity are different from typical values.

- iv. In this case, all the domains - tube, neck and cavity - are assigned to the Pressure Acoustics module. Neck and cavity can be also assigned to the 'Narrow region acoustics' option within the acoustics module to account for viscothermal losses.
- v. A plane wave radiation should be selected as the incident acoustic pressure wave, and the two extremities of the impedance tube should be the input and output locations of the wave.
- vi. A mesh can be selected from the list. For this simple model, a free tetrahedral mesh is a good choice.
- vii. A parametric sweep is then used to study the system response. The frequency range is selected to be between 40 Hz and 2000 Hz with a step size of 10 Hz.
- viii. By exporting the pressure at microphones to a different software, in this case MATLAB, it is possible to plot the reflection, transmission and absorption coefficients as shown in Fig. 3.11. It is worth noting that at 700 Hz the reflection is at maximum and transmission at minimum.
- ix. It is also possible to analyse the results in COMSOL, for example by plotting

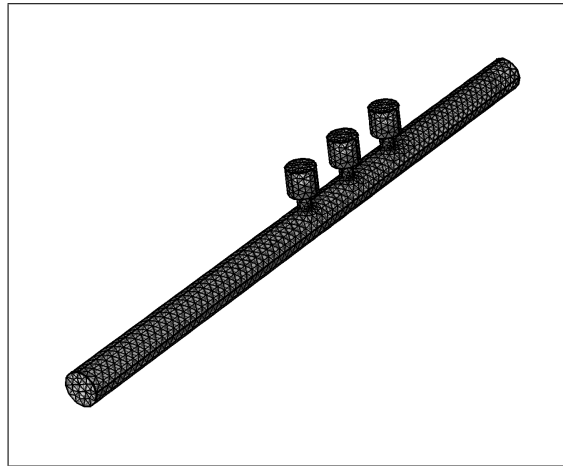


Figure 3.10: Free tetrahedral meshed geometry of Helmholtz resonators and impedance tube built with COMSOL Multiphysics.

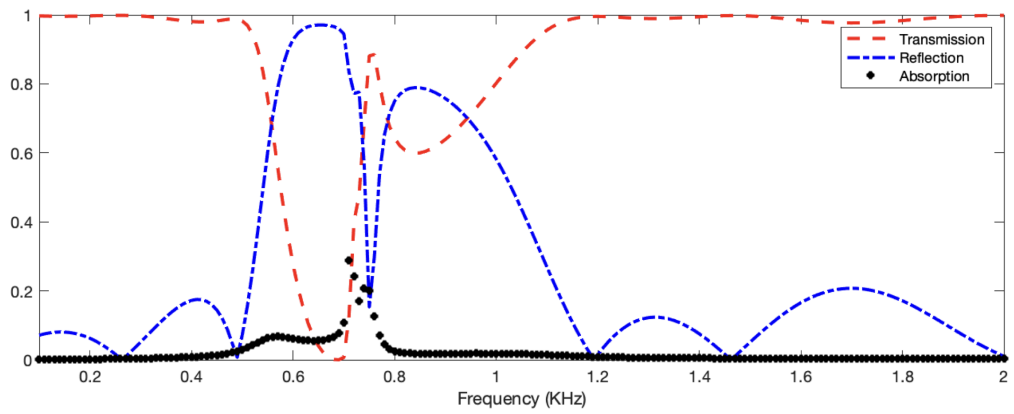


Figure 3.11: Transmission, reflection and absorption coefficients obtained by exporting acoustic pressure at microphones positions in COMSOL and plotted in MATLAB.

3.6. Finite Element Modelling Method

the sound pressure level at 700 Hz and 1500 Hz, to confirm the results shown in MATLAB.

These results can be compared with experimental results obtained in a real impedance tube. As done in the analytical transfer matrix model described in the previous section, if the two results differ, the parameters chosen to model the metamaterials can be iteratively fine tuned until measurements and model converge to the same results.

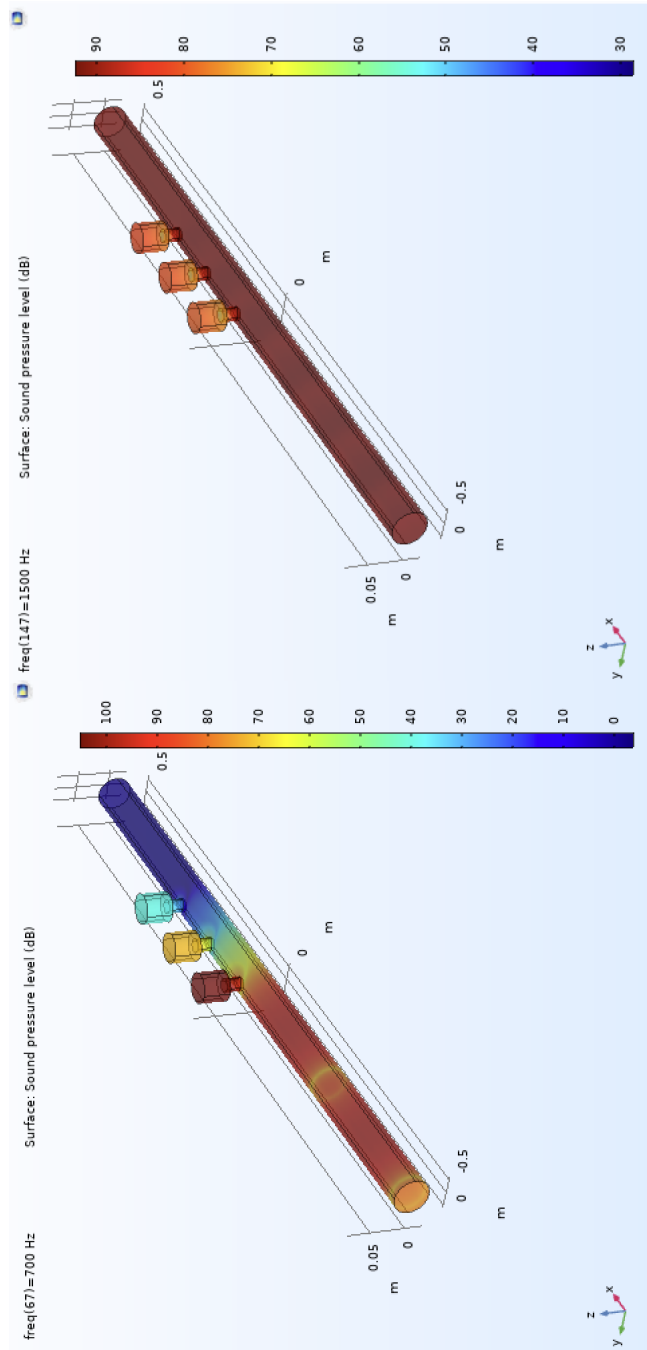


Figure 3.12: Sound Pressure Level at 700 Hz and 1500 Hz plotted in COMSOL Multiphysics.

Chapter 4

3D Printed Acoustic Metamaterials Based on Tunable Helmholtz Resonators

4.1 Introduction

This Chapter presents research and development of acoustic metamaterials based on three-dimensional printed small-scale Helmholtz resonators. This work started as a replication study of the research on soda cans conducted by Lemoult et al. [7]. Lemoult et al. utilised everyday objects shaped as Helmholtz resonators - namely soda cans - to create an array of periodically distributed unit-cells that in the bulk acted as acoustic metamaterials. As shown in Fig. 4.1 (a), they built a 7×7 array of identical soda cans having a resonance frequency at 420 Hz, hence a wavelength of 80 cm. The distance between the necks of soda cans was 6.6 cm, ensuring a deep subwavelength scale with respect to the resonance frequency. Fig. 4.1 (b) shows that they were able to measure a band gap in the frequency band above resonance, between 420 and 600 Hz. This band gap, exhibiting a negative effective modulus, was the result of resonant acoustic metamaterials, rather than Bragg scattering effect found in phononic crystals.

The first work presented in this Chapter replicates the study of Lemoult et al. and applies two changes: the samples are fabricated using a SLA three-

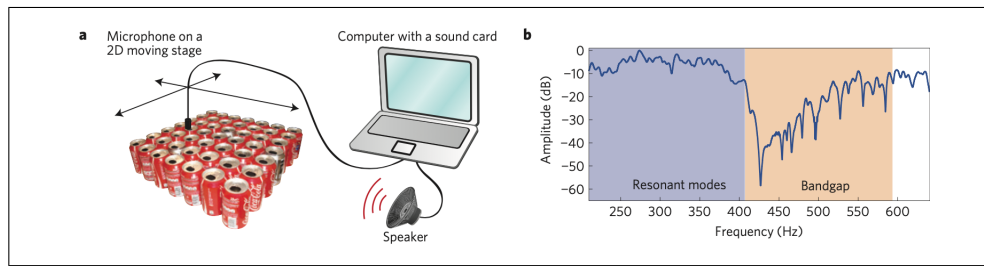


Figure 4.1: Setup and measurements of acoustic metamaterials based on soda cans by Lemoult et al. [7].

dimensional printing technique, and they are designed for small-scale applications. The reasons for these two changes derive from a question that has recently become important in the world of applied acoustic metamaterials. It has been phrased by Daraio [141] as follows: "Why are not there more metamaterials in our everyday life?". One answer to this question can be found in Cummer et al. [40], where it is stated that as fabrication techniques such as three-dimensional printing will become more popular and more accurate, it will become easier to move from the modelling and laboratory environment to a scalable product.

This replication study used a scaled-down version of soda cans dimensions and set as a primary application small-scale electroacoustic devices such as headphones, smart speakers, or hearing aids. Similar metamaterials dimensions can also be applied to panels for noise attenuation in buildings or the automotive and aerospace sectors. In general, attenuating noise in the audible frequency range (20 Hz to 20000 Hz) in the small-scale can be challenging, as the materials used for attenuation should be very dense or thick. Hence, setting small-scale products as a goal can help to define constraints. Once these constraints have been set, a parametric model can be built, and parameters such as materials and geometry can be optimised according to the specific application.

Many Universities have focused on modelling acoustic metamaterials, with few experimental works, usually relying on everyday objects for unit-cells. Furthermore, often the outcome of acoustic metamaterials models are unit-cells with complex shapes. For these reasons, one of the goals of this replication study was to develop accurate three-dimensional printing techniques that would

facilitate the process of shifting from a model to a real-world product and create a bridge between research and industrial fabrication. Another reason behind the problem of lack of metamaterials in our everyday lives can be found in how the design and modelling process is addressed. In many research works on metamaterials, models are created to find a new property or maximise one outcome - such as band gap width or depth - with little regard to the final application. Inverting this method, i.e., starting from the application and then optimising the parameters and outcomes, might be the key to accelerate the process of integrating more metamaterials in our everyday lives.

In the next sections, the primary methods used to design and fabricate the metamaterials presented in this Chapter will be reviewed, with appropriate references to the methods described in Chapter 3. The acoustic metamaterials based on Helmholtz resonators will then be modelled and measured. Data acquired through measurements will then be presented. Finally, a discussion of these results and future work related to this Chapter will be added in the last section.

4.2 Methods

This section describes the methods used to fabricate small-scale acoustic metamaterials based on Helmholtz resonators. Three versions of this type of metamaterials were fabricated and abbreviated as Helmholtz Resonators (HR) version 1, 2, and 3:

- i. HR1: a 3 x 3 array of Helmholtz resonators with the same dimensions of soda cans, scaled down by a factor of 20,
- ii. HR2: a 3 x 3 array of Helmholtz resonators with similar dimensions to point 1, but optimised to leverage the band gap produced by overtones,
- iii. HR3: a 3 x 3 array of Helmholtz resonators with the same dimensions as in point 1, and a thin plate on the cavity bottom.

Specifically, resonators in HR1 had the following dimensions: the neck of the resonator had an inner radius of 0.564 mm and a length of 0.5 mm, the cavity had an inner radius of 1.6 mm and a length of 5.8 mm. The thickness of the walls

was 0.5 mm. Resonators in HR2 had the following dimensions: a neck radius of 1 mm and a length of 0.5 mm, and a cavity with a radius of 1.6 mm and a length of 10.8 mm. The thickness of the walls was 0.5 mm. The resonators in HR3 had the same dimensions as those in HR1 and, instead of having a rigid base, they included a thin plate with a thickness of 170 μm . These dimensions were the results of analytic models. These models have been introduced in Chapter 3 and will be outlined in the next section. The samples used in this Chapter were fabricated with a Asiga (Sydney, Australia) Freeform Pico Plus SLA three-dimensional printer. To obtain the material used to fabricate the resonators in HR1 and HR2 we mixed the clear resin (Formlabs, Somerville, Massachusetts, U.S.) with 0.15% of Sudan I and 1% of Irgacure 819 (Sigma-Aldrich, St. Luis, Missouri, U.S.). The clear resin was chosen as monomer for its large Young's Modulus that allowed us to consider the walls of the resonators as rigid structures that do not influence their resonances. Autodesk Inventor 2018 was used to design the CAD model of the resonators. In HR3, PEGDA was used as monomer, since the clear resin used in HR1 and HR2 could not successfully allow the thin plate membrane to polymerise on top of the resonators' walls. CAD designs and pictures of HR1 are shown in Fig. 4.2.

The three finalised fluids were respectively PEGDA with 0.2% Sudan I and 1% of Irgacure 819, and BEMA (Sigma-Aldrich) with 0.125% Sudan I. To obtain the material for thin plates, various attempts were made in order to find a resin that could accurately produce a thin layer and at the same time could match the exposure time used to fabricate the resonators made with PEGDA. The Asiga three-dimensional printer did not allow to change the exposure time once the fabrication process is started, thus the same exposure time had to be used for the resonators material and the thin plate material. The final thickness depends on various factors: the amount of photo-initiator, absorber Sudan I and the duration of exposure time to light. Fig. 4.3 shows how different exposure times, between 1 s and 5 s, and fixed amount of Sudan I and Irgacure 819 produce various thicknesses. The three finalised fluids in Fig. 4.3 were respectively clear resin with 0.15% Sudan I, PEGDA with 0.2% Sudan I and BEMA with 0.125% Sudan I. An amount of 1% of Irgacure 819 was added to all the resins. BEMA with and exposure time of 5 s was chosen, as it could match the exposure time of PEGDA

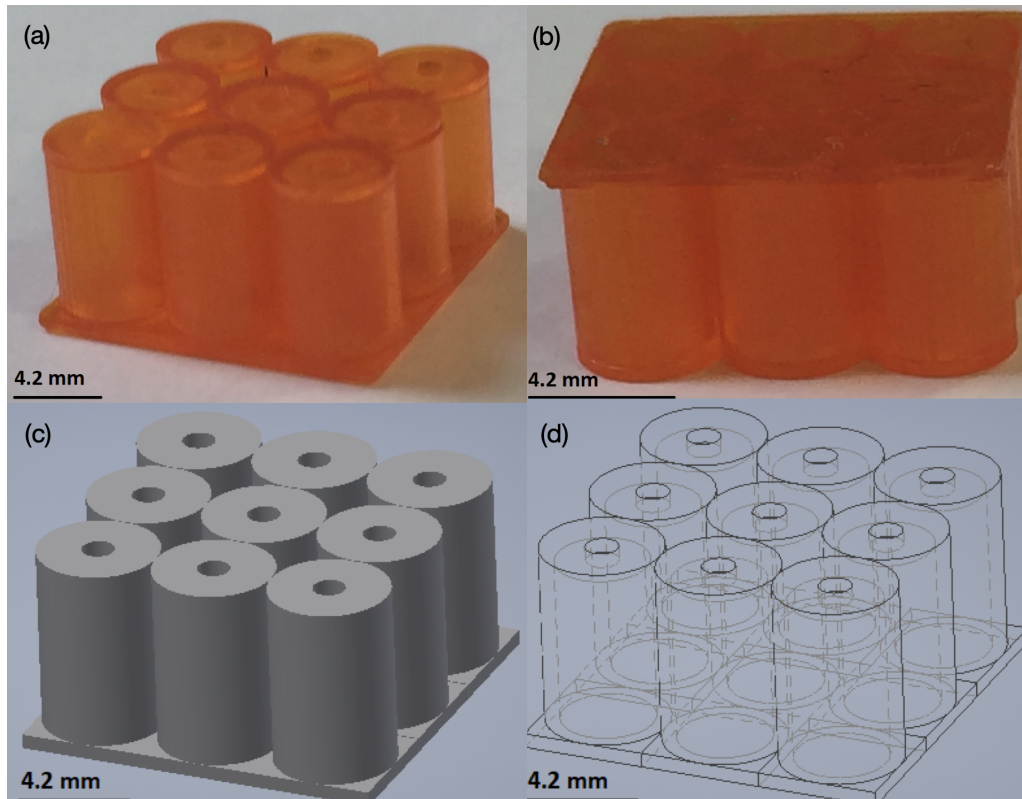


Figure 4.2: Front view (a) and bottom view (b) of the small-scale acoustic metamaterials based on a 3 X 3 array of Helmholtz resonators. Equivalent CAD model (c) and wireframe view (d).

and resulted in a thickness of $170\ \mu\text{m}$. Fig. 4.4 shows pictures and CAD designs of HR3.

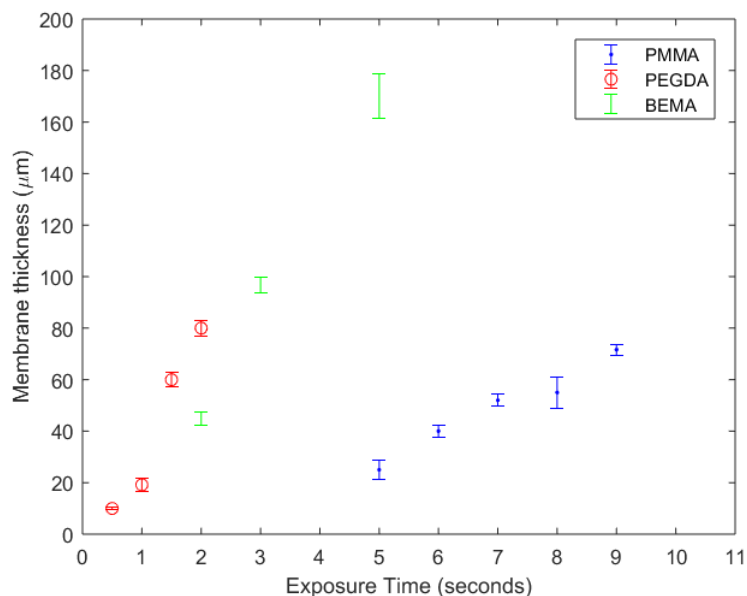


Figure 4.3: Thickness of the membranes against exposure time of UV light during the three-dimensional printing process. Longer exposure times will result in thicker membranes. The relation between these two parameters varies with the material used and the amount of absorber in the fluid.

The setup used to measure the metamaterials HR1, HR2 and HR3 presented in this Chapter is the one described in Section 3.2. Fig. 4.5 is a picture of the setup used in the laboratory [90]. The metamaterials HR1 were also measured using a modified version of this setup to understand if the measured band gaps were dependent on the location of the source with respect to the metamaterials. To answer this question, a study on the effects of the position of the source with respect to the stop band was conducted by utilising an industrial six Degree of Freedom (D.O.F.) robot [142]. This approach allowed for controlled and repeatable scanning not only of traditional 3 DOF (x, y, z) positions but also in roll, pitch and yaw orientations (Fig. 4.6). The robot arm was programmed to trace a quarter hemisphere around the sample, at a distance of 100, 200, 300 and 400 mm. A loudspeaker was mounted on the robot arm, and the execution of the robot path was controlled by custom MATLAB code interfaced with the

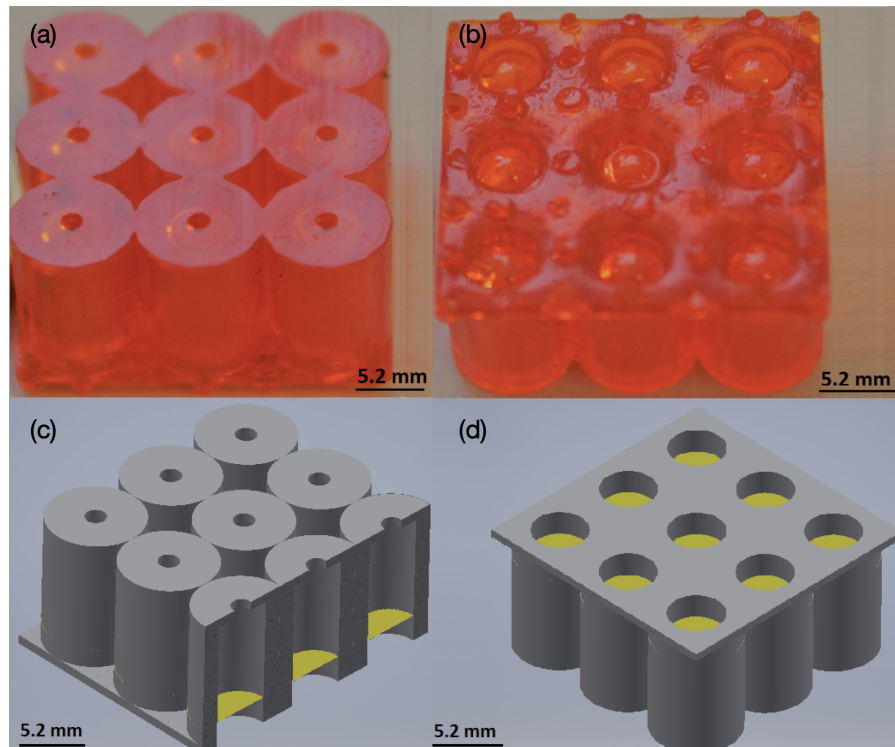


Figure 4.4: Front view (a) and bottom view (b) of acoustic metamaterials based on thin plates and Helmholtz resonators. Equivalent CAD model with cut away section (c) and bottom view (d). The membranes have been highlighted in yellow for a better understanding of the design.

robot controller through the KUKA Robot Sensor Interface (RSI) [143]. The data acquisition was synchronised with the progression of the robot path. Next, the collected data was encoded with the robot positional feedback, received through RSI. Two calibrated microphones measured the response above the sample and outside its near-field as a reference [91].

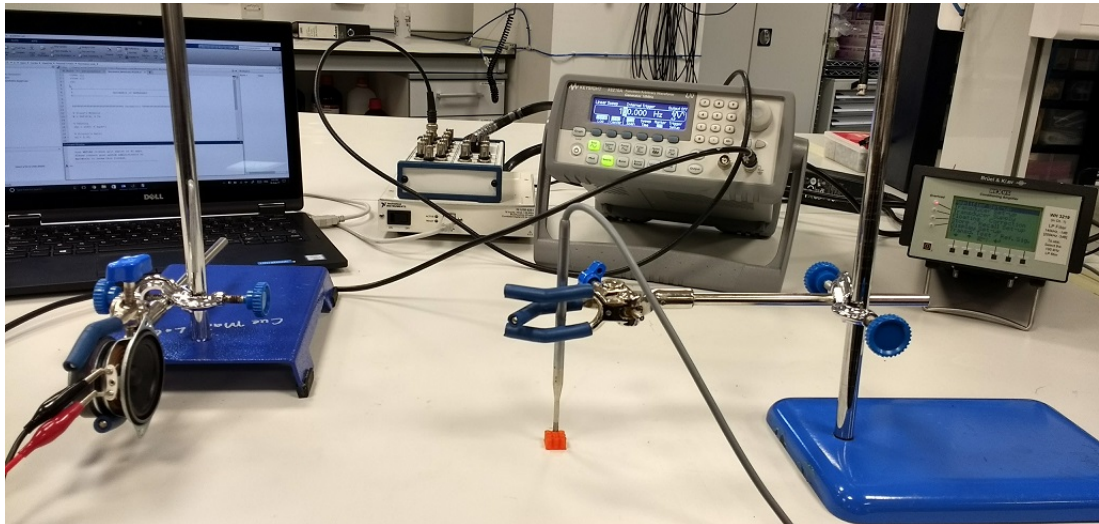


Figure 4.5: Experimental set-up: a speaker connected to a function generator emits a swept sine wave that impinges on the three-dimensional printed sample. A microphone, connected to a pre-amplifier and positioned right above the metamaterials, records the signal controlled by NI-DAQ hardware and MATLAB code running on a laptop.

The next sections will show how acoustic metamaterials HR1, HR2 and HR3 were modelled and will present the results and analysis of measurements.

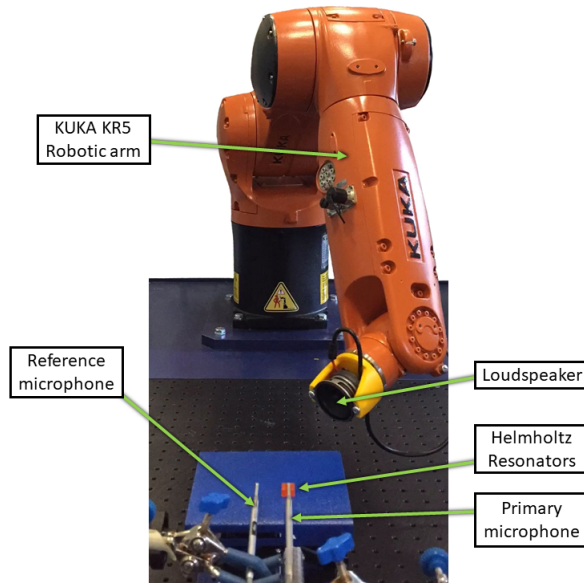


Figure 4.6: Robotic arm configuration. To verify that the attenuation of sound in the band gap happens at any incident angle of the source a robotic arm holding a loudspeaker traces a quarter hemisphere around the sample. A reference microphone measures the sound transmission in air while a second microphone measures the transmission above the sample.

4.3 Model

This Section first aims to develop a parametric model for small-scale Helmholtz resonators that receives as input the dimensions of neck and cavity and produces as output the band gaps of a single Helmholtz resonator. FEM models and transfer matrix models of resonators arrays are also presented.

Analytical Model of Single Helmholtz Resonator

Let's start by reviewing Eq. (2.31) for small-scale Helmholtz resonators introduced in Chapter 2. The fundamental frequency is given by:

$$f_0 = \frac{c}{2\pi} \sqrt{\frac{S}{L'V}}, \quad (4.1)$$

where c is the speed of sound in the gas filling the cavity, S is the cross-sectional area of the neck, $L' = l + 1.7a$ is the extended length of the neck, l is the length of the neck, a is the radius (for cylindrical Helmholtz resonators) or surface length

(for non cylindrical Helmholtz resonators) of the neck and V is the volume of the cavity [57]. In small-scale Helmholtz resonators the first overtone is:

$$f_n = (2n - 1) \frac{c}{4h'}, \quad (4.2)$$

with $n = 1, 2, 3, \dots, \text{etc.}$,

where c is the speed of sound in the host medium, $h' = h + 0.6r$ is the effective length of the cavity and r is its radius. First, we developed a model that shows how the band gap produced by the first resonance increases in depth as the number of resonators in an array increases. To illustrate the phenomenon, we considered the driven harmonic oscillator in which the response of N Helmholtz resonators was added to the input sound wave, such that we can describe a variable $y(t)$:

$$y(t) = \frac{F(t)}{\omega_0^2} + \alpha N x(t), \quad (4.3)$$

where α is a the ratio of pressure from the field generated by the Helmholtz resonators and the external field, chosen arbitrarily to match experimental data. The variable $y(t)$ represents the sum of the external driving force and the motion of the oscillator, which can be considered to be analogous to the acoustic pressure summed from both an external field and the pressure output from a driven Helmholtz resonator. Assuming that the external drive is sinusoidal, i.e. $F(t) = F e^{i\omega t}$, we can solve for $y(t)$ in the complex domain, such that the spectral response of $y(t)$ is given by:

$$Y(\omega) = \frac{Y}{\omega_0^2} \sqrt{\frac{\gamma^2 \omega^2 + (\omega^2 - (1 + \alpha N) \omega_0^2)^2}{\gamma^2 \omega^2 + (\omega^2 - \omega_0^2)^2}}. \quad (4.4)$$

Next, it is possible to build a parametric model, that, given different geometries for neck and cavities, outputs the frequencies of first and second modes of vibration. By doing so, the geometry of Helmholtz resonators can be modelled based on the sought frequency range to be attenuated. Fig. 4.8 shows the result of a model that outputs the fundamental frequency and first overtone of a cylindrical small-scale Helmholtz resonator when four parameters are varied across different values. These four parameters are height of the cavity, radius of the cavity,

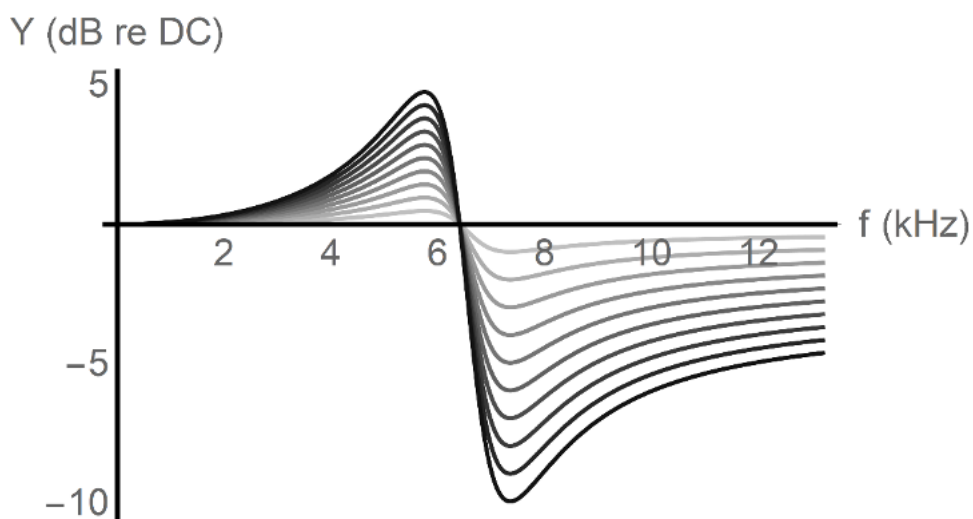


Figure 4.7: Plot of the sum of the response of N oscillators and an external sinusoidal driving force. The values of α (1%) and γ (2500) have been scaled to correlate with experimentally determined responses. Each curve represents the range of N from 1 to 10, with 10 being the darkest.

length of the neck and radius of the neck. Each set of permutations of two varying parameters is plotted and the two remaining parameters are fixed. The upper and lower limits of the parameters values are set according to constraints of the Asiga three-dimensional printer described in Chapter 3. The values of fixed parameters are set to be the mean of possible values.

It is also possible to optimise the choice of fixed parameters depending on a specific criterium. For example, one might want to maximise or minimise the difference between the fundamental frequency f_0 and the first overtone f_1 . By building two four-dimensional matrices with all the possible values for f_0 and f_1 and subtracting the two, it is possible to find the parameters that result in the maximum, minimum or specific difference. Setting the fixed values to these parameters, allows one to visualise similar solutions and eventually to choose the parameters that best optimise other constraints, such as damping, sound energy and dimensionality constraints. Fig. 4.9 is a modification of Fig. 4.8 where the fixed parameters are chosen in order to minimise the distance between f_0 and f_1 . By assigning to fixed parameters the mean values of selected ranges, f_0 is 1871 Hz and f_1 is 2781 Hz. If the fixed parameters are optimised for maximum

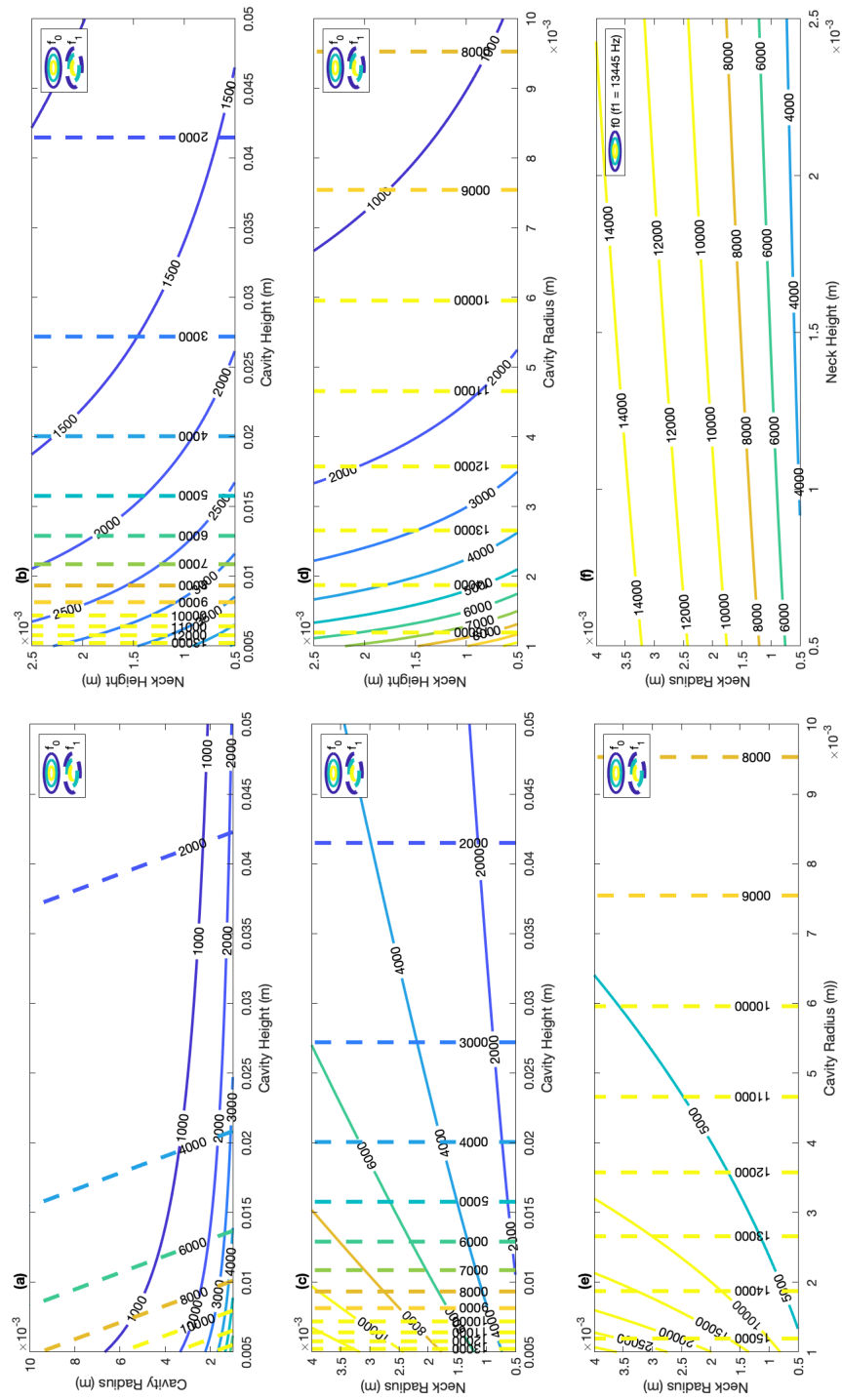


Figure 4.9: Variation of two parameters, while keeping the other two parameters at a fixed optimised value that maximises the difference between f_0 and f_1 .

distance between fundamental frequency and overtone, f_0 is 2905 Hz and f_1 is 13445 Hz. The plots in Fig. 4.8 and Fig. 4.9 provide a way to find the best geometries given constraints of a specific application, a sought frequency range and a desired distance between f_0 and f_1 . However, other factors need to be taken into account, and that are not considered in this parametric model. For example, damping and coupling with other elements of an application can have a crucial effect on the amount of attenuation and some geometries that would match the required frequency range and $f_0 - f_1$ distance could not be suitable for a particular situation. Therefore, this parametric model can be useful as a starting point to select some candidate geometries that can be used as input in FEM models that consider the interaction between more elements. The models shown in Fig. 4.8 and Fig. 4.9 have been coded in MATLAB[®] and can be found in Appendix A.1.

4.4 Results

In this Section results from experiments described in Section 4.2 are presented and analysed. The main goal of these experiments was to show that it is possible to fabricate small-scale acoustic metamaterials based on Helmholtz resonators using additive manufacturing technology. Although these metamaterials were designed without the constraints of a specific application, their small-scale dimensions and noise attenuation frequency range would make them suitable for applications such as headphones, smart speakers, automotive and aerospace industries. Once an application has been chosen, models presented in Section 4.3 can be leveraged in order to find suitable geometries and the designs presented in this Section can be modified accordingly. Four different designs and measurements are discussed. Dimensions and materials used are reported in Section 4.2.

The first measurement compares band gaps obtained with acoustic metamaterials composed of 3×3 , 3×6 and 6×6 arrays of Helmholtz resonators. Fig. 4.10 shows that a stop band is generated where the sound is attenuated. It is worth noting that by increasing the number of resonators, the stop band has greater peak attenuation and the incoming sound wave is attenuated approximately 10 dB, 20 dB and 30 dB respectively (peak values). This behaviour is reflected in the model shown in Fig. 4.7. The measurements are normalised with respect to

a measurement in the free field where no structures or resonators are present. The slight de-tuning in frequency can be an effect of coupling between the resonators, as well as of increased damping with increased number of resonators, since damping can de-tune resonators as explained in Chapter 2.

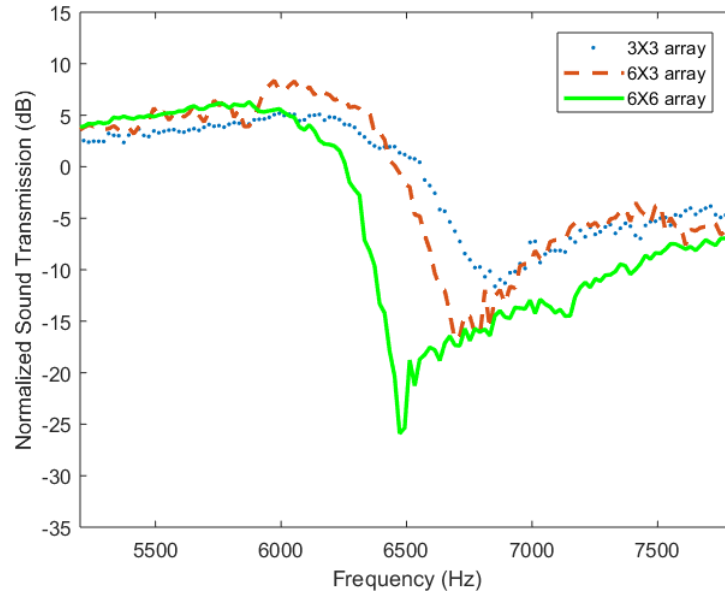


Figure 4.10: Plot of normalised sound transmission as a function of frequency, showing an increase in sound attenuation with higher number of resonators. It can be noticed that the band gap is detuned with increased number of resonators. This is due to increased damping with higher number of resonators.

The second measurement is a study on how the position of the sound source affects noise attenuation. This study was performed with the robot setup described in Chapter 3. As shown in Fig. 4.11, the sound is attenuated in the band gap (i.e. at 6600 Hz) for each source position, with an increasing attenuation when the loudspeaker is above the sample, i.e. facing the front of the aperture of the neck of the resonators. The effect of sound attenuation is present for measurement spheres of different radiuses, namely 100, 200, 300 and 400 mm and it is consistent for all the chosen distances. The source is always positioned in the far field with respect to the samples, since the frequencies of interest are higher than the minimum distance ($f = c_s/\lambda = 343 \text{ (m/s)} / 0.1\text{(s)} = 3430\text{(Hz)}$).

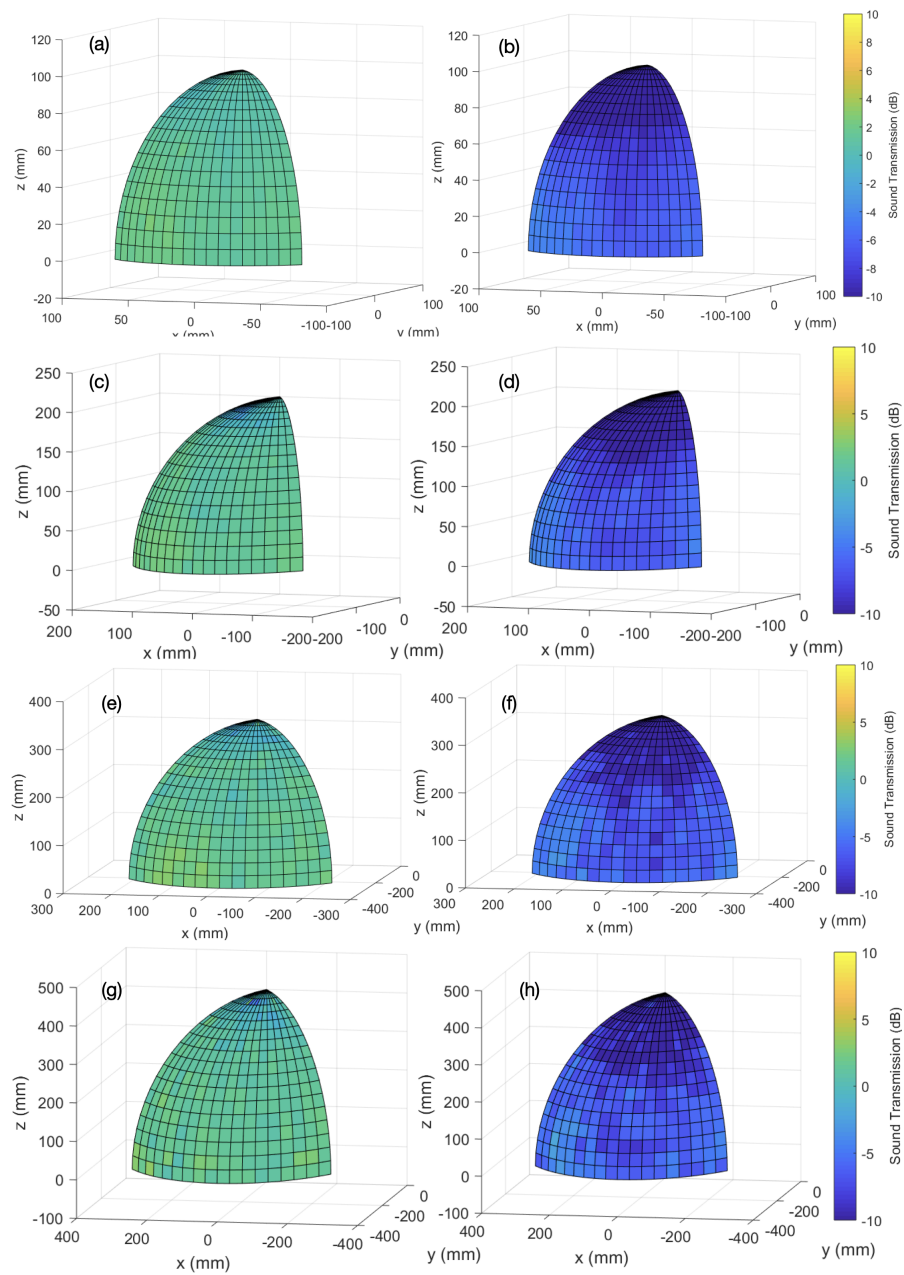


Figure 4.11: Sound transmission measured above the sample at 5000 Hz (left) and 6600 Hz (right) with respect to the source playing a swept sine wave and positioned along a quarter hemisphere with a radius of 100 ((a), (b)), 200 ((c), (d)), 300 ((e), (f)), and 400 ((g), (h)) mm.

The third measurement compares the distance of first and second band gap when using resonators having the dimensions of a soda can scaled down by a factor of 20 and resonators designed to achieve band gaps hybridisation, respectively. In the first case, shown in plot (a) of Fig. 4.12, the first and second band gaps are approximately 6.5 kHz apart. In the second case, shown in plot (b) of Fig. 4.12, the second band gap has been designed to be closer to the first one, and hybridisation - i.e. the process of merging two band gaps - has been achieved. Previously, hybridisation had been achieved by merging the first band gap with band gaps produced by Bragg scattering, a byproduct of the periodicity of acoustic metamaterials and depending on the lattice distance. Here, hybridisation of band gaps of fundamental frequency and first overtone is proposed for the first time. Although the two band gaps are clearly separated at a distance of approximately 2.5 kHz, they are close enough to achieve hybridisation. In other words, the frequency band in-between the two band gaps is still attenuated, due to damping and air non-linearities.

The fourth measurement aims to evaluate the effect of adding a thin plate inside the Helmholtz resonators and to enhance the band gap of the first resonance by leveraging the band gap created by the resonance of the thin plate. Fig. 4.13 shows that the resonance of thin plates widens the band gaps produced by the resonators alone: a band gap at 9 kHz that is not present in the samples containing simple resonators is visible and the band gap of the first overtone is shifted onto a 2 kHz lower band and enhanced by 10 dB. The nature of this result is mainly experimental. However, a comprehensive work on thin plates modelling, fabrication and characterisation is presented in the next Chapter.

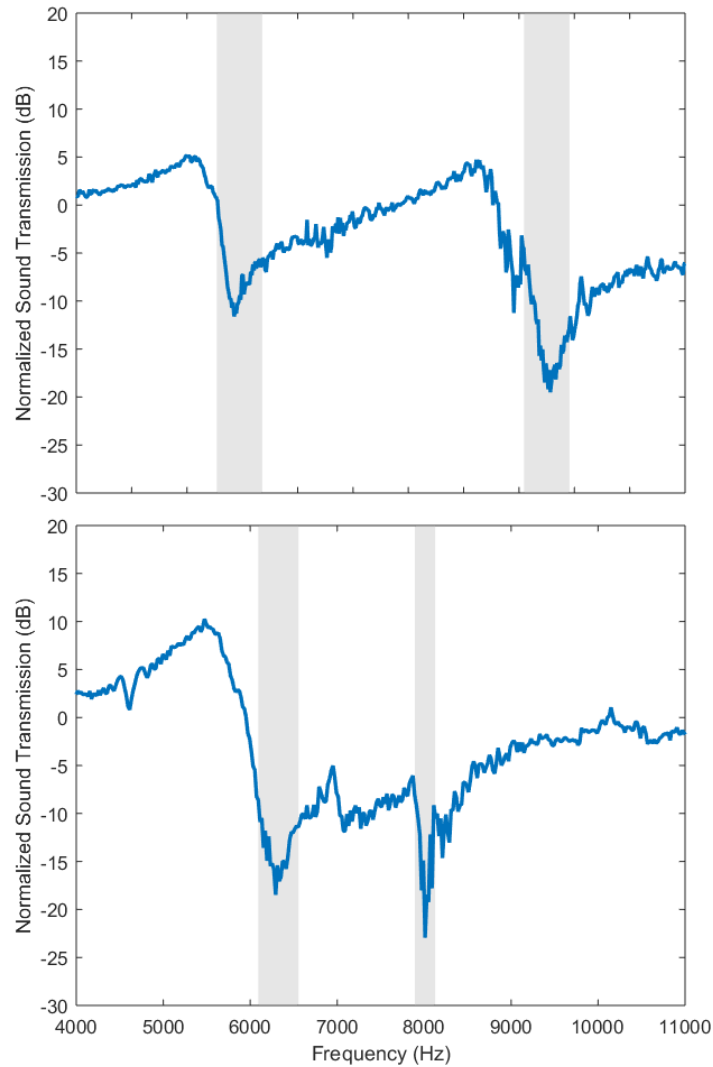


Figure 4.12: Narrow stop bands 6.5 kHz apart, originated in acoustic metamaterials with unit cells having the dimensions of a soda can scaled down by a factor of 20 (a). Closer stop bands 2.5 kHz apart and hybridised by a band gap where the sound is still attenuated by 10 dB, generated by acoustic metamaterials with tuned overtones (b).

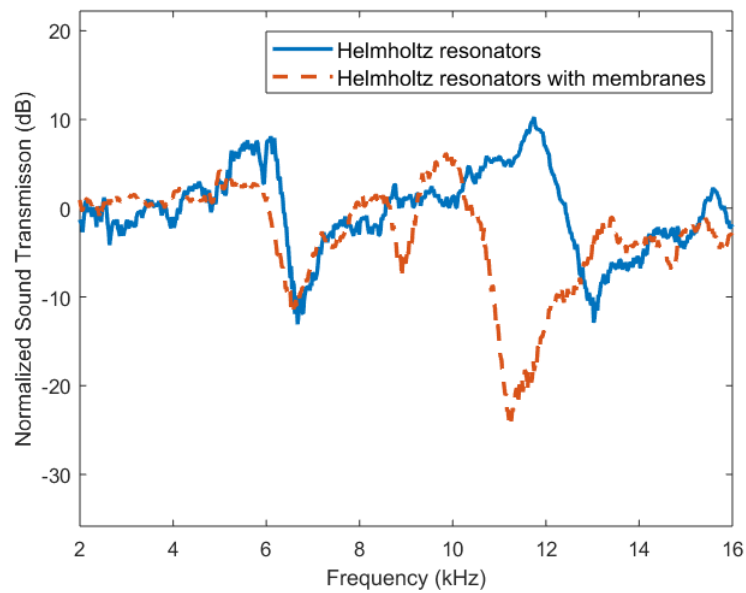


Figure 4.13: Sound transmission of the acoustic metamaterials based Helmholtz resonators (blue) and based on Helmholtz resonators with thin plates (red). The signal has been acquired above the resonator in the middle of a 3×3 array.

4.5 Conclusion and Future Work

Chapter 4 discussed research on noise attenuation using acoustic metamaterials based on small-scale three-dimensional printed Helmholtz resonators. The first work presented as part of this research aimed to replicate previous studies on large-scale Helmholtz resonators such as soda cans and to show that it was possible to achieve similar effects in small-scale Helmholtz resonators that had been fabricated using additive manufacturing technology. By increasing the number of unit-cells, it was shown - with a model and experiments - that noise attenuation increases. The second work answered a question on how the position of the acoustic source affects noise attenuation. To do so, a robotic arm moved a loudspeaker around a quarter-hemisphere trajectory, while a microphone was placed on top of a fixed array of unit-cells. The effect of source position was determined to not have an influence on the band gap for this setup and this type of acoustic metamaterials. The third work proposed to tune Helmholtz resonators at the design stage to create a larger "hybridisation" band gap that merged the band gap created by the fundamental frequency and the band gap created by the first overtone. To facilitate design, a parametric model allowed to choose the best

geometry to attenuate a specific band gap. An optimisation algorithm allowed to select a specific band gap depth. By successfully measuring the hybridisation band gap, it was possible to show that leveraging multiple resonances - such as overtones - in the same unit-cell is a new way to achieve a broad band gap. Finally, the fourth work expanded the concept of leveraging multiple resonances by inserting a resonant thin plate inside Helmholtz resonators. It is worth noting that the thin plates and the Helmholtz resonators were fabricated using a novel three-dimensional printing technique that allowed to obtain these unit cells using multiple materials - one for the thin plate and one for the resonators - in one print. These results were published in IEEE Sensors Proceedings [90] and IEEE Sensors Journal [91] and were presented through posters and oral presentation in multiple events, symposia and workshops.

The results presented above show that it is possible to innovate in the field of acoustics today, even starting from well-known concepts such as the working mechanism of a Helmholtz resonator. The field of acoustic metamaterials can offer new ways to attenuate sound that have not been explored in the past. However, the work needed to start from theoretical studies or proof-of-concept experimental work and build real-world products is still in progress and laborious. One way to develop a bridge between theoretical work and production is to start from applications that need improvement and then build models, designs and develop fabrication techniques that are specific to that application. Models are a powerful tool that can inform the design stage, but they need to consider multiple parameters such as geometry, depth and breadth of band gap, coupling with housing and other elements. By defining an application, it is possible to reduce the initial complexity of the models, and leverage their full potential. Finally, new technologies such as advance manufacturing techniques that are developed to optimise a certain parameter, such as for example thickness of a layer, can unleash creativity, as they allow rapid trial and error. These new technologies also allow to create complex shapes - such as customised Helmholtz resonators that fit a loudspeaker enclosure and include resonant or active layers - that were difficult to build in the past or required the help of expensive chains of manufacturing.

Future work on three-dimensional printed acoustic metamaterials based on

Helmholtz resonators will present interesting challenges. It will try to answer questions such as "Which and how many resonant structures can be used inside Helmholtz resonators?", or "Which applications will benefit from this technology?". Some research, also presented in this thesis, is looking at how to actively control the parameters such as frequency range of band gap of this type of metamaterials. Of course, the research on materials used to fabricate the resonators is also very important, including a search for sustainable materials or resonators already presented in nature that can be used as unit-cells.

The next Chapter will further look into the process of three-dimensional printing a thin plate, developing a method to go beyond the initial thickness constraints of a printer and obtaining a characterisation of the thin plates. Chapter 6 will explore the possibility of modifying the resonators presented in this Chapter to obtain active metamaterials that can be tuned in real-time.

Chapter 5

Fabrication and Characterisation of Thin Plates for Acoustic Metamaterials Applications

5.1 Introduction

This Chapter presents the research and development of acoustic metamaterials based on three-dimensional printed thin plates. A novel technique was developed to fabricate thin resonant layers using additive manufacturing. The material parameters of these thin plates have been characterised by models and various measurement techniques. The motivations behind this project are driven by the opportunity to grow the field of acoustic metamaterials and to create a bridge between theoretical work, laboratory experiments, and the realisation of real-world products. In the past decade, many publications have proposed new acoustic metamaterials based on membranes and thin plates [45]. However, many of these publications are models, and few present experimental work. This is also due to the difficulty of fabricating membranes with comparison to simpler unit-cells such as Helmholtz resonators. Some laboratories rely on manually gluing membranes to supports, and this can result in unit-cells that are slightly different and that are not suitable for the periodic and bulk requirements of acoustic metamaterials. Although some techniques for three-dimensional printing membranes have been proposed, they usually present thick layers [144, 145].

The first goal of this work was to develop a technique for three-dimensional printing thin plates having a low resonance frequency. Thin plates can potentially be ideal unit-cells for attenuating low frequencies in small-scale and lightweight applications. While other unit-cells such as pipes need a larger structure to resonate at low frequencies, thin plates have a resonant frequency that is directly proportional to their thickness. Therefore, thin plates are good candidates for low frequency, thin, lightweight, small-scale applications. As explained in Chapter 3, most additive manufacturing printers do not offer a system to fabricate layers thinner than 0.1 mm. Hence, developing a technique to fabricate thinner layers and also include them within other structures such as supports, pipes, Helmholtz resonators is a fundamental first step for contributing to the field of acoustic metamaterials. Once this fabrication technique has been developed, the second goal was to build a parametric model, similar to the one developed in Chapter 4 for Helmholtz resonators, to control geometry and materials and to inform the final design of acoustic metamaterials. Finally, an experimental characterisation of three-dimensional printed thin layers was carried out to validate the parametric models and to quantify both the physical parameters, such as density and Young's modulus, as well as the absorption, reflection, and transmission characteristics of thin layers.

The next sections will describe the methods used to fabricate thin layers, and to build the parametric model. Results of experimental characterisations will be shown and a final discussion will reflect on the results and on future work.

5.2 Methods

The Asiga three-dimensional printer introduced in Chapter 3 was used to fabricate the two samples that are presented in this work. Both samples have the same dimensions and are shown in Fig. 5.1. The shape of three-dimensional printed layers is circular and they are fabricated on top of a hollow cylinder 1 mm in height and with 1 mm thick walls. The three-dimensional printer build plate size is $33.49 \times 20.99 \times 76$ mm, and the outer diameters of the support and plate were set at 20 mm, which is the maximum diameter. Therefore, the effective diameter of

the thin plate was 15 mm. There are two main reasons for selecting the maximum possible diameter. Firstly, in order to characterise the plate with an impedance tube, the diameter should be as large as possible, given the standard dimension of the tube, in this case having a 30 mm diameter. Secondly, since the resonance of a thin plate is inversely proportional to the square of its radius, a larger diameter would result in a lower frequency, as required for noise applications.

The first sample had as main component PEGDA 250 and the second PEGDA 700. The numbers 250 and 700 represent the molecular weights of the two different types of PEGDA. In particular, PEGDA 700 was preferred for this work as it is characterised by a lower Young's modulus than PEGDA 250 and hence a lower resonance frequency, that could match and attenuate lower frequencies. BaTiO₃ nano-powder with a 500 nm diameter average particle size, purchased from US-NANO, was added to the resin with a 50% weight with respect to PEGDA when fabricating the plate. BaTiO₃ main function was to scatter the light in a uniform way on the horizontal plane, to obtain a flat plate, since previous attempts that did not include BaTiO₃ resulted in a curved plate. An explanation of the relationship between light exposure and degree of polymerisation is provided in Chapter 3. It is important to notice that by adding BaTiO₃ to the resin, a piezoelectric material can be obtained, and its properties are explored in the next Chapter. Irgacure 819 was added to both mixtures as a photo-initiator with a 1% weight with respect to PEGDA and 0.1% Sudan I was added as absorber to better control the amount of light that could contribute to the polymerisation of the resin. While the resin described above was used to print the thin plate, the support material was made of PEGDA 250, 0.1% Sudan I and 1% Irgacure 819. Since the Asiga three-dimensional printer software does not allow to change the exposure time to light or other parameters while the print has started, the chosen exposure time of 5 seconds was of a duration that allowed to print both the materials of the support and the materials of the membrane. This exposure time was chosen as a result of a trial and error process. Nevertheless, it is possible to build models based on Beer's methods (see Chapter 3) that allow to predict the optimal exposure time for different materials.

The samples were modelled using the transfer matrix method described in

Chapter 3. They were measured using an impedance tube described in Chapter 3 shown in Fig. 5.2 and schematised in Fig. 5.3.

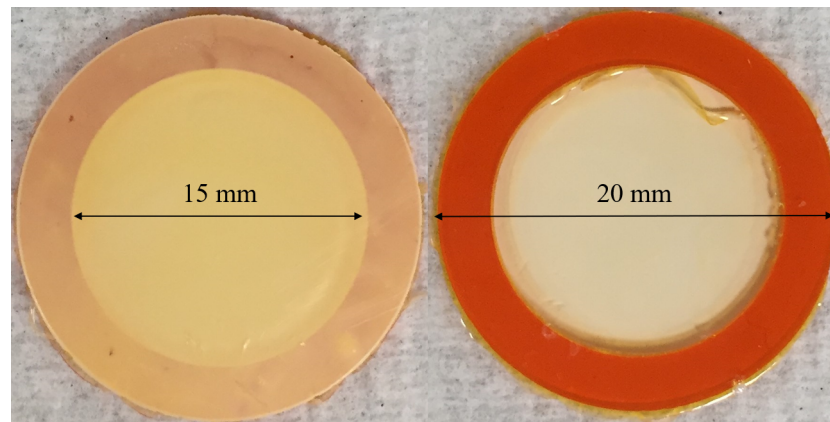


Figure 5.1: Three-dimensional printed thin plates front (left) and back (right).

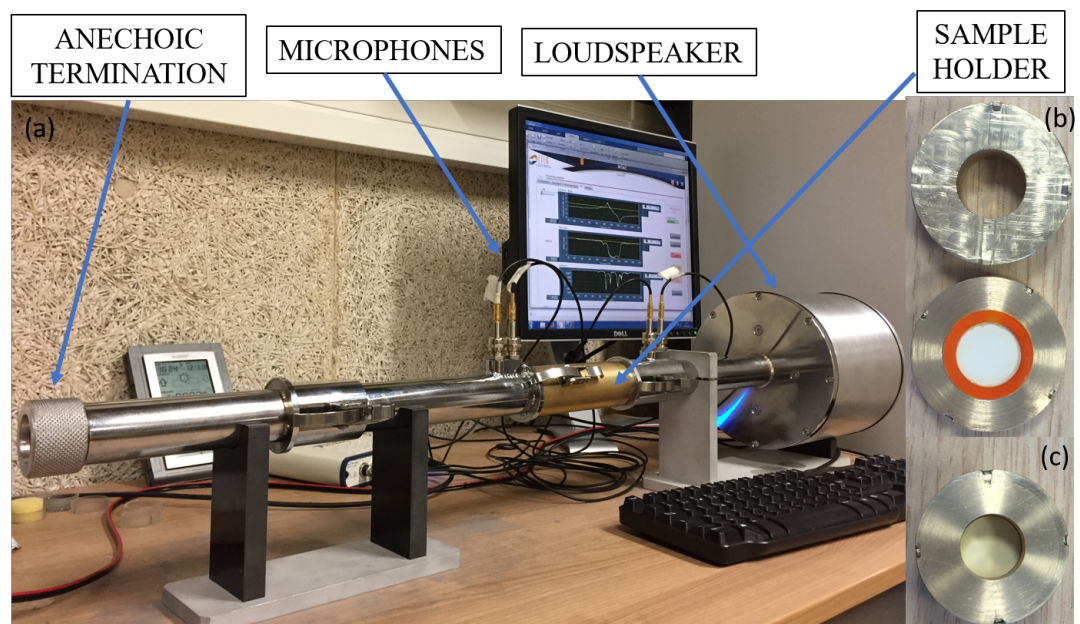


Figure 5.2: Impedance tube used to measure the acoustic coefficients of the plate under test (a). Open sample holder with plate inserted (b) and closed sample holder with plate (c).

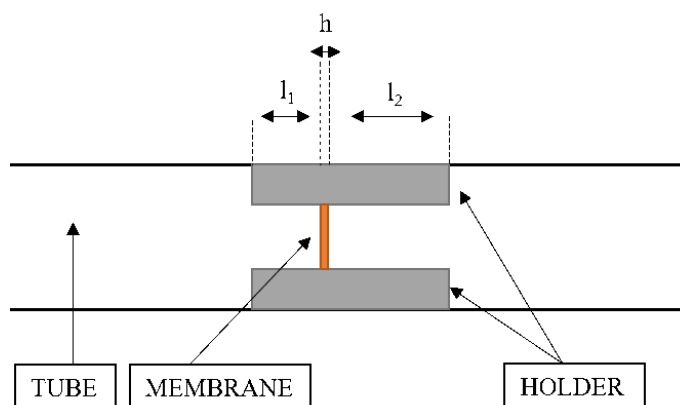


Figure 5.3: Scheme of the system modelled through the transfer matrix method. As in the experiments, the impedance tube contains a sample holder that supports the plate.

5.3 Model

This Section first aims to develop a parametric model for thin plates that receives as input the material and geometry parameters and produces as output the resonance of a single thin plate. Then, a transfer matrix model of thin plates is also introduced and validated by experiments in the next Section. Four different parametric models are shown. All these parametric models take as input Young's Modulus, Density, Poisson's Ratio, Thickness and Radius of a circular thin plate. In each model, every set of permutations of two varying parameters is varied across a range while the three remaining parameters are fixed. The value of the fixed parameters is chosen in each model by running an algorithm that optimises those values based on a specific goal, such as maximising or minimising the resonance, or obtaining a resonance within a specific range, such as frequencies between 300 Hz and 3000 Hz, where most of human speech fundamental frequencies are found.

The first model shown in Fig. 5.4 selects values for the fixed parameters that maximise the value of f_0 within the given parameters' ranges. The second model shown in Fig. 5.5 selects values for the fixed parameters that obtain a mid-frequency values for f_0 . The third model shown in Fig. 5.6 selects values for the fixed parameters that minimise the value of f_0 within the given parameters'

ranges. The fourth model shown in Fig. 5.7 selects values for the fixed parameters that obtain a value for f_0 within the frequency range where most human speech fundamental frequencies are found, namely between 300 Hz and 3000 Hz. The models shown below have been coded in MATLAB[®] and can be found in Appendix A.2.

A transfer matrix model has also been developed to retrieve the thin plate's material parameters and simulate the experimental measurements conducted in the impedance tube. The transfer matrix model described in Chapter 3 has been applied to this specific sample. The transfer matrix

$$T = \begin{bmatrix} T_{11} & T_{12} \\ T_{21} & T_{22} \end{bmatrix} \quad (5.1)$$

is equal to:

$$T = M_{endcorr} M_{tube_1} M_{plate} M_{tube_2} M_{endcorr}, \quad (5.2)$$

where $M_{endcorr}$ is the transfer matrix of the end correction Δl [146]:

$$M_{endcorr} = \begin{bmatrix} 1 & iZ_t k t \Delta l \\ 0 & 1 \end{bmatrix}. \quad (5.3)$$

M_{tube_j} is the transfer matrix of the sample holder on the left ($j = 1$) and right ($j = 2$) sides of the plate [147]:

$$M_{tube_j} = \begin{bmatrix} \cos(k_t l_j) & iZ_t \sin(k_t l_j) \\ \frac{i \sin(k_t l_j)}{Z_t} & \cos(k_t l_j) \end{bmatrix}. \quad (5.4)$$

M_{plate} is the transfer matrix of the thin plate:

$$M_{plate} = \begin{bmatrix} 1 & Z_m \\ 0 & 1 \end{bmatrix}, \quad (5.5)$$

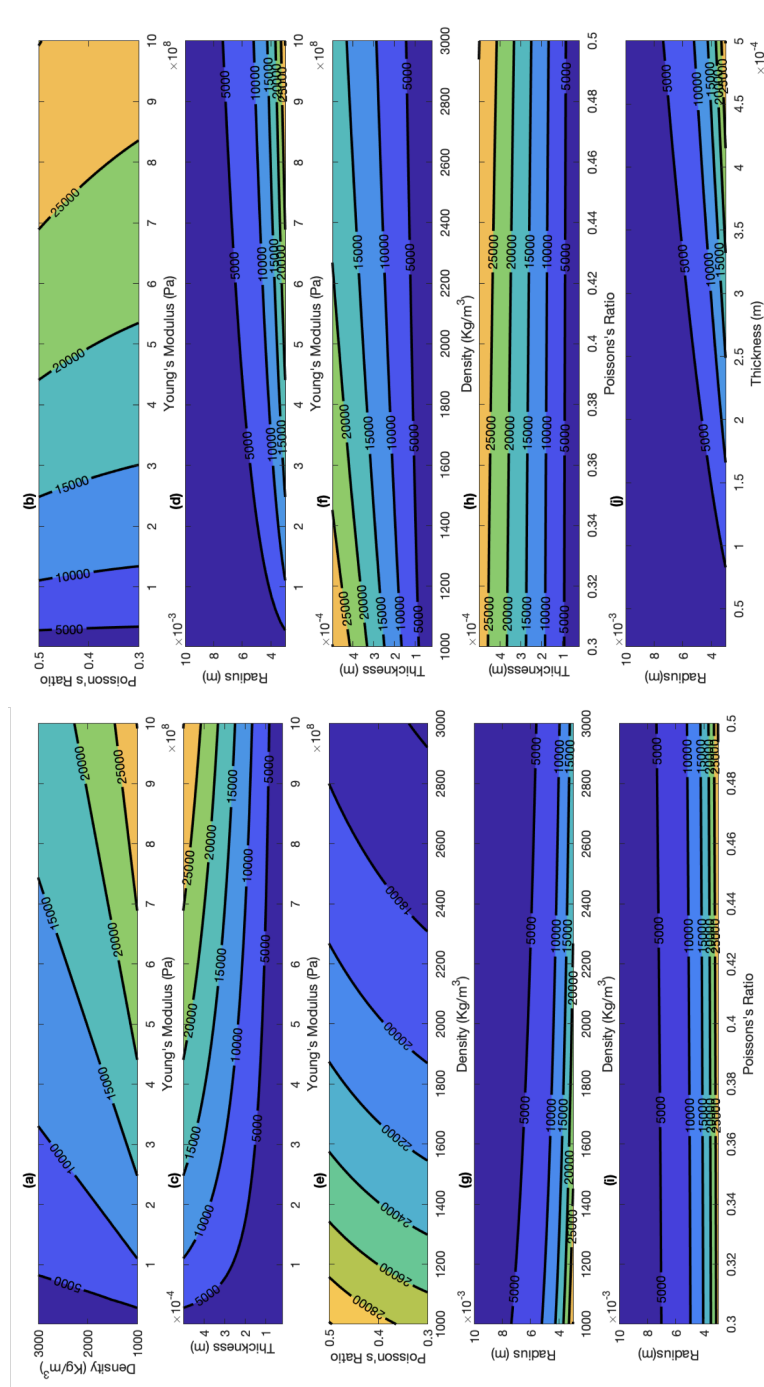


Figure 5.4: Variation of two parameters, while keeping the other two parameters at a fixed value, allows one to choose a desired value for f_0 and f_1 . The values of the fixed parameters are chosen to maximise f_0 .

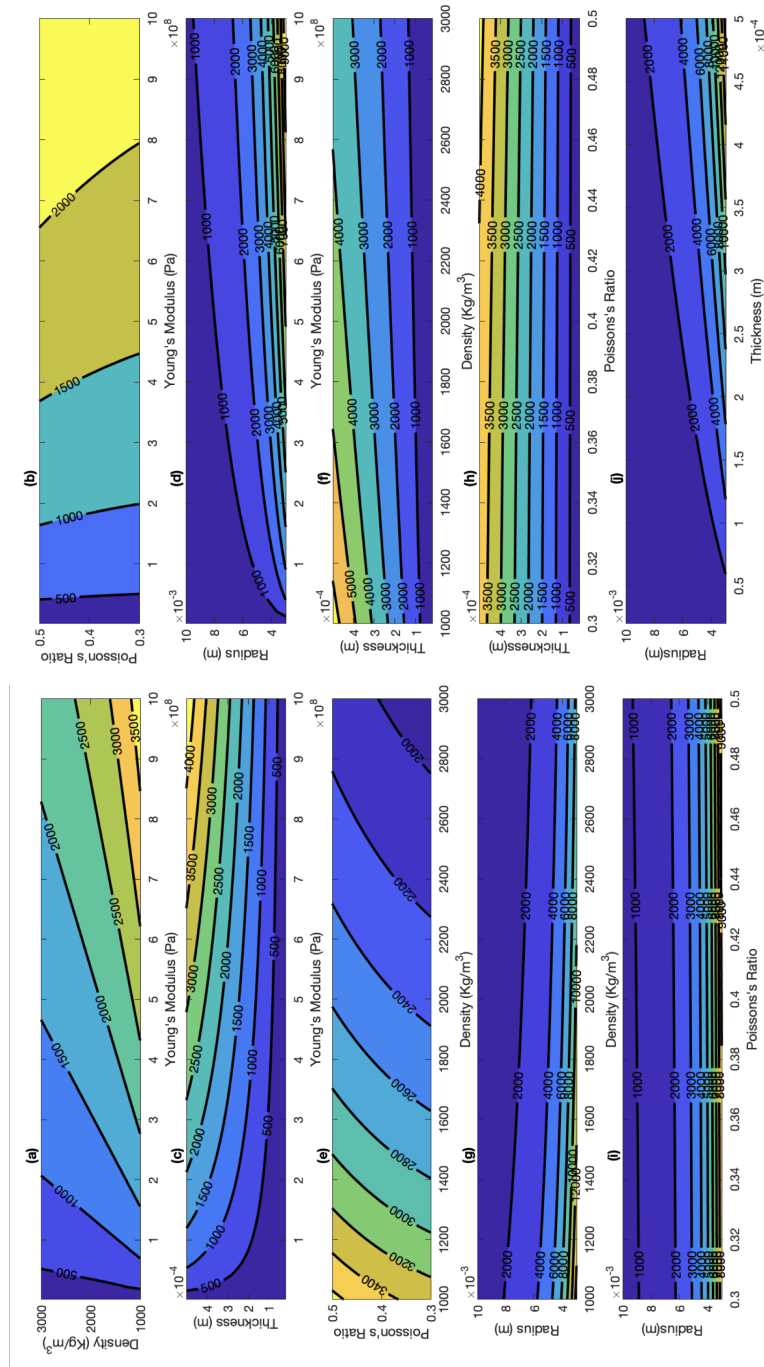


Figure 5.5: Variation of two parameters, while keeping the other two parameters at a fixed value, allows one to choose a desired value for f_0 and f_1 . The values of the fixed parameters are chosen to obtain a mid-frequencies value for f_0 .

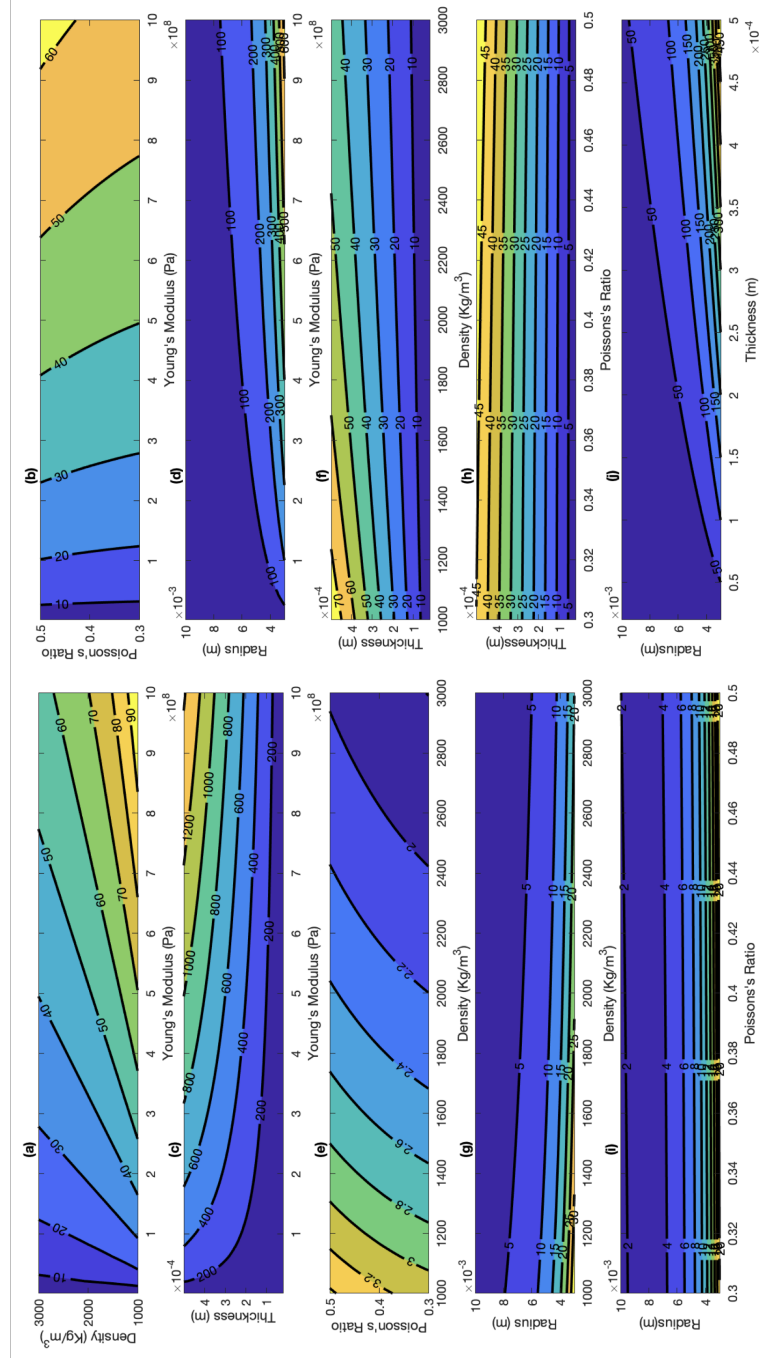


Figure 5.6: Variation of two parameters, while keeping the other two parameters at a fixed value, allows one to choose a desired value for f_0 and f_1 . The values of the fixed parameters are chosen to minimise f_0 .

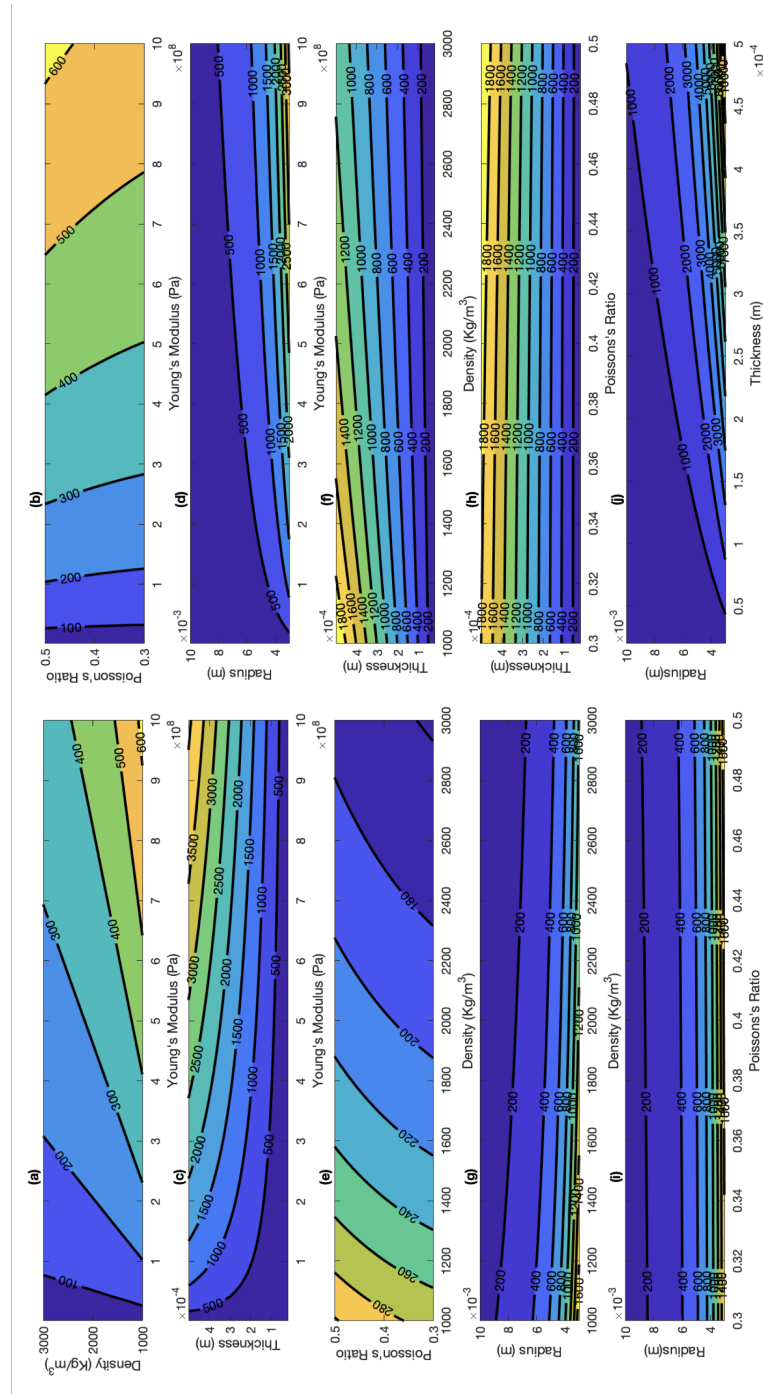


Figure 5.7: Variation of two parameters, while keeping the other two parameters at a fixed value, allows one to choose a desired value for f_0 and f_1 . The values of the fixed parameters are chosen to obtain a value for f_0 within the speech frequencies range.

where Z_m is the acoustic impedance of the thin plate [148].

The results from this model and the corresponding measurements gathered in the impedance tube are reported in the next Section.

5.4 Results

The measurements obtained using laser Doppler vibrometer method showed that the three-dimensional printed samples presented in this paper behave as thin plates. Two models exist in the literature to predict the modes of vibration of circular thin layers. The model of a membrane considers a thin layer only dependent on tension, while the model of the plate is only dependent on stiffness. Furthermore, a membrane resonance frequency is inversely proportional to its thickness, while a plate is directly proportional to it [53]. These two models successfully represent many vibrating layers present in nature and in our everyday life. Nevertheless, in real-world scenarios, it is possible to encounter objects that manifest a behaviour in-between membranes and plates. While fabricating the samples presented in this Chapter, it became clear that a thicker sample had a higher resonance frequency and therefore a thin plate model was chosen (see Chapter 2. As shown in Fig. 5.8 (a) for PEGDA 250 and in Fig. 5.8 (b) for PEGDA 700, it can be clearly seen that the plates present several modes of vibration, both radial and circular modes. It is possible to predict the frequency of the modes of vibration of a circular plate as reported in Chapter 2, where modes (1,1) and (0,2) are predicted to be respectively 2.091 and 3.909 times higher than mode (0,1). The three-dimensional printed plates present all the modes of vibrations predicted by Chapter 2 and their frequencies are in good agreement with those predicted in the literature. Table 5.1 shows the average resonance frequency for the two types of PEGDA samples. These values were useful while modelling the plates with the transfer matrix method, as they were used as initial guess to initiate the optimisation procedure to retrieve the other parameters.

To characterise the material parameters of the two thin plates, the impedance tube described in Chapter 3 was used, with a sine sweep between 20 Hz and 2500 Hz as input. Each sample was measured 10 times to assess the repeatability

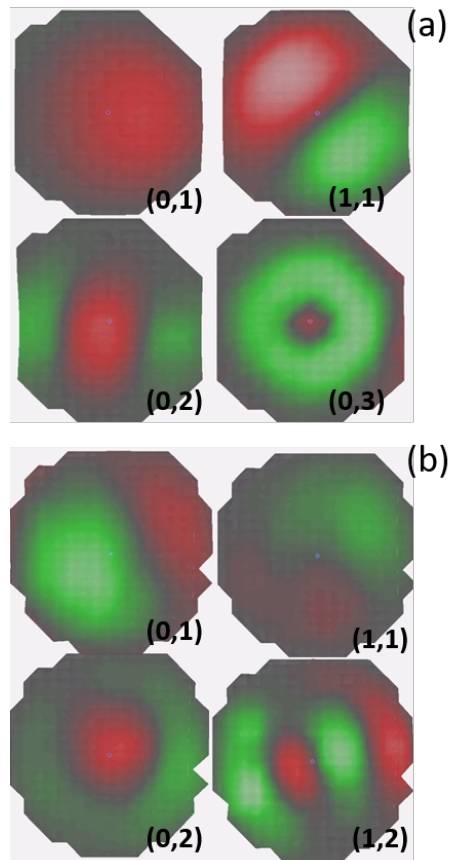


Figure 5.8: Modes (0,1), (1,1), (0,2), (0,3) for the PEGDA 250 sample (a). Modes (0,1), (1,1), (0,2), (1,2) for the PEGDA 700 sample (b).

Table 5.1: Values of fundamental frequency and first circular and radial modes for samples of PEGDA 250 and PEGDA 700 having a 15 mm diameter, measured using a 3D laser vibrometer.

Mode	Quantity	PEGDA 250	PEGDA 700
(0, 1)	Fundamental Frequency (Hz)	940	400
(1, 1)	First radial mode (Hz)	1500	1070
(0, 2)	First circular mode (Hz)	2300	1530

of the measurements. The reflection, transmission and absorption coefficients were retrieved from the measurements. Then, the physical quantities, chosen to initialise the model introduced above, namely density, Poisson's ratio, loss factor and Young's modulus, were optimised to fit the experiments. The transmission and reflection coefficients were first retrieved through impedance tube measurements and are represented respectively by the solid magenta and green lines in Fig. 5.9 for PEGDA 250 (a) and 700 (b). The same coefficients together with absorption were then retrieved using the transfer matrix model and initialised using the values given by laser Doppler vibrometer for the resonance frequency and by vendors data sheets and literature values for density, Young's modulus, Poisson's ratio and loss factor. To minimise the difference between transmission, reflection and absorption coefficients obtained experimentally with those obtained analytically, the values of density, Young's modulus, Poisson's ratio and loss factor assumed at the modelling stage were changed iteratively during an optimisation process, until the modelled coefficients graph in Fig. 5.9 fit into the graph representing the experimental coefficients. Therefore, the density, Young's modulus, Poisson's ratio and loss factor parameters retrieved in this section result from the process of minimisation of the difference between experimental coefficients obtained through measurements in the impedance tube and theoretical transmission, reflection and absorption coefficients modelled with the transfer matrix approach. Through this inverse method it was therefore possible to obtain the values of Young's modulus, density, Poisson's ratio, loss factor and fundamental frequency listed in Table 5.2. The differences between the values of fundamental frequency given by laser vibrometer and the impedance tube approach are due to the differences in samples preparation. In the first case, the plate is in the free field and its support is glued to a piece of glass. Hence, a tiny volume of air is created between the plate and the support. In the second case, there is no support to separate the plate from its measurement environment, which is a tube instead than the free field. The values retrieved through LDV measurements should therefore be used just as initial values for our model and to show the presence of the modes in the plates. Fig. 5.9 shows that the plates fabricated in this work would be suitable for acoustic metamaterials applications. In fact, both kinds of samples show a high reflection coefficient hence low transmission before the first mode of resonance, which corresponds to

a region of negative effective density [149–151]. PEGDA 700 presents a lower frequencies, therefore a peak corresponding to a higher mode is visible in these measurements.

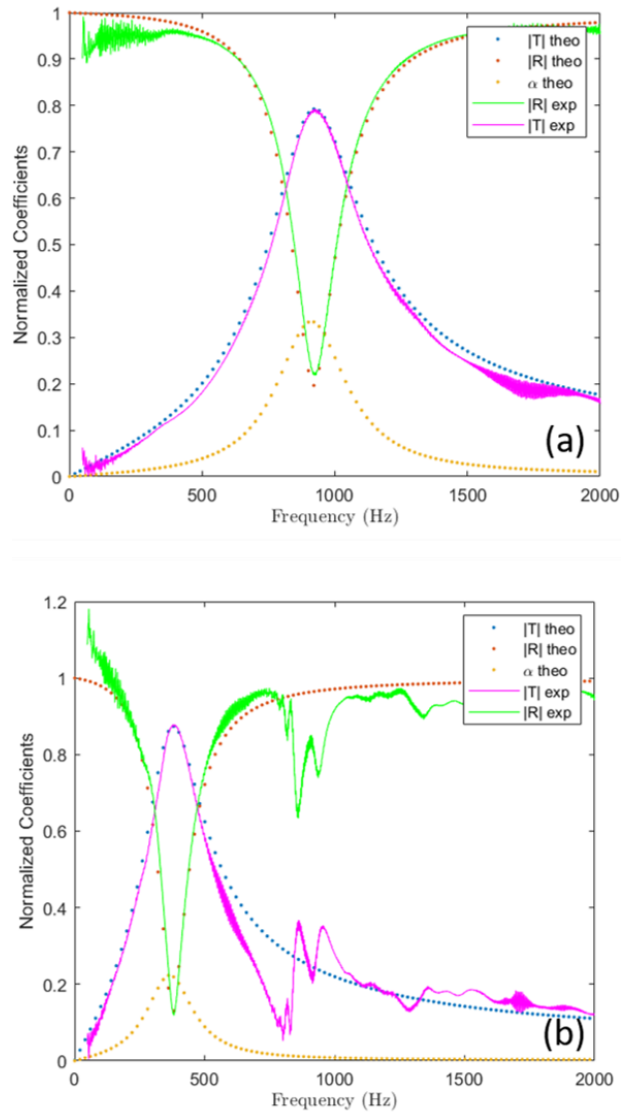


Figure 5.9: Transmission, reflection and absorption coefficients represented by the dotted lines correspond to the parameters retrieved with the optimised transfer matrix model. The solid lines show reflection and transmission coefficients measured through the impedance tube and normalised to the input signal. PEGDA 250 values are shown in graph (a) and PEGDA 700 in graph (b).

Table 5.2: Properties of the materials used to 3D print the plates as retrieved by using the transfer matrix approach and optimisation with the impedance tube measurements.

Symbol	Quantity	PEGDA 250	PEGDA 700
E	Young's Modulus (GPa)	3.04	0.67
ρ	Density (kg/m ³)	1730	2170
η	Loss	0.070	0.075
ν	Poisson's Ratio	0.35	0.35
f_0	Fundamental Frequency (Hz)	827	346

Finally, nanoindentation measurements were gathered on both top and bottom sides of the samples. By looking at Fig. 5.10, it can be seen that the particles distribution is different on the two sides of the plate. The bottom side tends to contain more BaTiO₃ particles than the top side. Therefore, two different values for the Young's Modulus of both PEGDA 250 and PEGDA 700 samples were retrieved, as outlined in Table 5.3. This non-homogeneous distribution of particles in the plate can possibly explain the different values of Young's modulus given by nanoindentation and retrieved through impedance tube measurements. Since the tip used for nanoindentation is small in comparison to the dimension of the particles of PEGDA and BaTiO₃ in the plate, it can be inferred that, for this specific type of plates, impedance tube measurements are more reliable than nanoindentation. Moreover, the sample required for nanoindentation must be small and cut from the support, hence possibly eliminating the small stress that the plate could have received while being attached to the support during the three-dimensional printing process. This sample preparation process could cause a modification of the physical properties of the plate. Therefore, in future designs containing these plates, the results from impedance tube measurements will be preferred when modelling the system.

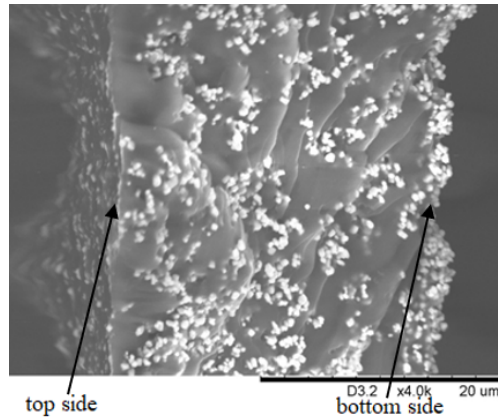


Figure 5.10: Cross-section of the PEGDA 250 sample used for nanoindentation and obtained with scanning electron microscope. It can be noticed that the top and bottom side contain different amounts of BaTiO₃ and PEGDA.

Table 5.3: Young's modulus of PEGDA 250 and PEGDA 700 obtained through nanoindentation measurements. Both top and bottom of the samples have been measured because of non-homogeneous distribution of BaTiO₃ in the sample, as highlighted by scanning electron microscopy.

Symbol	Quantity	PEGDA 250	PEGDA 700
E	Young's Modulus (GPa) Top	0.30	0.062
E	Young's Modulus (GPa) Bottom	0.12	0.059

5.5 Conclusion and Future Work

Chapter 5 discussed research on developing a three-dimensional printing technique to fabricate thin resonant plates. This new technique allowed to control the thickness of layers by using a customised resin containing absorbers and scatterers such as Sudan I and BaTiO₃. The materials used to fabricate the thin plates were chosen to have properties - such as Young's Modulus and density - that resulted in a resonance in the low-frequency range. To the best of our knowledge, this was the first example of three-dimensional printed resonant thin plates fabricate for low-frequency attenuation. The thin plates were modelled using an analytic parametric model as well as a transfer matrix method. Absorption, Transmission, and Reflection coefficients were retrieved by impedance tube measurements. Material parameters were obtain by characterisation using impedance tube, 3D laser Doppler vibrometer and nanoindentation. Different characterisation techniques produced results that were consistent, but slightly different due to the preparation of the samples with an open or closed cavity. A scanning electron microscope was also used to show the different distributions of the constituting materials.

The results presented above show that it is now possible to fabricate thin layers and supports - in one print - using 3D printers that can be affordable and purchased by Universities and research laboratories. This work also shows the importance of starting from a specific goal, such as attenuation at low-frequencies using lightweight and small-scale materials. The number of material and geometry parameters that determines the final outcome is so large that only a specific goal can help initialise and optimise these parameters. The process of selecting a goal, developing a three-dimensional printing technique and fabricating complex shapes could pave the way to fabricating acoustic metamaterials in laboratory environments where it was considered difficult to obtain such samples and where the outcome of research mainly consisted in models and not in fabrication.

Future work on three-dimensional printed thin plates could focus on building full products that include these samples. Many variations to the presented samples

5.5. Conclusion and Future Work

are also possible. For example, it is possible to fabricate thin plates with masses attached, or to control higher modes of vibration by dividing the plate in quadrants and changing the thickness of the thin plate in different regions. Thin plates can also be embedded in other resonators, as shown in Chapter 4. The next Chapter will further look into the process of three-dimensional printing a thin plate, by showing how an active piezoelectric thin plate can be tuned to a desired frequency in real-time.

Chapter 6

Three-Dimensional Printed Acoustic Metamaterials Devices and Applications

6.1 Introduction

This Chapter presents two final projects that apply the techniques developed in previous chapters of this thesis to acoustic and audio devices. The first project is a proof-of-concept work on active acoustic metamaterials that will be further developed within our laboratory in the upcoming years. This active acoustic metamaterial consists of a three-dimensional printed Helmholtz resonator having a piezoelectric plate at the bottom of its cavity. Fabricating an active acoustic metamaterial is an opportunity to enable a user to control parameters such as Q factor, to modify the effective damping, and possibly even the stiffness of a system. By providing additional energy, at the right phase, an active acoustic metamaterial will enhance the pressure output from for example a Helmholtz resonator, and increase the out-of-phase acoustic wave resonating in the cavity and destructively interfering with the incoming sound. In the second project, wearable devices such as headphones, or simple ear mufflers, were 3D printed to leverage the properties of acoustic metamaterials to attenuate external noise in chosen frequency bands. Although the use of passive foam in headphones and the addition of active noise cancellation systems represent an efficient and established

way to attenuate noise in wearable devices, some frequency bands - for example between 500 Hz and 2000 Hz - are not successfully covered by the existing noise attenuation techniques [152, 153]. The work here presented proposes to design and fabricate acoustic metamaterials that can be inserted in headsets or other devices to tackle noise attenuation in specific frequency bands. For example, mechanical and electric noise produced by industrial machines, as well as electric devices such as hair dryers, or vacuum machines are usually narrowband.

6.2 Three-Dimensional Printed Printed Active Acoustic Metamaterials

Introduction

Although the nature of the work here presented is mainly experimental, the thin plates models developed in Chapter 5 have been used as a reference for the initial design. The concept of active acoustic metamaterials has become increasingly popular in recent years [41, 154, 155]. Changing the band gap position can be a convenient property in applications that need to attenuate or control sound waves that change frequency over time, such as in headphones, sound barriers, or similar devices that respond to environmental noise. Tuning the band gap is also practical for scalability of production, where for example, acoustic metamaterials could be fabricated in large batches and then tuned once integrated into a specific application. In particular, piezoelectric thin plates have been recently proposed as unit-cells for acoustic metamaterials [119, 156, 157]. Building on these ideas, here we investigate the possibility of three-dimensional printing piezoelectric thin plates that, after poling, can be controlled in real-time. Firstly, an off-the-shelf piezoelectric buzzer embedded in a three-dimensional printed Helmholtz resonator was assembled, controlled in real-time, and measured. This device was used to enhance the attenuation of a Helmholtz resonator at its band gap by driving the piezoelectric stack in phase with the vibration of the resonator. Secondly, we used a 3D printer to fabricate a thin plate and then we manually added silver coating as a conductive layer. The possibility of entirely three-

dimensional printing an active acoustic metamaterial such as a thin plate could pave the way to developing complex active noise-reducing structures that could be tuned to a specific application. This type of acoustic metamaterials would enable the development of new devices, with new shapes and functionalities that were difficult or even impossible to fabricate before. This work was made possible by using new techniques to control the materials and thickness of three-dimensional printed layers [47]. The next sections will discuss methods used to fabricate these unit-cells, models, and results. Finally, a conclusion section will summarise the work and reflect on possible outcomes and future developments.

Methods

A first way to enhance the band gap is to 3D print a Helmholtz resonator and glue it to an off-the-shelf piezoelectric buzzer or stack. As shown in Fig. 6.1, an external driver is set at the band gap frequency of the resonator, in this case, 2200 Hz. A microphone placed on top of the resonator will sense the sound field and measure the band gap, as displayed through an oscilloscope or similar visualisation method. The piezoelectric buzzer is driven at the band gap frequency, and its phase is iteratively changed until the signal measured by the microphone on top of the resonator is minimised. To better control the band gap, a custom real-time algorithm is implemented using the framework JUCE, based on C++. JUCE is an open-source cross-platform framework that is used to rapidly prototype desktop and mobile applications. This framework allows to control the signal in real-time and is preferred to others due to the low latency required for this experiment. The developed user interface is shown in Fig. 6.2.

Next, as shown in Fig. 6.3, the off-the-shelf piezoelectric buzzer is substituted with a 3D printed piezoelectric thin plate with silver paint sprayed on top. The plate has been fabricated with the same techniques and specifications described in Chapter 5. The piezoelectric properties are obtained by adding 50% BaTiO₃ to the mix and by exposing the thin plate to poling for several hours. Poling is done by applying 10kV / mm to the 3D printed sample, and its main function is to align dipoles that are randomly oriented. After poling, the piezoelectric properties of the sample can be used and the sample can function as a sensor or

6.2. Three-Dimensional Printed Printed Active Acoustic Metamaterials

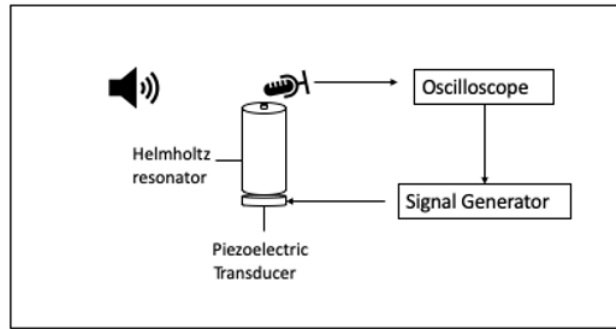


Figure 6.1: Setup used to measure the response of the Helmholtz resonator and to drive the piezoelectric transducer in phase with the signal.



Figure 6.2: User Interface developed to measure the signal and control the phase and frequency of piezoelectric transducer in real-time.

6.2. Three-Dimensional Printed Printed Active Acoustic Metamaterials

as an actuator.

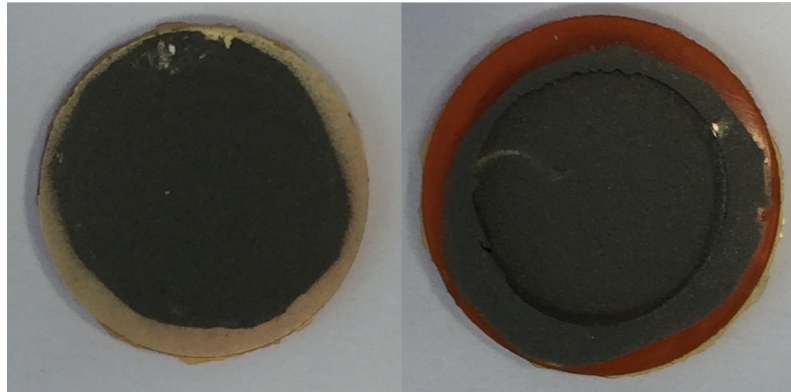


Figure 6.3: Front (left) and bottom (right) picture of a three-dimensional printed piezoelectric thin-plate with silver paint sprayed on top.

Results

The results in Fig. 6.4 show that it is possible to enhance the band gap of a simple passive Helmholtz resonator up to 4 dB (peak measurement), when driving an off-the-shelf piezoelectric transducer in phase with the resonator. The blue continuous line in Fig. 6.4 represents the measured transmission amplitude of a passive Helmholtz resonator when the plate situated at its base is not active. The blue starred line highlights the band gap created by this passive device. The read line show that when the piezoelectric buzzer is active and its phase is controlled to be in-phase with the natural vibration of the resonator it is possible to enhance the depth of the band gap by 4 dB.

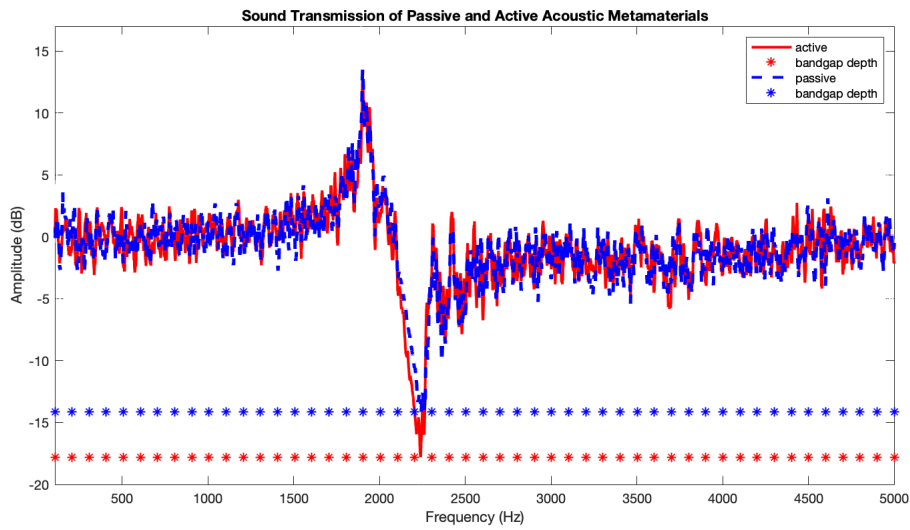


Figure 6.4: Measured transmission for simple passive Helmholtz resonator (blue) and active metamaterial (red) composed of a Helmholtz resonator and an active piezoelectric stack. The active metamaterial has a 4 dB deeper band gap, i.e. enhanced noise attenuation.

6.3 3D Printed Quiet Headphones Based on Acoustic Metamaterials

Introduction

The second project presented in this Chapter presents the development of portable devices such as headphones or ear mufflers based on acoustic metamaterials designed in the previous chapters of this thesis. By designing and fabricating these wearable devices we aim to tackle the problem of attenuation of acoustic noise, an unresolved engineering challenge, that has a negative effect on the population health and wellbeing. Active noise cancellation is effective for low frequency – generally up to 500 Hz - steady noise such as traffic noise in roads and airplanes and is based on the waves interference principle. Foams usually address higher frequencies, by absorbing the incoming external sound waves and at the same time they avoid the reflection of waves between the speaker and the eardrum. The absorption property of foams do not provide complete acoustic insulation, since - according to the mass-law - the transmission of sound is inversely

6.3. 3D Printed Quiet Headphones Based on Acoustic Metamaterials

proportional to the thickness, density and frequency of the wave. In this project, headphones and ear mufflers devices based on acoustic metamaterials are designed to improve the noise cancellation properties of traditional headsets. These novel devices leverage the properties of acoustic metamaterials to attenuate external noise in chosen frequency bands. The metamaterials chosen for this project tackle external noise in the frequency band of speech, in particular between 1000 Hz and 3000 Hz. This choice derives from the fact that lower frequencies are already successfully attenuated by active noise cancellation, that fails to successfully cancel higher frequencies. Nevertheless, future versions of this project could cancel the entire audible frequency spectrum, or could address problems such as single high frequency machine noise in work environments. An advantage of headphones based on metamaterials, is that they benefit from the passage of air to cancel the acoustic noise, hence are lighter and breathable. Furthermore, unlike active noise cancellation based devices, the passive mechanism here provided by acoustic metamaterials does not require a source of electricity to work. The technology here presented is scalable and could be included in other audio devices, such as smart speakers or VR headsets.

Methods

The headphones here presented (see Fig. 6.5) are the first proof-of-concept audio device. In this first version, the ear cup of the headphones includes metamaterials based on Helmholtz resonators. The geometry of the Helmholtz resonators has been designed to obtain a band gap where frequencies are attenuated between 1000 Hz and 3000 Hz. A second band gap at higher frequencies is also expected. Different meta-atoms geometries have been tried during the design process to tackle different frequency bands, and in this Chapter we present a first version where speech frequencies are attenuated. Other designs could for example use membranes as meta-atoms instead of Helmholtz resonators, which would result in a thinner product. After placing the metamaterials inside the headphones, a standard inset containing a loudspeaker is inserted in both ear cups, that are connected by a headband (see Fig. 6.6). While the casing of the headphones has been fabricated via Fusion Deposition Modelling 3D printers, the metamaterials fabrication necessitates of a more accurate and finer 3D printing fabrication

6.3. 3D Printed Quiet Headphones Based on Acoustic Metamaterials

method based on stereolithography.



Figure 6.5: Headphones based on acoustic metamaterials.

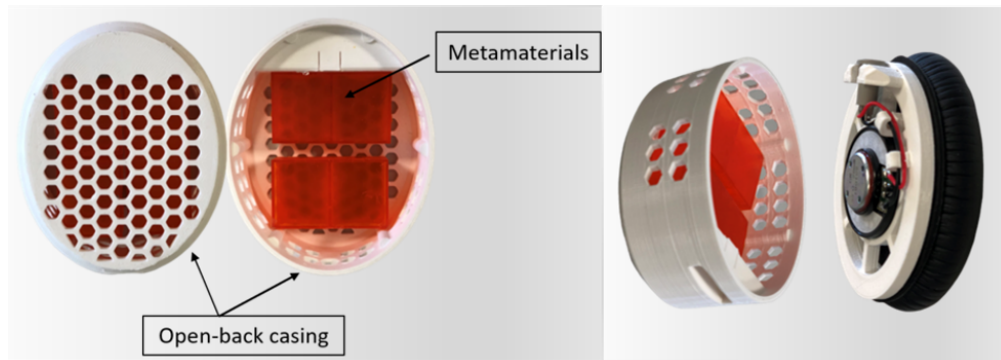


Figure 6.6: Cut-through view of headphones based on acoustic metamaterials.

To test the effect of metamaterials on external noise, two types of measurements have been employed. The first test is an open-field measurement (see Fig. 6.7) obtained inside an acoustic booth by placing a microphone near the inner side of the headphone while a loudspeaker plays a chirp in the audible frequency range. This was a preliminary test to check the correct position of the band gap. The attenuation effects could be lower in this case, because of the open-field condition. In the second test, the headphones have been placed on a B&K Head &

6.3. 3D Printed Quiet Headphones Based on Acoustic Metamaterials

Torso Simulator (HATS), equipped with a $\frac{1}{2}$ " B&K microphone and standard-size pinna, while a pink noise signal in the audible frequency range was played by a loudspeaker (see Fig. 6.8). In both cases, the effect of metamaterials was tested by measuring the headphones with and without the metamaterials and by comparing the two results. Ear muffers – i.e. headphones without the loudspeakers – have also been tested in both cases.

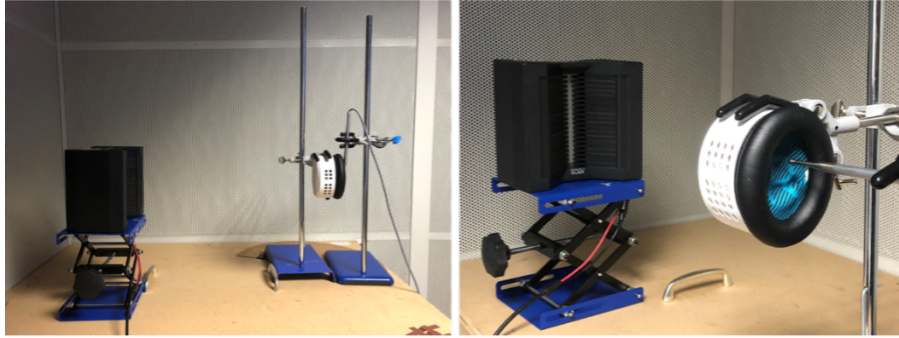


Figure 6.7: Free-field measurement of noise attenuation properties of headphones based on acoustic metamaterials.

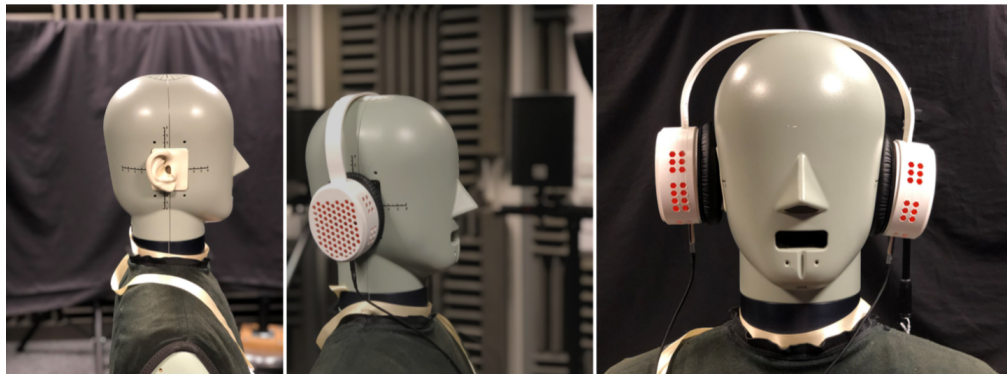


Figure 6.8: Head and torso simulator measurement of noise attenuation properties of headphones based on acoustic metamaterials.

Results

The measurements of noise attenuation by headphones based on acoustic metamaterials described in the previous section show that it is possible to attenuate external noise at chosen frequency bands. Specifically, free-field

6.3. 3D Printed Quiet Headphones Based on Acoustic Metamaterials

measurements conducted in the acoustic booth showed that it was possible to attenuate noise up to 4 dB in a frequency range where most speech frequencies are located and also at higher frequencies (see Fig. 6.9). By measuring the noise attenuation in a more realistic scenario, i.e. by placing the headphones on a B&K Head & Torso Simulator inside an acoustic booth, it was possible to show that the wanted frequency range corresponding to the speech frequency band external noise was attenuated up to 10 dB. Higher frequencies were also attenuated up to 20 dB (see Fig. 6.10).

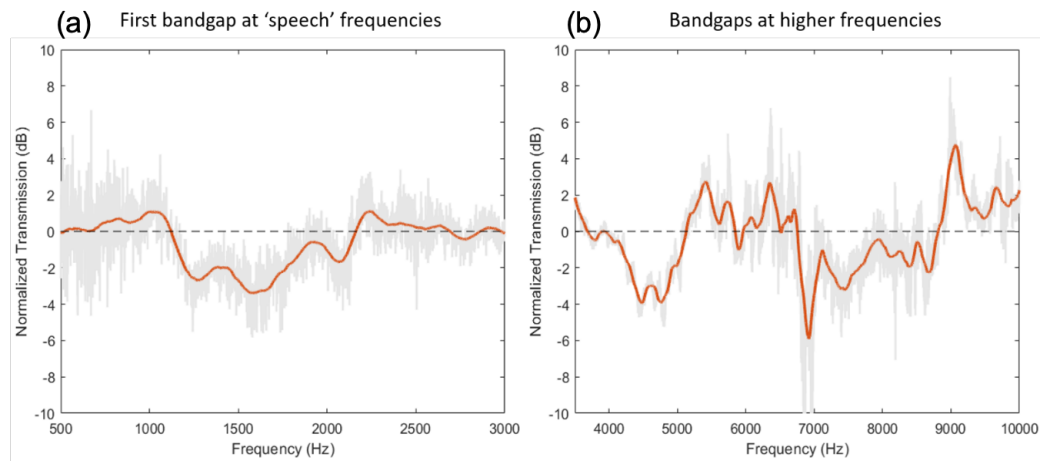


Figure 6.9: Free-field sound transmission of headphones based on acoustic metamaterials measured in acoustic booth. A frequency band around the speech frequencies shows that it is possible to attenuate noise up to 4 dB in this region (a). Higher frequency bands are also attenuated due to overtones of the resonant meta-atoms (b).

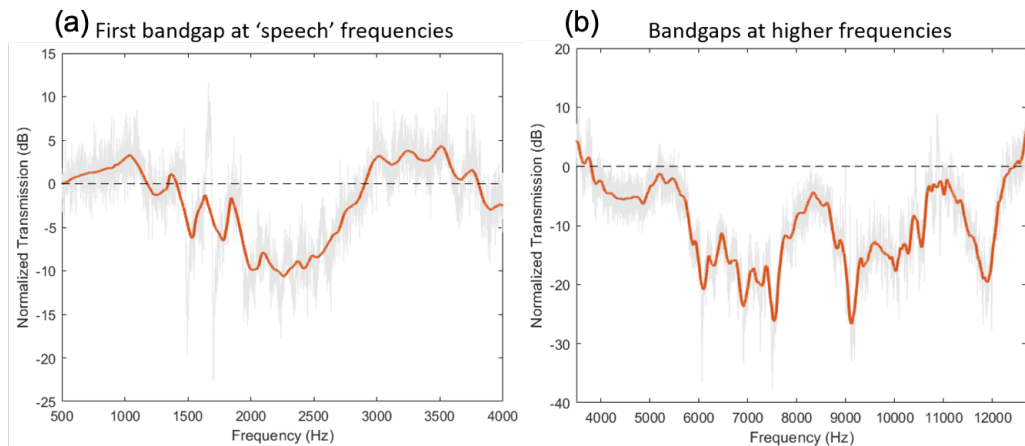


Figure 6.10: Sound transmission of headphones based on acoustic metamaterials placed on a B&K Head & Torso Simulator inside an acoustic booth. A frequency band around the speech frequencies shows that it is possible to attenuate noise up to 10 dB in this region (a). Higher frequency bands are also attenuated up to 20 dB due to overtones of the resonant meta-atoms (b).

6.4 Conclusion and Future Work

This Chapter presented two applications of acoustic metamaterials. The first application was an active acoustic metamaterial made of Helmholtz resonators and piezoelectric plates. The second application was a headset wearable device based on acoustic metamaterials.

Active acoustic metamaterials made it possible to enhance the attenuation of a Helmholtz resonator at its band gap by 4 dB. This result was obtained by driving a piezoelectric stack situated at the base of the resonator in phase with the vibration of the resonator. A setup made of an oscilloscope, a function generator, and an external microphone was used to manually find the phase that minimised the measured signal on top of the resonator. A real-time algorithm was also developed in C++ to obtain the same results. A piezoelectric thin plate with added silver paint was also three-dimensional printed as proof-of-concept for new types of active acoustic metamaterial. Future work will focus on further improving the real-time algorithm to automatically match the phase of the transducer without a manual search. A feedback loop could be employed to match the phase automatically. Specifically, a piezoelectric transducer with at

least two ports would make it possible to leverage a feedback loop. The design of a new device with two electrically independent and mechanically coupled ports could be three-dimensional printed to build a full system.

The first headphones based on acoustic metamaterials were designed and fabricated. It was possible to attenuate noise up to 10 dB in the ‘speech’ frequency spectrum. Higher frequency band gaps reached up to 20 dB noise attenuation. This result was achieved thanks to an open-back design and to acoustic metamaterials based on Helmholtz resonators. The properties of metamaterials make it possible to achieve noise attenuation in the subwavelength scale, using lightweight materials and allow the passage of air, in contrast with traditional passive attenuation methods. Future work could optimise the results as well as tackle other frequency bands. A switch mechanism could be added to the design to enable or disable noise attenuation. A user study could be designed to test the perception of noise attenuation in listeners. Other metamaterial types such as membranes or resonators with different geometries and shapes could be used in future versions. In the future, headphones and ear muffers designs could entirely rely on metamaterials to attenuate external noise as well as on hybrid solutions including active noise cancellation, foams and metamaterials. This idea is scalable to other technologies, such as smart speakers, VR headsets, sound-bars, TVs, IoT and smart devices.

Chapter 7

Conclusion and Future Work

Over the last few years, we have witnessed rapid advances in the field of acoustic metamaterials for noise control. Initially predicted by Veselago in 1968 within electromagnetism, metamaterials are a class of materials that present unusual properties different from those of conventional materials. In the field of acoustics, phononic crystals had first been proposed as a new way to attenuate noise by leveraging the Bragg scattering effect that reduced noise at wavelengths of the same order of the distance between periodically arranged rods or structures. Acoustic metamaterials, initially developed in 2000 by Liu, can control sound at a subwavelength scale, thanks to the change of phase near the resonances of unit-cells. Since the work of Liu, the field of acoustic metamaterials has rapidly expanded, and researchers have proposed numerous options for resonant unit-cells, introduced new models to predict sound transmission, and conducted experimental work that shows how to control sound. In particular, noise control could greatly benefit from the use of new techniques. Noise is a significant public hazard and affects the well-being and health of the population. These promising new sound control techniques could be applied to attenuate noise at the source, such as in pieces of machinery, during the propagation path by building better noise barriers and the receiver side by improving noise cancellation in ear-mufflers and headphones.

Despite significant advances, only a few products, such as sound reducing metamaterials in automobiles, have been integrated into real-world products.

For example, the automobile producer Nissan [158] presented a new car cabins design that integrated acoustic metamaterials weighing one-fourth of traditional materials and providing the same degree of sound isolation in the 500 - 1200 Hz regime. One reason for the lack of acoustic metamaterials in industrial applications might be the difficulty of fabricating abstract shapes and complex unit-cells in university laboratories. The development of new three-dimensional printing techniques that can facilitate the fabrication of resonant structures such as thin membranes and resonators could be the first step to solve this challenge. Furthermore, narrowing the research to specific applications starting at the modelling and design stage could also facilitate the process of integrating more acoustic metamaterials in everyday life. This thesis presented new ways to three-dimensional printing unit-cells for acoustic metamaterials. Its primary focus was to apply these methods to small-scale applications such as headphones, hearing aids, smart speakers, and electroacoustic devices. The automotive and aerospace industries could also benefit from these techniques due to their requirements for low-weight and thin structures for noise control.

In Chapter 4, we have designed, three-dimensional printed, and measured acoustic metamaterials based on small-scale Helmholtz resonators. We have shown that, in the free-field, an increasing number of unit-cells corresponds to a deeper band gap. The maximum attenuation in the band gap was -25 dB in a 6×6 array. By changing the position of a loudspeaker with a robotic arm we showed that this effect was mostly independent from the source's location. We have also presented a new design that leverages the first overtone of Helmholtz resonators to obtain a hybridisation band gap - up to 2000 Hz broad - between the band gap near the fundamental resonance and the band gap near the first overtone. The position of the hybridisation band gap can be predicted by a parametric model and it was situated between mid and high audible frequencies range. A second way to enhance the band gap was shown experimentally by three-dimensional printing Helmholtz resonators with embedded thin plates. This complex structure was made possible by advanced and novel active manufacturing techniques. The dimensions of the unit-cells were chosen to fit small-scale applications.

In Chapter 5, we have further developed techniques for three-dimensional printing

thin plates, with a thickness between 20 μm and 100 μm . By fabricating very thin layers, it was possible to obtain thin plates with a small radius, having a fundamental resonance at low frequencies, between 300 Hz and 900 Hz. This is a desirable geometry for applications that want to tackle low-frequency noise control and require low-weight attenuating materials. The thin plates were modelled using the transfer matrix method. Their material parameters and absorption, reflection, and transmission coefficients were characterised using an impedance tube. Other characterisation methods were used to highlight other properties: a 3D laser Doppler vibrometer showed the vibration modes, nanoindentation further characterised material parameters, and scanning electron microscopy was used to study the distribution of particles in the three-dimensional printed material.

In Chapter 6, we have presented two devices that apply acoustic metamaterials to real-world scenarios. In the first project, we experimentally investigated the use of piezoelectric sensors as unit-cells. Firstly, an off-the-shelf piezoelectric buzzer was glued at the base of a Helmholtz resonator. By manually controlling the phase of the piezoelectric buzzer driven at the same frequency as the Helmholtz resonator's resonance it was possible to enhance the band gap by 4 dB. Secondly, a piezoelectric thin plate was 3D printed by applying the techniques developed in the previous Chapter. After poling and applying silver paste and attaching electrodes it was possible to show that the plate could be used as a sensor or actuator. This proof-of-concept could be further developed to build a fully three-dimensional printed active acoustic metamaterial, tunable in real-time. In the second project, a prototype of headphones based on acoustic metamaterials was fabricated by using three-dimensional printing technology and assembled to include off-the-shelf loudspeakers. It was possible to attenuate external noise up to 10 dB in the frequency range between 1000 and 3000 Hz which is usually difficult to tackle with traditional noise attenuation techniques.

In summary, in this thesis, we have applied a novel additive manufacturing fabrication technique to the fabrication of acoustic metamaterials. The principal unit-cells used in this work were small-scale Helmholtz resonators, thin plates, and piezoelectric buzzers. We have also shown that more complex structures,

such as thin plates embedded in Helmholtz resonators and piezoelectric active plates, can be fabricated in one print via additive manufacturing. These complex structures are able to improve the peak attenuation of the band gaps without increasing the dimensions of a simple unit-cell. Two final prototypes have been fabricated to apply these techniques to real-world devices. We hope that this research will contribute to advancing the field of acoustic metamaterials and to the development of new ways to attenuate noise in acoustic devices, such as headphones, smart speakers, in the automotive industry and the aerospace industry.

Finally, it is useful to reflect on future work beyond this dissertation. Despite recent rapid advancement in the field of acoustic metamaterials, many challenges remain. Some of these challenges are highlighted as follows [39, 40, 159]:

- As discussed throughout this dissertation, it has become clear that starting from an application can be an advantage in the process of integrating acoustic metamaterials in industrial products. One way to do so is to define a type of product or set of devices that require improvements in dealing with noise control. Next, a study of geometrical constraints, weight, and materials requirements can help select the type of resonator that forms the unit-cell.
- Models should be able to predict the position of band gaps and evaluate the sound transmission loss of acoustic metamaterials when inserted in products. This would require knowledge and modelling of the device where the metamaterial is inserted. Furthermore, the development of new optimisation methods to maximise noise attenuation is also crucial in the modelling phase.
- From a fabrication point of view, developing reliable techniques to scale the production of metamaterials is essential. Three-dimensional printing technology is offering new exciting solutions to these challenges. However, improvements need to be made to control the fabrication process and make it easier and economically affordable to research labs to rapidly prototype complex shapes.

- Similarly to models, also experimental setups should reflect the real-world scenario where the metamaterials will be integrated. In the case of noise attenuation for hearing protection, psychoacoustic techniques that evaluate the effectiveness of acoustic metamaterials and subjective measurements should be developed and compared to objective measurements.
- Finally, particular attention should be focused on the use of sustainable materials. As acoustic metamaterials can control acoustic waves in new ways, it is essential to rethink the list of common materials used in traditional noise attenuation techniques and to offer a new sustainable alternative. Although current 3D printers are mainly fabricating plastics and polymers, great advances have been presented in the field of 3D printable sustainable materials and it is a topic worth investigating in order to successfully redesign sustainable noise attenuators.

To realise further progress, it is these sets of challenges that we should focus on next.

Appendix A

APPENDIX

A.1 MATLAB Codes for Parametric Models of Helmholtz Resonators

```
1 close all
2 clear all
3 clc
4
5 %%%%%%%%%%% PARAMETRIC STUDY - HELMHOLTZ RESONATORS %%%%%%%%%%%
6 %
7 % This code plots the first and second resonance of Helmholtz
8 % resonators. Four geometrical parameters
9 % are varied across different values. These four parameters are
10 % height of the cavity, radius of the cavity, length of the neck
11 % and radius of the neck. Each set of permutations of two varying
12 % parameters is plotted and the two remaining parameters are fixed.
13 %
14 % The second section of this code optimizes the choice of fixed
15 % parameters by selecting the values that maximize the distance
16 % between f0 and f1.
17 %
18 %%%%%%%%%%%
19
20 %% Non Parametric Code for Helmholtz Resonator Resonances
21
```

A.1. MATLAB Codes for Parametric Models of Helmholtz Resonators

```
22 %~~~~~Parameters~~~~~%
23
24 % Neck radius (m)
25 r_n = 0.0023; % p4 (0.0005 - 0.004)
26
27 % Neck length (m)
28 l_n = 0.0015; % p3 (0.0005 - 0.0025)
29
30 % Cavity radius (m)
31 r_c = 0.0055; % p2 (0.001 - 0.01)
32
33 % Cavity height (m)
34 h_c = 0.0275; % p1 (0.005 - 0.05)
35
36 % Effective length parameter
37 D1 = 1.7; % fundamental frequency
38 D2 = 0.6; % first overtone
39
40 % Speed of sound (m/s)
41 c = 343;
42
43 %~~~~~Derived values~~~~~%
44
45 % Derived cavity volume
46 V = (r_c.^2*pi.*h_c);
47
48 % Derived neck cross sectional area
49 S = (r_n.^2*pi);
50
51 % Derived effective neck length
52 L = (l_n+D1.*r_n);
53
54 % Derived effective cavity length
55 H = (h_c+D2.*r_c);
56
57 %~~~~~Resonant Frequency~~~~~%
58
59 f0 = (c/(2*pi))*sqrt(S./(V.*L));
60 f0 = round(f0);
61 fprintf('The resonance frequency is at %f Hz\n', f0);
62
```

A.1. MATLAB Codes for Parametric Models of Helmholtz Resonators

```
63 f1 = c/(4*(h_c+D2.*r_c));
64 fprintf('The overtone is at %f Hz\n', f1);
65
66 %% Parametric Code for Helmholtz Resonator Resonances
67
68 % f0 function
69 f0 = @(h_c,r_c,l_n,r_n)((c/(2*pi))*sqrt((r_n.^2*pi)./((r_c.^2*...
70     pi.*h_c).*(l_n+D1.*r_n))));
71
72 % f1 function
73 f1 = @(h_c,r_c,l_n,r_n)(c./(4*(h_c+D2.*r_c)));
74
75 % Fixed values (mid vector)
76 h_c_fix = h_c;
77 r_c_fix = r_c;
78 l_n_fix = l_n;
79 r_n_fix = r_n;
80
81 % Resonances f0 and f1
82 f0_fix = (c/(2*pi))*sqrt((r_n_fix.^2*pi)./((r_c_fix.^2*pi.*...
83     h_c_fix).*(l_n_fix+D1.*r_n_fix)));
84 f1_fix = c./(4*(h_c_fix+D2.*(r_c_fix)));
85
86 % Number of points in vectors
87 tot = 100;
88
89 % Vectors of possible values
90 h_c_v = linspace(0.005, 0.05,tot);
91 r_c_v = linspace(0.001, 0.01,tot);
92 l_n_v = linspace(0.0005, 0.0025,tot);
93 r_n_v = linspace(0.0005, 0.004,tot);
94
95 % Plot
96 figure()
97
98 subplot(3,2,1)
99
100 [H_C_V,R_C_V] = meshgrid(h_c_v,r_c_v);
101 [p1p2_0, h0] = contour(H_C_V,R_C_V,f0(H_C_V,R_C_V,l_n_fix, r_n_fix));
102 h0.LineWidth = 2;
103 clabel(p1p2_0, h0);
```

A.1. MATLAB Codes for Parametric Models of Helmholtz Resonators

```
104 caxis([500 10000]);
105 xlabel('Cavity Height (m)');
106 ylabel('Cavity Radius (m)');
107 t = title('(a)
    ', 'FontSize', 11);
108
109 hold on
110 [p1p2_1, h1] = contour(H_C_V,R_C_V,f1(H_C_V,R_C_V,l_n-fix, r_n-fix));
111 h1.LineWidth = 3;
112 h1.LineStyle = '--';
113 clabel(p1p2_1, h1);
114 caxis([500 10000]);
115 legend('f_0','f_1');
116
117 subplot(3,2,2)
118
119 [H_C_V,L_N_V] = meshgrid(h_c_v,l_n-v);
120 [p1p2_0, h0] = contour(H_C_V,L_N_V,f0(H_C_V,r_c-fix, L_N_V, r_n-fix));
121 h0.LineWidth = 2;
122 clabel(p1p2_0, h0);
123 caxis([500 10000]);
124 xlabel('Cavity Height (m)');
125 ylabel('Neck Height (m)');
126 t = title('(b)
    ', 'FontSize', 11);
127
128 hold on
129 [p1p2_1, h1] = contour(H_C_V,L_N_V,f1(H_C_V,r_c-fix, L_N_V, r_n-fix));
130 h1.LineWidth = 3;
131 h1.LineStyle = '--';
132 clabel(p1p2_1, h1);
133 caxis([500 10000]);
134 legend('f_0','f_1');
135
136 subplot(3,2,3)
137
138 [H_C_V,R_N_V] = meshgrid(h_c_v,r_n-v);
139 [p1p2_0, h0] = contour(H_C_V,R_N_V,f0(H_C_V,r_c-fix, l_n-fix, R_N_V));
140 h0.LineWidth = 2;
141 clabel(p1p2_0, h0);
142 caxis([500 10000]);
```


A.1. MATLAB Codes for Parametric Models of Helmholtz Resonators

```
143 xlabel('Cavity Height (m)');
144 ylabel('Neck Radius (m)');
145 t = title(' (c)
    ', 'FontSize', 11);
146
147 hold on
148 [p1p2_1, h1] = contour(H_C_V,R_N_V,f1(H_C_V,r_c_fix, l_n_fix, R_N_V));
149 h1.LineWidth = 3;
150 h1.LineStyle = '--';
151 clabel(p1p2_1, h1);
152 caxis([500 10000]);
153 legend('f_0','f_1');
154
155 subplot(3,2,4)
156
157 [R_C_V,L_N_V] = meshgrid(r_c_v,l_n_v);
158 [p1p2_0, h0] = contour(R_C_V,L_N_V,f0(h_c_fix,R_C_V, L_N_V, r_n_fix));
159 h0.LineWidth = 2;
160 clabel(p1p2_0, h0);
161 caxis([500 10000]);
162 xlabel('Cavity Radius (m)');
163 ylabel('Neck Height (m)');
164 t = title(' (d)
    ', 'FontSize', 11);
165
166
167 hold on
168 [p1p2_1, h1] = contour(R_C_V,L_N_V,f1(h_c_fix,R_C_V, L_N_V, r_n_fix));
169 h1.LineWidth = 3;
170 h1.LineStyle = '--';
171 clabel(p1p2_1, h1);
172 caxis([500 10000]);
173 legend('f_0','f_1');
174
175 subplot(3,2,5)
176
177 [R_C_V,R_N_V] = meshgrid(r_c_v,r_n_v);
178 [p1p2_0, h0] = contour(R_C_V,R_N_V,f0(h_c_fix,R_C_V, l_n_fix, R_N_V));
179 h0.LineWidth = 2;
180 clabel(p1p2_0, h0);
181 caxis([500 10000]);
```

A.1. MATLAB Codes for Parametric Models of Helmholtz Resonators

```
182 xlabel('Cavity Radius (m)');
183 ylabel('Neck Radius (m)');
184 t = title('e)
      ', 'FontSize', 11);
185
186 hold on
187 [p1p2_1, h1] = contour(R_C_V,R_N_V,f1(h_c_fix,R_C_V, l_n_fix, R_N_V));
188 h1.LineWidth = 3;
189 h1.LineStyle = '--';
190 clabel(p1p2_1, h1);
191 caxis([500 10000]);
192 legend('f_0','f_1');
193
194 subplot(3,2,6)
195
196 [L_N_V,R_N_V] = meshgrid(l_n_v,r_n_v);
197 [p1p2_0, h0] = contour(L_N_V,R_N_V,f0(h_c_fix,r_c_fix, L_N_V, R_N_V));
198 h0.LineWidth = 2;
199 clabel(p1p2_0, h0);
200 caxis([500 10000]);
201 xlabel('Neck Height (m)');
202 ylabel('Neck Radius (m)');
203 t = title('f)
      ', 'FontSize', 11);
204
205 % hold on
206 % [p1p2_1, h1] = contour(L_N_V,W_N_V,f1(h_c_fix,r_c_fix, L_N_V, R_N_V));
207 % h1.LineWidth = 3;
208 % h1.LineStyle = '--';
209 % clabel(p1p2_1, h1);
210 caxis([500 10000]);
211 legend('f_0, (f_1 = 2784 Hz)');
212
213 %suptitle('Parametric Evaluation of Resonance f_0...
214 %and First Overtone f_1');
215
216
217 %% Optimization for Maximum Distance between f0 and f1
218
219 Z_opt = 2;
220 Z_opt_old = 0;
```

A.1. MATLAB Codes for Parametric Models of Helmholtz Resonators

```
221 k = 0;
222
223 while Z_opt-Z_opt_old>1e-5
224
225     Z_opt_old = Z_opt;
226     [X1,X2,X3,X4] = ndgrid(h_c_v,r_c_v,l_n_v,r_n_v);
227     Y0 = f0(X1,X2,X3,X4);
228     Y1 = f1(X1,X2,X3,X4);
229     Z = Y1-Y0;
230     [Z_opt,idx] = max(Z(:));
231     if sum(Z==max(Z(:)))>1
232         fprintf('Caution! Multiple values found!');
233     end
234     [i1,i2,i3,i4] = ind2sub(size(Z),idx);
235     h_c_opt = h_c_v(i1)
236     r_c_opt = r_c_v(i2)
237     l_n_opt = l_n_v(i3)
238     r_n_opt = r_n_v(i4)
239     f0_opt = f0(h_c_opt,r_c_opt,l_n_opt,r_n_opt);
240     f1_opt = f1(h_c_opt,r_c_opt,l_n_opt,r_n_opt);
241
242     h_c_v = linspace(h_c_v(max(i1-2,1)),h_c_v(min(i1+2,tot)),tot);
243     r_c_v = linspace(r_c_v(max(i2-2,1)),r_c_v(min(i2+2,tot)),tot);
244     l_n_v = linspace(l_n_v(max(i3-2,1)),l_n_v(min(i3+2,tot)),tot);
245     r_n_v = linspace(r_n_v(max(i4-2,1)),r_n_v(min(i4+2,tot)),tot);
246     k = k+1;
247     fprintf('\n %d - %f \n',k,Z_opt)
248 end
249
250 h_c_fix = h_c_opt;
251 r_c_fix = r_c_opt;
252 l_n_fix = l_n_opt;
253 r_n_fix = r_n_opt;
254
255 % Vectors of possible values
256 h_c_v = linspace(0.005, 0.05,tot);
257 r_c_v = linspace(0.001, 0.01,tot);
258 l_n_v = linspace(0.0005, 0.0025,tot);
259 r_n_v = linspace(0.0005, 0.004,tot);
260
261 f1_fix_opt = c./(4*(h_c_fix+D2.*(r_c_fix)));
```

A.1. MATLAB Codes for Parametric Models of Helmholtz Resonators

```
262 f0_fix_opt = (c/(2*pi))*sqrt((r_n_fix.^2*pi)./...
263     ((r_c_fix.^2*pi.*h_c_fix).*(l_n_fix+Dl.*r_n_fix)));
264
265 % Plot
266 figure()
267
268 subplot(3,2,1)
269
270 [H_C_V,R_C_V] = meshgrid(h_c_v,r_c_v);
271 [p1p2_0, h0] = contour(H_C_V,R_C_V,f0(H_C_V,R_C_V,l_n_fix, r_n_fix));
272 h0.LineWidth = 2;
273 clabel(p1p2_0, h0);
274 caxis([500 10000]);
275 xlabel('Cavity Height (m)');
276 ylabel('Cavity Radius (m)');
277
278 hold on
279 [p1p2_1, h1] = contour(H_C_V,R_C_V,f1(H_C_V,R_C_V,l_n_fix, r_n_fix));
280 h1.LineWidth = 3;
281 h1.LineStyle = '--';
282 clabel(p1p2_1, h1);
283 caxis([500 10000]);
284 legend('f_0','f_1');
285 t = title('a)
    ', 'FontSize', 11);
286
287 subplot(3,2,2)
288
289 [H_C_V,L_N_V] = meshgrid(h_c_v,l_n_v);
290 [p1p2_0, h0] = contour(H_C_V,L_N_V,f0(H_C_V,r_c_fix, L_N_V, r_n_fix));
291 h0.LineWidth = 2;
292 clabel(p1p2_0, h0);
293 caxis([500 10000]);
294 xlabel('Cavity Height (m)');
295 ylabel('Neck Height (m)');
296
297 hold on
298 [p1p2_1, h1] = contour(H_C_V,L_N_V,f1(H_C_V,r_c_fix, L_N_V, r_n_fix));
299 h1.LineWidth = 3;
300 h1.LineStyle = '--';
301 clabel(p1p2_1, h1);
```

A.1. MATLAB Codes for Parametric Models of Helmholtz Resonators

```
302 caxis([500 10000]);
303 legend('f_0','f_1');
304 t = title(' (b)
      ', 'FontSize', 11);
305
306 subplot(3,2,3)
307
308 [H-C-V,W-N-V] = meshgrid(h-c-v,r-n-v);
309 [p1p2_0, h0] = contour(H-C-V,W-N-V,f0(H-C-V,r-c-fix, l-n-fix, W-N-V));
310 h0.LineWidth = 2;
311 clabel(p1p2_0, h0);
312 caxis([500 10000]);
313 xlabel('Cavity Height (m)');
314 ylabel('Neck Radius (m)');
315
316 hold on
317 [p1p2_1, h1] = contour(H-C-V,W-N-V,f1(H-C-V,r-c-fix, l-n-fix, W-N-V));
318 h1.LineWidth = 3;
319 h1.LineStyle = '--';
320 clabel(p1p2_1, h1);
321 caxis([500 10000]);
322 legend('f_0','f_1');
323 t = title(' (c)
      ', 'FontSize', 11);
324
325 subplot(3,2,4)
326
327 [R-C-V,L-N-V] = meshgrid(r-c-v,l-n-v);
328 [p1p2_0, h0] = contour(R-C-V,L-N-V,f0(h-c-fix,R-C-V, L-N-V, r-n-fix));
329 h0.LineWidth = 2;
330 clabel(p1p2_0, h0);
331 caxis([500 10000]);
332 xlabel('Cavity Radius (m)');
333 ylabel('Neck Height (m)');
334
335 hold on
336 [p1p2_1, h1] = contour(R-C-V,L-N-V,f1(h-c-fix,R-C-V, L-N-V, r-n-fix));
337 h1.LineWidth = 3;
338 h1.LineStyle = '--';
339 clabel(p1p2_1, h1);
340 caxis([500 10000]);
```

A.1. MATLAB Codes for Parametric Models of Helmholtz Resonators

```
341 legend('f_0','f_1');
342 t = title('(d)
      ', 'FontSize', 11);
343
344
345 subplot(3,2,5)
346
347 [R-C-V,W-N-V] = meshgrid(r-c-v,r-n-v);
348 [p1p2_0, h0] = contour(R-C-V,W-N-V,f0(h-c-fix,R-C-V, l-n-fix, W-N-V));
349 h0.LineWidth = 2;
350 clabel(p1p2_0, h0);
351 caxis([500 10000]);
352 xlabel('Cavity Radius (m)');
353 ylabel('Neck Radius (m)');
354
355 hold on
356 [p1p2_1, h1] = contour(R-C-V,W-N-V,f1(h-c-fix,R-C-V, l-n-fix, W-N-V));
357 h1.LineWidth = 3;
358 h1.LineStyle = '--';
359 clabel(p1p2_1, h1);
360 caxis([500 10000]);
361 legend('f_0','f_1');
362 t = title('(e)
      ', 'FontSize', 11);
363
364 subplot(3,2,6)
365
366 [L-N-V,W-N-V] = meshgrid(l-n-v,r-n-v);
367 [p1p2_0, h0] = contour(L-N-V,W-N-V,f0(h-c-fix,r-c-fix, L-N-V, W-N-V));
368 h0.LineWidth = 2;
369 clabel(p1p2_0, h0);
370 caxis([500 10000]);
371 xlabel('Neck Height (m)');
372 ylabel('Neck Radius (m)');
373 t = title('(f)
      ', 'FontSize', 11);
374 % hold on
375 % [p1p2_1, h1] = contour(L-N-V,W-N-V,f1(h-c-fix,r-cdouble-fix,...
376 %L-N-V, W-N-V));
377 % h1.LineWidth = 3;
378 % h1.LineStyle = '--';
```

A.2. MATLAB Codes for Parametric Models of Thin Plates

```
379 % clabel(plp2_1, h1);
380 caxis([500 10000]);
381 legend('f0 (f1 = 13445 Hz)');
382
383 %suptitle('Optimized Parametric Evaluation of Resonance ...
384 %f0 and First Overtone f1');
```

A.2 MATLAB Codes for Parametric Models of Thin Plates

```
1 clear all
2 close all
3 clc
4
5 %%%%%%%%%%% PARAMETRIC STUDY - THIN PLATES %%%%%%%%%%%
6 %
7 % This code plots the first mode of vibration of thin plates.
8 % Geometrical and material parameters are varied across
9 % different values. These five parameters are Youngs Modulus,
10 % Density, Poissons Ratio, Thickness and Radius of a circular
11 % thin plate. Each set of permutations of two varying
12 % parameters is plotted and the three remaining parameters are fixed.
13 %
14 % The second section of this code optimizes the choice of fixed
15 % parameters by selecting the values according to different criteria.
16 % The first optimization aims to maximize the value of f0. The second
17 % aims to obtain f0 within mid frequency range. The third minimizes f0.
18 % The fourth model optimizes f0 to be in the speech frequency range.
19 %
20 %%%%%%%%%%%
21
22 %% %%%%%%%%%%% Parameters %%%%%%%%%%%
23
24 % Young's Modulus
25 E_v_fix = 200*10^6;
26 E_v = linspace(1*10^6, 1*10^9, 50);
27 % loss=0.05;
28 % E = 200*10^7*(1+1i*loss);
```

A.2. MATLAB Codes for Parametric Models of Thin Plates

```

29
30 % Density
31 rho_fix = 1180;
32 rho = linspace(1000, 3000, 50); % Kg/m^3
33
34 % Poisson's Ratio
35 nu_fix = 0.35;
36 nu = linspace(0.3, 0.5, 50);
37
38 % Thickness
39 d_fix = 70*10^(-6); % m
40 d = linspace(20*10^(-6), 0.5*10^(-3), 50);
41
42 % Radius
43 r_fix = 15*10^(-3)/2; % m
44 r = linspace(3*10^(-3), 10*10^(-3), 50);
45
46 % Constant for circular membrane
47 K = 10.22;
48
49
50 %% %%%%%%%%%%% Fixed Formula %%%%%%%%%%%
51
52 %f0 = K*d/(r^2*2*pi)*sqrt(E/(rho*12*(1-nu^2)));
53
54
55 %fprintf('The resonant frequency is %f Hz\n', f0);
56
57 %% %%%%%%%%%%% Parametric Formula %%%%%%%%%%%
58
59 % f0 function
60 f0 = @(E_v, rho, nu, d, r)(K*d./(r.^2*2*pi)...
61     .*sqrt(E_v./(rho*12.*(1-nu.^2))));
62
63
64 %% Plot
65
66 figure()
67
68 subplot(5,2,1)
69

```


A.2. MATLAB Codes for Parametric Models of Thin Plates

```
70 [E-V,RHO] = meshgrid(E-v,rho);
71 [p1p2_0, h0] = contourf(E-V,RHO,f0(E-V,RHO,nu_fix, d_fix, r_fix));
72 h0.LineWidth = 2;
73 clabel(p1p2_0, h0);
74 %caxis([500 3000]);
75 xlabel('Young''s Modulus (Pa)');
76 ylabel('Density (Kg/m^3)');
77 t = title('(a)
    ', 'FontSize', 11);
78 %caxis([500 3000]);
79 %legend('f0 (Hz)');
80
81 subplot(5,2,2)
82
83 [E-V,NU] = meshgrid(E-v,nu);
84 [p1p2_0, h0] = contourf(E-V,NU,f0(E-V,rho_fix,NU, d_fix, r_fix));
85 h0.LineWidth = 2;
86 clabel(p1p2_0, h0);
87 %caxis([500 3000]);
88 xlabel('Young''s Modulus (Pa)');
89 ylabel('Poisson''s Ratio');
90 t = title('(b)
    ', 'FontSize', 11);
91 %caxis([500 3000]);
92 %legend('f0 (Hz)');
93
94 subplot(5,2,3)
95
96 [E-V,D] = meshgrid(E-v,d);
97 [p1p2_0, h0] = contourf(E-V,D,f0(E-V,rho_fix,nu_fix, D, r_fix));
98 h0.LineWidth = 2;
99 clabel(p1p2_0, h0);
100 %caxis([500 3000]);
101 xlabel('Young''s Modulus (Pa)');
102 ylabel('Thickness (m)');
103 t = title('(c)
    ', 'FontSize', 11);
104 %caxis([500 3000]);
105 %legend('f0 (Hz)');
106
107 subplot(5,2,4)
```

A.2. MATLAB Codes for Parametric Models of Thin Plates

```
108
109 [E_V,R] = meshgrid(E_v,r);
110 [p1p2_0, h0] = contourf(E_V,R,f0(E_V,rho_fix,nu_fix, d_fix, R));
111 h0.LineWidth = 2;
112 clabel(p1p2_0, h0);
113 %caxis([500 3000]);
114 xlabel('Young''s Modulus (Pa)');
115 ylabel('Radius (m)');
116 t = title('(d)
    ', 'FontSize', 11);
117 %caxis([500 3000]);
118 %legend('f0 (Hz)');
119
120 subplot(5,2,5)
121
122 [RHO,NU] = meshgrid(rho,nu);
123 [p1p2_0, h0] = contourf(RHO,NU,f0(E_v_fix,RHO,NU, d_fix, r_fix));
124 h0.LineWidth = 2;
125 clabel(p1p2_0, h0);
126 %caxis([500 3000]);
127 xlabel('Density (Kg/m^3)');
128 ylabel('Poisson''s Ratio');
129 t = title('(e)
    ', 'FontSize', 11);
130 %caxis([500 3000]);
131 %legend('f0 (Hz)');
132
133 subplot(5,2,6)
134
135 [RHO,D] = meshgrid(rho,d);
136 [p1p2_0, h0] = contourf(RHO,D,f0(E_v_fix,RHO,nu_fix, D, r_fix));
137 h0.LineWidth = 2;
138 clabel(p1p2_0, h0);
139 %caxis([500 3000]);
140 xlabel('Density (Kg/m^3)');
141 ylabel('Thickness (m)');
142 t = title('(f)
    ', 'FontSize', 11);
143 %caxis([500 3000]);
144 %legend('f0 (Hz)');
145
```

A.2. MATLAB Codes for Parametric Models of Thin Plates

```
146 subplot(5,2,7)
147
148 [RHO,R] = meshgrid(rho,r);
149 [p1p2_0, h0] = contourf(RHO,R,f0(E_v_fix,RHO,nu_fix, d_fix, R));
150 h0.LineWidth = 2;
151 clabel(p1p2_0, h0);
152 %caxis([500 3000]);
153 xlabel('Density (Kg/m^3)');
154 ylabel('Radius (m)');
155 t = title('g)
    ', 'FontSize', 11);
156 %caxis([500 3000]);
157 %legend('f0 (Hz)');
158
159 subplot(5,2,8)
160
161 [NU,D] = meshgrid(nu,d);
162 [p1p2_0, h0] = contourf(NU,D,f0(E_v_fix,rho_fix,NU, D, r_fix));
163 h0.LineWidth = 2;
164 clabel(p1p2_0, h0);
165 %caxis([500 3000]);
166 xlabel('Poissons's Ratio');
167 ylabel('Thickness (m)');
168 t = title('h)
    ', 'FontSize', 11);
169 %caxis([500 3000]);
170 %legend('f0 (Hz)');
171
172 subplot(5,2,9)
173
174 [NU,R] = meshgrid(nu,r);
175 [p1p2_0, h0] = contourf(NU,R,f0(E_v_fix,rho_fix,NU, d_fix, R));
176 h0.LineWidth = 2;
177 clabel(p1p2_0, h0);
178 %caxis([500 3000]);
179 xlabel('Poissons's Ratio');
180 ylabel('Radius (m)');
181 t = title('i)
    ', 'FontSize', 11);
182 %caxis([500 3000]);
183 %legend('f0 (Hz)');
```

A.2. MATLAB Codes for Parametric Models of Thin Plates

```
184
185 subplot(5,2,10)
186
187 [D,R] = meshgrid(d,r);
188 [p1p2_0, h0] = contourf(D,R,f0(E_v_fix,rho_fix,nu_fix, D, R));
189 h0.LineWidth = 2;
190 clabel(p1p2_0, h0);
191 %caxis([500 3000]);
192 xlabel('Thickness (m)');
193 ylabel('Radius (m)');
194 t = title('j)
    ', 'FontSize', 11);%caxis([500 3000]);
195 %legend('f0 (Hz)');
196
197 %suptitle('Parametric Evaluation of Thin Plates Resonance...
198 % (Hz) - Speech Frequencies Optimization');
199
200 %% Low Frequency Optimization
201
202 [X1,X2,X3,X4, X5] = ndgrid(E_v,rho,nu, d, r);
203 F0 = f0(X1,X2,X3,X4, X5);
204
205 [F0_low,idx] = min(F0(:));
206
207 if sum(F0==max(F0(:)))>1
208     fprintf('Caution! Multiple values found!');
209 end
210 [i1,i2,i3,i4, i5] = ind2sub(size(F0),idx);
211
212 E_v_low = E_v(i1)
213 rho_low = rho(i2)
214 nu_low = nu(i3)
215 d_low = d(i4)
216 r_low = r(i5)
217
218 %% Plot Low Freq
219
220 figure()
221
222 subplot(5,2,1)
223
```

A.2. MATLAB Codes for Parametric Models of Thin Plates

```
224 [E-V,RHO] = meshgrid(E-v,rho);
225 [p1p2_0, h0] = contourf(E-V,RHO,f0(E-V,RHO,nu_low, d_low, r_low));
226 h0.LineWidth = 2;
227 clabel(p1p2_0, h0);
228 %caxis([500 3000]);
229 xlabel('Young''s Modulus (Pa)');
230 ylabel('Density (Kg/m^3)');
231 t = title(' (a)
    ', 'FontSize', 11);
232 %caxis([500 3000]);
233 %legend('f0 (Hz)');
234
235 subplot(5,2,2)
236
237 [E-V,NU] = meshgrid(E-v,nu);
238 [p1p2_0, h0] = contourf(E-V,NU,f0(E-V,rho_low,NU, d_low, r_low));
239 h0.LineWidth = 2;
240 clabel(p1p2_0, h0);
241 %caxis([500 3000]);
242 xlabel('Young''s Modulus (Pa)');
243 ylabel('Poisson''s Ratio');
244 t = title(' (b)
    ', 'FontSize', 11);
245 %caxis([500 3000]);
246 %legend('f0 (Hz)');
247
248 subplot(5,2,3)
249
250 [E-V,D] = meshgrid(E-v,d);
251 [p1p2_0, h0] = contourf(E-V,D,f0(E-V,rho_low,nu_low, D, r_low));
252 h0.LineWidth = 2;
253 clabel(p1p2_0, h0);
254 %caxis([500 3000]);
255 xlabel('Young''s Modulus (Pa)');
256 ylabel('Thickness (m)');
257 t = title(' (c)
    ', 'FontSize', 11);
258 %caxis([500 3000]);
259 %legend('f0 (Hz)');
260
261 subplot(5,2,4)
```

A.2. MATLAB Codes for Parametric Models of Thin Plates

```
262
263 [E-V,R] = meshgrid(E-v,r);
264 [p1p2_0, h0] = contourf(E-V,R,f0(E-V,rho_low,nu_low, d_low, R));
265 h0.LineWidth = 2;
266 clabel(p1p2_0, h0);
267 %caxis([500 3000]);
268 xlabel('Young's Modulus (Pa)');
269 ylabel('Radius (m)');
270 t = title('(d)
    ', 'FontSize', 11);
271 %caxis([500 3000]);
272 %legend('f0 (Hz)');
273
274 subplot(5,2,5)
275
276 [RHO,NU] = meshgrid(rho,nu);
277 [p1p2_0, h0] = contourf(RHO,NU,f0(E-v_low,RHO,NU, d_low, r_low));
278 h0.LineWidth = 2;
279 clabel(p1p2_0, h0);
280 %caxis([500 3000]);
281 xlabel('Density (Kg/m^3)');
282 ylabel('Poisson's Ratio');
283 t = title('(e)
    ', 'FontSize', 11);
284 %caxis([500 3000]);
285 %legend('f0 (Hz)');
286
287 subplot(5,2,6)
288
289 [RHO,D] = meshgrid(rho,d);
290 [p1p2_0, h0] = contourf(RHO,D,f0(E-v_low,RHO,nu_low, D, r_low));
291 h0.LineWidth = 2;
292 clabel(p1p2_0, h0);
293 %caxis([500 3000]);
294 xlabel('Density (Kg/m^3)');
295 ylabel('Thickness (m)');
296 t = title('(f)
    ', 'FontSize', 11);
297 %caxis([500 3000]);
298 %legend('f0 (Hz)');
299
```

A.2. MATLAB Codes for Parametric Models of Thin Plates

```
300 subplot(5,2,7)
301
302 [RHO,R] = meshgrid(rho,r);
303 [p1p2_0, h0] = contourf(RHO,R,f0(E_v_low,RHO,nu_low, d_low, R));
304 h0.LineWidth = 2;
305 clabel(p1p2_0, h0);
306 %caxis([500 3000]);
307 xlabel('Density (Kg/m^3)');
308 ylabel('Radius (m)');
309 t = title('(g)
      ', 'FontSize', 11);
310 %caxis([500 3000]);
311 %legend('f0 (Hz)');
312
313 subplot(5,2,8)
314
315 [NU,D] = meshgrid(nu,d);
316 [p1p2_0, h0] = contourf(NU,D,f0(E_v_low,rho_low,NU, D, r_low));
317 h0.LineWidth = 2;
318 clabel(p1p2_0, h0);
319 %caxis([500 3000]);
320 xlabel('Poissons''s Ratio');
321 ylabel('Thickness (m)');
322 t = title('(h)
      ', 'FontSize', 11);
323 %caxis([500 3000]);
324 %legend('f0 (Hz)');
325
326 subplot(5,2,9)
327
328 [NU,R] = meshgrid(nu,r);
329 [p1p2_0, h0] = contourf(NU,R,f0(E_v_low,rho_low,NU, d_low, R));
330 h0.LineWidth = 2;
331 clabel(p1p2_0, h0);
332 %caxis([500 3000]);
333 xlabel('Poissons''s Ratio');
334 ylabel('Radius (m)');
335 t = title('(i)
      ', 'FontSize', 11);
336 %caxis([500 3000]);
337 %legend('f0 (Hz)');
```

A.2. MATLAB Codes for Parametric Models of Thin Plates

```
338
339 subplot(5,2,10)
340
341 [D,R] = meshgrid(d,r);
342 [p1p2_0, h0] = contourf(D,R,f0(E_v_low,rho_low,nu_low, D, R));
343 h0.LineWidth = 2;
344 clabel(p1p2_0, h0);
345 %caxis([500 3000]);
346 xlabel('Thickness (m)');
347 ylabel('Radius (m)');
348 t = title('(j)
    ', 'FontSize', 11);%caxis([500 3000]);
349 %legend('f0 (Hz)');
350
351 % subtitle('Parametric Evaluation of Thin Plates Resonance (Hz)...
352 %- Low Frequency Optimization');
353
354
355 %% High Frequency Optimization
356
357 [X1,X2,X3,X4, X5] = ndgrid(E_v,rho,nu, d, r);
358 F0 = f0(X1,X2,X3,X4, X5);
359
360 [F0_low,idx] = max(F0(:));
361
362 if sum(F0==max(F0(:))>1
363     fprintf('Caution! Multiple values found!');
364 end
365 [i1,i2,i3,i4, i5] = ind2sub(size(F0),idx);
366
367 E_v_high = E_v(i1)
368 rho_high = rho(i2)
369 nu_high = nu(i3)
370 d_high = d(i4)
371 r_high = r(i5)
372
373 %% Plot High Freq
374
375 figure()
376
377 subplot(5,2,1)
```


A.2. MATLAB Codes for Parametric Models of Thin Plates

```
378
379 [E-V,RHO] = meshgrid(E-v,rho);
380 [p1p2_0, h0] = contourf(E-V,RHO,f0(E-V,RHO,nu_high, d_high, r_high));
381 h0.LineWidth = 2;
382 clabel(p1p2_0, h0);
383 %caxis([500 3000]);
384 xlabel('Young''s Modulus (Pa)');
385 ylabel('Density (Kg/m^3)');
386 t = title('(a)
      ', 'FontSize', 11);
387 %caxis([500 3000]);
388 %legend('f0 (Hz)');
389
390 subplot(5,2,2)
391
392 [E-V,NU] = meshgrid(E-v,nu);
393 [p1p2_0, h0] = contourf(E-V,NU,f0(E-V,rho_high,NU, d_high, r_high));
394 h0.LineWidth = 2;
395 clabel(p1p2_0, h0);
396 %caxis([500 3000]);
397 xlabel('Young''s Modulus (Pa)');
398 ylabel('Poisson''s Ratio');
399 t = title('(b)
      ', 'FontSize', 11);
400 %caxis([500 3000]);
401 %legend('f0 (Hz)');
402
403 subplot(5,2,3)
404
405 [E-V,D] = meshgrid(E-v,d);
406 [p1p2_0, h0] = contourf(E-V,D,f0(E-V,rho_high,nu_high, D, r_high));
407 h0.LineWidth = 2;
408 clabel(p1p2_0, h0);
409 %caxis([500 3000]);
410 xlabel('Young''s Modulus (Pa)');
411 ylabel('Thickness (m)');
412 t = title('(c)
      ', 'FontSize', 11);
413 %caxis([500 3000]);
414 %legend('f0 (Hz)');
415
```

A.2. MATLAB Codes for Parametric Models of Thin Plates

```
416 subplot(5,2,4)
417
418 [E-V,R] = meshgrid(E-v,r);
419 [p1p2_0, h0] = contourf(E-V,R,f0(E-V,rho-high,nu-high, d-high, R));
420 h0.LineWidth = 2;
421 clabel(p1p2_0, h0);
422 %caxis([500 3000]);
423 xlabel('Young''s Modulus (Pa)');
424 ylabel('Radius (m)');
425 t = title('(d)
    ', 'FontSize', 11);
426 %caxis([500 3000]);
427 %legend('f0 (Hz)');
428
429 subplot(5,2,5)
430
431 [RHO,NU] = meshgrid(rho,nu);
432 [p1p2_0, h0] = contourf(RHO,NU,f0(E-v_high,RHO,NU, d-high, r_high));
433 h0.LineWidth = 2;
434 clabel(p1p2_0, h0);
435 %caxis([500 3000]);
436 xlabel('Density (Kg/m^3)');
437 ylabel('Poisson''s Ratio');
438 t = title('(e)
    ', 'FontSize', 11);
439 %caxis([500 3000]);
440 %legend('f0 (Hz)');
441
442 subplot(5,2,6)
443
444 [RHO,D] = meshgrid(rho,d);
445 [p1p2_0, h0] = contourf(RHO,D,f0(E-v_high,RHO,nu-high, D, r_high));
446 h0.LineWidth = 2;
447 clabel(p1p2_0, h0);
448 %caxis([500 3000]);
449 xlabel('Density (Kg/m^3)');
450 ylabel('Thickness (m)');
451 t = title('(f)
    ', 'FontSize', 11);
452 %caxis([500 3000]);
453 %legend('f0 (Hz)');
```

A.2. MATLAB Codes for Parametric Models of Thin Plates

```
454
455 subplot(5,2,7)
456
457 [RHO,R] = meshgrid(rho,r);
458 [p1p2_0, h0] = contourf(RHO,R,f0(E_v_high,RHO,nu_high, d_high, R));
459 h0.LineWidth = 2;
460 clabel(p1p2_0, h0);
461 %caxis([500 3000]);
462 xlabel('Density (Kg/m^3)');
463 ylabel('Radius (m)');
464 t = title(' (g)
    ', 'FontSize', 11);
465 %caxis([500 3000]);
466 %legend('f0 (Hz)');
467
468 subplot(5,2,8)
469
470 [NU,D] = meshgrid(nu,d);
471 [p1p2_0, h0] = contourf(NU,D,f0(E_v_high,rho_high,NU, D, r_high));
472 h0.LineWidth = 2;
473 clabel(p1p2_0, h0);
474 %caxis([500 3000]);
475 xlabel('Poissons''s Ratio');
476 ylabel('Thickness (m)');
477 t = title(' (h)
    ', 'FontSize', 11);
478 %caxis([500 3000]);
479 %legend('f0 (Hz)');
480
481 subplot(5,2,9)
482
483 [NU,R] = meshgrid(nu,r);
484 [p1p2_0, h0] = contourf(NU,R,f0(E_v_high,rho_high,NU, d_high, R));
485 h0.LineWidth = 2;
486 clabel(p1p2_0, h0);
487 %caxis([500 3000]);
488 xlabel('Poissons''s Ratio');
489 ylabel('Radius (m)');
490 t = title(' (i)
    ', 'FontSize', 11);
491 %caxis([500 3000]);
```

A.2. MATLAB Codes for Parametric Models of Thin Plates

```
492 %legend('f0 (Hz)');
493
494 subplot(5,2,10)
495
496 [D,R] = meshgrid(d,r);
497 [p1p2_0, h0] = contourf(D,R,f0(E_v_high,rho_high,nu_high, D, R));
498 h0.LineWidth = 2;
499 clabel(p1p2_0, h0);
500 %caxis([500 3000]);
501 xlabel('Thickness (m)');
502 ylabel('Radius(m)');
503 t = title('j)
    ', 'FontSize', 11);%caxis([500 3000]);
504 %legend('f0 (Hz)');
505
506 %suptitle('Parametric Evaluation of Thin Plates Resonance (Hz)...
507 % - High Frequencies Optimization');
508
509
510 %% Mid Frequency Optimization
511
512 [X1,X2,X3,X4,X5] = ndgrid(E_v,rho,nu,d,r);
513 F0 = f0(X1,X2,X3,X4,X5);
514
515 F0_mean = mean(F0,'all');
516 F0_mean_eval = abs(F0-F0_mean);
517 [F0_mean_val,F0_mean_idx] = min(F0_mean_eval(:));
518
519 if sum(F0==max(F0(:)))>1
520     fprintf('Caution! Multiple values found!');
521 end
522 [i1,i2,i3,i4, i5] = ind2sub(size(F0),F0_mean_idx);
523
524 E_v_mean = E_v(i1);
525 rho_mean = rho(i2);
526 nu_mean = nu(i3);
527 d_mean = d(i4);
528 r_mean = r(i5);
529
530 %% Plot Mid Freq
531
```

A.2. MATLAB Codes for Parametric Models of Thin Plates

```
532 figure()
533
534 subplot(5,2,1)
535
536 [E_V,RHO] = meshgrid(E_v,rho);
537 [p1p2_0, h0] = contourf(E_V,RHO,f0(E_V,RHO,nu_mean, d_mean, r_mean));
538 h0.LineWidth = 2;
539 clabel(p1p2_0, h0);
540 %caxis([500 3000]);
541 xlabel('Young''s Modulus (Pa)');
542 ylabel('Density (Kg/m^3)');
543 t = title(' (a)
    ', 'FontSize', 11);
544 %caxis([500 3000]);
545 %legend('f0 (Hz)');
546
547 subplot(5,2,2)
548
549 [E_V,NU] = meshgrid(E_v,nu);
550 [p1p2_0, h0] = contourf(E_V,NU,f0(E_V,rho_mean,NU, d_mean, r_mean));
551 h0.LineWidth = 2;
552 clabel(p1p2_0, h0);
553 %caxis([500 3000]);
554 xlabel('Young''s Modulus (Pa)');
555 ylabel('Poisson''s Ratio');
556 t = title(' (b)
    ', 'FontSize', 11);
557 %caxis([500 3000]);
558 %legend('f0 (Hz)');
559
560 subplot(5,2,3)
561
562 [E_V,D] = meshgrid(E_v,d);
563 [p1p2_0, h0] = contourf(E_V,D,f0(E_V,rho_mean,nu_mean, D, r_mean));
564 h0.LineWidth = 2;
565 clabel(p1p2_0, h0);
566 %caxis([500 3000]);
567 xlabel('Young''s Modulus (Pa)');
568 ylabel('Thickness (m)');
569 t = title(' (c)
    ', 'FontSize', 11);
```

A.2. MATLAB Codes for Parametric Models of Thin Plates

```
570 %caxis([500 3000]);
571 %legend('f0 (Hz)');
572
573 subplot(5,2,4)
574
575 [E-V,R] = meshgrid(E-v,r);
576 [p1p2_0, h0] = contourf(E-V,R,f0(E-V,rho_mean,nu_mean, d_mean, R));
577 h0.LineWidth = 2;
578 clabel(p1p2_0, h0);
579 %caxis([500 3000]);
580 xlabel('Young''s Modulus (Pa)');
581 ylabel('Radius (m)');
582 t = title('(d)
    ', 'FontSize', 11);
583 %caxis([500 3000]);
584 %legend('f0 (Hz)');
585
586 subplot(5,2,5)
587
588 [RHO,NU] = meshgrid(rho,nu);
589 [p1p2_0, h0] = contourf(RHO,NU,f0(E-v_mean,RHO,NU, d_mean, r_mean));
590 h0.LineWidth = 2;
591 clabel(p1p2_0, h0);
592 %caxis([500 3000]);
593 xlabel('Density (Kg/m^3)');
594 ylabel('Poisson''s Ratio');
595 t = title('(e)
    ', 'FontSize', 11);
596 %caxis([500 3000]);
597 %legend('f0 (Hz)');
598
599 subplot(5,2,6)
600
601 [RHO,D] = meshgrid(rho,d);
602 [p1p2_0, h0] = contourf(RHO,D,f0(E-v_mean,RHO,nu_mean, D, r_mean));
603 h0.LineWidth = 2;
604 clabel(p1p2_0, h0);
605 %caxis([500 3000]);
606 xlabel('Density (Kg/m^3)');
607 ylabel('Thickness (m)');
608 t = title('(f)
```

A.2. MATLAB Codes for Parametric Models of Thin Plates

```
    ', 'FontSize', 11);
609 %caxis([500 3000]);
610 %legend('f0 (Hz)');
611
612 subplot(5,2,7)
613
614 [RHO,R] = meshgrid(rho,r);
615 [p1p2_0, h0] = contourf(RHO,R,f0(E_v_mean,RHO,nu_mean, d_mean, R));
616 h0.LineWidth = 2;
617 clabel(p1p2_0, h0);
618 %caxis([500 3000]);
619 xlabel('Density (Kg/m^3)');
620 ylabel('Radius (m)');
621 t = title('(g)
    ', 'FontSize', 11);
622 %caxis([500 3000]);
623 %legend('f0 (Hz)');
624
625 subplot(5,2,8)
626
627 [NU,D] = meshgrid(nu,d);
628 [p1p2_0, h0] = contourf(NU,D,f0(E_v_mean,rho_mean,NU, D, r_mean));
629 h0.LineWidth = 2;
630 clabel(p1p2_0, h0);
631 %caxis([500 3000]);
632 xlabel('Poissons''s Ratio');
633 ylabel('Thickness (m)');
634 t = title('(h)
    ', 'FontSize', 11);
635 %caxis([500 3000]);
636 %legend('f0 (Hz)');
637
638 subplot(5,2,9)
639
640 [NU,R] = meshgrid(nu,r);
641 [p1p2_0, h0] = contourf(NU,R,f0(E_v_mean,rho_mean,NU, d_mean, R));
642 h0.LineWidth = 2;
643 clabel(p1p2_0, h0);
644 %caxis([500 3000]);
645 xlabel('Poissons''s Ratio');
646 ylabel('Radius (m)');
```

A.2. MATLAB Codes for Parametric Models of Thin Plates

```
647 t = title(' (i)
      ', 'FontSize', 11);
648 %caxis([500 3000]);
649 %legend('f0 (Hz)');
650
651 subplot(5,2,10)
652
653 [D,R] = meshgrid(d,r);
654 [p1p2_0, h0] = contourf(D,R,f0(E_v_mean,rho_mean,nu_mean, D, R));
655 h0.LineWidth = 2;
656 clabel(p1p2_0, h0);
657 %caxis([500 3000]);
658 xlabel('Thickness (m)');
659 ylabel('Radius (m)');
660 t = title(' (j)
      ', 'FontSize', 11);%caxis([500 3000]);
661 %legend('f0 (Hz)');
662
663 % supitle('Parametric Evaluation of Thin Plates Resonance (Hz)...
664 % - Mid Frequencies Optimization');
```


Bibliography

- [1] R. B. Lindsay, “Erratum: Report to the National Science Foundation on the Conference on Education in Acoustics [J. Acoust. Soc. Am. 36, 2241–2243 (1964); p. 2242],” *The Journal of the Acoustical Society of America*, vol. 37, p. 758, apr 1965.
- [2] T. Rossing, ed., *Springer Handbook of Acoustics*. 2nd ed., 2014.
- [3] Z. Liu, X. Zhang, Y. Mao, Y. Y. Zhu, Z. Yang, C. T. Chan, and P. Sheng, “Locally resonant sonic materials,” *Science*, 2000.
- [4] R. Martínez-Sala, J. Sancho, J. V. Sánchez, V. Gómez, J. Llinares, and F. Meseguer, “Sound attenuation by sculpture,” *Nature*, 1995.
- [5] T. Miyashita, R. Taniguchi, and H. Sakamoto, “Experimental full band-gap of a sonic-crystal slab structure of a 2D lattice of aluminum rods in air,” in *Proc. 5th World Congress on Ultrasonics TO-PM04.02*, 2003.
- [6] N. Fang, D. Xi, J. Xu, M. Ambati, W. Srituravanich, C. Sun, and X. Zhang, “Ultrasonic metamaterials with negative modulus,” *Nature Materials*, vol. 5, no. 6, pp. 452–456, 2006.
- [7] F. Lemoult, N. Kaina, M. Fink, and G. Lerosey, “Wave propagation control at the deep subwavelength scale in metamaterials,” *Nat Phys*, vol. 9, pp. 55–60, jan 2013.
- [8] Z. Yang, H. M. Dai, N. H. Chan, G. C. Ma, and P. Sheng, “Acoustic metamaterial panels for sound attenuation in the 50–1000 Hz regime,” *Applied Physics Letters*, vol. 96, no. 4, p. 41906, 2010.
- [9] Y. Xie, T.-H. Tsai, A. Konneker, B.-I. Popa, D. J. Brady, and S. A. Cummer, “Single-sensor multispeaker listening with acoustic metamaterials,” *Proceedings of the National Academy of Sciences*, vol. 112, pp. 10595–10598, aug 2015.
- [10] H. Esfahlani, S. Karkar, H. Lissek, and J. R. Mosig, “Exploiting the leaky-wave properties of transmission-line metamaterials for single-microphone direction finding,” *The Journal of the Acoustical Society of America*, vol. 139, no. 6, pp. 3259–3266, 2016.

- [11] R. Ghaffarivardavagh, J. Nikolajczyk, S. Anderson, and X. Zhang, “Ultra-open acoustic metamaterial silencer based on Fano-like interference,” *Physical Review B*, vol. 99, p. 24302, jan 2019.
- [12] L. Zigoneanu, B. I. Popa, and S. A. Cummer, “Three-dimensional broadband omnidirectional acoustic ground cloak,” *Nature Materials*, 2014.
- [13] N. Jiménez, T. J. Cox, V. Romero-García, and J.-P. Groby, “Metadiffusers: Deep-subwavelength sound diffusers,” *Scientific Reports*, vol. 7, no. 1, p. 5389, 2017.
- [14] K. Deng, Y. Ding, Z. He, H. Zhao, J. Shi, and Z. Liu, “Theoretical study of subwavelength imaging by acoustic metamaterial slabs,” in *Journal of Applied Physics*, 2009.
- [15] L. Y. Wu, L. W. Chen, and C. M. Liu, “Acoustic energy harvesting using resonant cavity of a sonic crystal,” *Applied Physics Letters*, 2009.
- [16] J. S. Bolton, R. J. Yun, J. Pope, and D. Apfel, “Development of a new sound transmission test for automotive sealant materials,” in *SAE Technical Papers*, 1997.
- [17] B. H. Song and J. S. Bolton, “A transfer-matrix approach for estimating the characteristic impedance and wave numbers of limp and rigid porous materials,” *The Journal of the Acoustical Society of America*, vol. 107, pp. 1131–1152, feb 2000.
- [18] World Health Organization., “Environmental noise guidelines for the European region.,” 2018.
- [19] A. Hansell, Y. S. Cai, and J. Gulliver, “Cardiovascular Health Effects of Road Traffic Noise,” in *Environmental Impacts of Road Vehicles: Past, Present and Future*, pp. 107–132, The Royal Society of Chemistry, 2017.
- [20] C. Clark, H. Sbihi, L. Tamburic, M. Brauer, L. D. Frank, and H. W. Davies, “Association of Long-Term Exposure to Transportation Noise and Traffic-Related Air Pollution with the Incidence of Diabetes: A Prospective Cohort Study,” *Environmental health perspectives*, vol. 125, p. 87025, aug 2017.
- [21] B. Shield, R. Conetta, J. Dockrell, D. Connolly, T. Cox, and C. Mydlarz, “A survey of acoustic conditions and noise levels in secondary school classrooms in England,” *The Journal of the Acoustical Society of America*, vol. 137, pp. 177–188, jan 2015.
- [22] A. L. Bronzaft, “The effect of a noise abatement program on reading ability,” *Journal of Environmental Psychology*, vol. 1, no. 3, pp. 215–222, 1981.
- [23] K. D. Kryter, D. H. K. Lee, E. W. Hewson, and C. F. Gurnham, *The Effects of Noise on Man*. Elsevier Science, 2013.

- [24] J. Méline, A. Van Hulst, F. Thomas, and B. Chaix, “Road, rail, and air transportation noise in residential and workplace neighborhoods and blood pressure (RECORD Study),” *Noise & health*, vol. 17, no. 78, pp. 308–319, 2015.
- [25] C. Mydlarz, M. Sharma, Y. Lockerman, B. Steers, C. Silva, and J. P. Bello, “The Life of a New York City Noise Sensor Network,” *Sensors (Basel, Switzerland)*, vol. 19, p. 1415, mar 2019.
- [26] J. P. Bello, C. Silva, O. Nov, R. L. Dubois, A. Arora, J. Salamon, C. Mydlarz, and H. Doraiswamy, “SONYC: A System for Monitoring, Analyzing, and Mitigating Urban Noise Pollution,” *Commun. ACM*, vol. 62, pp. 68–77, jan 2019.
- [27] R. Benocci, P. Bellucci, L. Peruzzi, A. Bisceglie, F. Angelini, C. Confalonieri, and G. Zambon, “Dynamic Noise Mapping in the Suburban Area of Rome (Italy),” *Environments*, vol. 6, no. 7, 2019.
- [28] H. E. Ware, C. J. W. McClure, J. D. Carlisle, and J. R. Barber, “A phantom road experiment reveals traffic noise is an invisible source of habitat degradation,” *Proceedings of the National Academy of Sciences*, vol. 112, pp. 12105 LP – 12109, sep 2015.
- [29] P. J. O. Miller, N. Biassoni, A. Samuels, and P. L. Tyack, “Whale songs lengthen in response to sonar,” *Nature*, vol. 405, no. 6789, p. 903, 2000.
- [30] G. Shannon, M. F. McKenna, L. M. Angeloni, K. R. Crooks, K. M. Fristrup, E. Brown, K. A. Warner, M. D. Nelson, C. White, J. Briggs, S. McFarland, and G. Wittemyer, “A synthesis of two decades of research documenting the effects of noise on wildlife,” *Biological Reviews*, vol. 91, pp. 982–1005, nov 2016.
- [31] C. D. Francis and J. R. Barber, “A framework for understanding noise impacts on wildlife: an urgent conservation priority,” *Frontiers in Ecology and the Environment*, vol. 11, pp. 305–313, aug 2013.
- [32] T. J. Cox, *Acoustic Absorbers and Diffusers*. 2018.
- [33] D. A. Bies and C. H. Hansen, *Engineering noise control : theory and practice*. 2003.
- [34] G. Müller and M. Möser, *Handbook of engineering acoustics*. Springer Berlin Heidelberg, jan 2013.
- [35] L. L. Beranek and A. S. of America, *Acoustics*. Electrical and electronic engineering, American Institute of Physics, 1986.
- [36] M. J. Crocker, *Handbook of Noise and Vibration Control*. 2008.
- [37] S. M. Kuo and D. R. Morgan, “Active noise control: a tutorial review,” *Proceedings of the IEEE*, 1999.

- [38] S. J. Elliott and P. A. Nelson, “The Active Control of Sound,” *Electronics and Communication Engineering Journal*, 1990.
- [39] G. Ma and P. Sheng, “Acoustic metamaterials: From local resonances to broad horizons,” *Science Advances*, vol. 2, no. 2, pp. e1501595–e1501595, 2016.
- [40] S. A. Cummer, J. Christensen, and A. Alù, “Controlling sound with acoustic metamaterials,” *Nature Reviews Materials*, vol. 1, no. 3, p. 16001, 2016.
- [41] F. Zangeneh-Nejad and R. Fleury, “Active times for acoustic metamaterials,” *Reviews in Physics*, vol. 4, p. 100031, 2019.
- [42] S. H. Lee, C. M. Park, Y. M. Seo, Z. G. Wang, and C. K. Kim, “Acoustic metamaterial with negative modulus,” *Journal of Physics Condensed Matter*, 2009.
- [43] S. H. Lee, C. M. Park, Y. M. Seo, Z. G. Wang, and C. K. Kim, “Acoustic metamaterial with negative density,” *Physics Letters A*, vol. 373, no. 48, pp. 4464–4469, 2009.
- [44] J. Christensen, L. Martín-Moreno, and F. J. García-Vidal, “All-angle blockage of sound by an acoustic double-fishnet metamaterial,” *Applied Physics Letters*, 2010.
- [45] T.-Y. Huang, C. Shen, and Y. Jing, “Membrane- and plate-type acoustic metamaterials,” *The Journal of the Acoustical Society of America*, vol. 139, no. 6, pp. 3240–3250, 2016.
- [46] B. E. Kelly, I. Bhattacharya, H. Heidari, M. Shusteff, C. M. Spadaccini, and H. K. Taylor, “Volumetric additive manufacturing via tomographic reconstruction,” *Science*, vol. 363, pp. 1075 LP – 1079, mar 2019.
- [47] B. Tiller, A. Reid, B. Zhu, J. Guerreiro, R. Domingo-Roca, J. Curt Jackson, and J. F. C. Windmill, “Piezoelectric microphone via a digital light processing 3D printing process,” *Materials & Design*, vol. 165, p. 107593, 2019.
- [48] E. Behroodi, H. Latifi, and F. Najafi, “A compact LED-based projection microstereolithography for producing 3D microstructures,” *Scientific Reports*, vol. 9, no. 1, p. 19692, 2019.
- [49] D. T. Blackstock, *Fundamentals of physical acoustics*. John Wiley & Sons, 2000.
- [50] A. D. Pierce, *Acoustics: An Introduction to Its Physical Principles and Applications*. McGraw-Hill Book Company, 1981.
- [51] G. Loy, *Musimathics: The Mathematical Foundations of Music, Volume 1*. The MIT Press, 2006.
- [52] N. H. N. H. Fletcher, *Acoustic systems in biology*. Oxford University Press, 1992.

- [53] P. M. C. Morse, *Vibration and Sound*. International series in pure and applied physics, McGraw-Hill Book Company, 1948.
- [54] W. H. Bragg and W. L. Bragg, “The Reflection of X-rays by Crystals,” *Proc. R. Soc. Lond.*, vol. 88, no. A, pp. 428–438, 1913.
- [55] DENORMS COST Action 15125, “Training School on Sound Waves in Metamaterials and Porous Media,” 2016.
- [56] H. L. F. von Helmholtz and A. J. Ellis, *On the sensations of tone as a physiological basis for the theory of music*. 1875.
- [57] L. E. Kinsler, A. R. Frey, A. B. Coppens, and V. Sanders, James, *Fundamentals of acoustics*. Wiley, 3rd editio ed., 1982.
- [58] B. Parker, *Good vibrations: The physics of music*. 2009.
- [59] S. Singh, “Acoustic Materials and Metamaterials,” *IIT Roorkee*, https://onlinecourses.nptel.ac.in/noc21_me48/preview, 2020.
- [60] M. Lapine and S. Tretyakov, “Contemporary notes on metamaterials,” *Microwaves, Antennas & Propagation, IET*, vol. 1, pp. 3–11, 2007.
- [61] W. S. Weiglhofer and A. Lakhtakia, *Introduction to Complex Mediums for Optics and Electromagnetics*. Press Monographs, SPIE Press, 2003.
- [62] A. Sihvola, “Electromagnetic Emergence in Metamaterials,” in *Advances in Electromagnetics of Complex Media and Metamaterials* (S. Zouhdi, A. Sihvola, and M. Arsalane, eds.), pp. 3–17, Dordrecht: Springer Netherlands, 2002.
- [63] V. G. Veselago, “The electrodynamics of substances with simultaneously negative values of epsilon and mu,” *Soviet Physics Uspekhi*, 1968.
- [64] D. J. Griffiths, *Introduction to Electrodynamics*. Cambridge University Press, 4 ed., 2017.
- [65] E. Yablonovitch, “Inhibited spontaneous emission in solid-state physics and electronics,” *Physical Review Letters*, 1987.
- [66] E. Yablonovitch, T. J. Gmitter, and K. M. Leung, “Photonic band structure: The face-centered-cubic case employing nonspherical atoms,” *Physical Review Letters*, 1991.
- [67] A. Z. Genack and N. Garcia, “Observation of photon localization in a three-dimensional disordered system,” *Physical Review Letters*, 1991.
- [68] J. B. Pendry, A. J. Holden, D. J. Robbins, and W. J. Stewart, “Magnetism from conductors and enhanced nonlinear phenomena,” *IEEE Transactions on Microwave Theory and Techniques*, 1999.

BIBLIOGRAPHY

- [69] J. B. Pendry, “Negative refraction makes a perfect lens,” *Physical Review Letters*, 2000.
- [70] D. R. Smith, D. C. Vier, N. Kroll, and S. Schultz, “Direct calculation of permeability and permittivity for a left-handed metamaterial,” *Applied Physics Letters*, 2000.
- [71] D. R. Smith, W. J. Padilla, D. C. Vier, S. C. Nemat-Nasser, and S. Schultz, “Composite medium with simultaneously negative permeability and permittivity,” *Physical Review Letters*, 2000.
- [72] A. J. Hoffman, L. Alekseyev, S. S. Howard, K. J. Franz, D. Wasserman, V. A. Podolskiy, E. E. Narimanov, D. L. Sivco, and C. Gmachl, “Negative refraction in semiconductor metamaterials,” *Nature Materials*, vol. 6, no. 12, pp. 946–950, 2007.
- [73] D. Schurig, J. J. Mock, B. J. Justice, S. A. Cummer, J. B. Pendry, A. F. Starr, and D. R. Smith, “Metamaterial Electromagnetic Cloak at Microwave Frequencies,” *Science*, vol. 314, pp. 977 LP – 980, nov 2006.
- [74] R. Liu, C. Ji, J. J. Mock, J. Y. Chin, T. J. Cui, and D. R. Smith, “Broadband Ground-Plane Cloak,” *Science*, vol. 323, pp. 366 LP – 369, jan 2009.
- [75] J. Valentine, J. Li, T. Zentgraf, G. Bartal, and X. Zhang, “An optical cloak made of dielectrics,” *Nature Materials*, vol. 8, no. 7, pp. 568–571, 2009.
- [76] M. M. Sigalas and E. N. Economou, “Elastic and acoustic wave band structure,” 1992.
- [77] M. S. Kushwaha, P. Halevi, L. Dobrzynski, and B. Djafari-Rouhani, “Acoustic band structure of periodic elastic composites,” *Physical Review Letters*, 1993.
- [78] M. Kafesaki, M. M. Sigalas, and E. N. Economou, “Elastic wave band gaps in 3-D periodic polymer matrix composites,” *Solid State Communications*, 1995.
- [79] F. R. Montero de Espinosa, E. Jiménez, and M. Torres, “Ultrasonic band gap in a periodic two-dimensional composite,” *Physical Review Letters*, 1998.
- [80] N. W. Ashcroft and N. D. Mermin, *Solid State Physics*. Philadelphia: Saunders College, 1976.
- [81] T. Miyashita, “Sonic crystals and sonic wave-guides,” *Measurement Science and Technology*, vol. 16, no. 5, pp. R47–R63, 2005.
- [82] M. Kafesaki and E. N. Economou, “Multiple-scattering theory for three-dimensional periodic acoustic composites,” *Physical Review B - Condensed Matter and Materials Physics*, 1999.

- [83] I. Psarobas, N. Stefanou, and A. Modinos, "Scattering of elastic waves by periodic arrays of spherical bodies," *Physical Review B - Condensed Matter and Materials Physics*, 2000.
- [84] P. Sheng, X. X. Zhang, Z. Liu, and C. T. Chan, "Locally resonant sonic materials," in *Physica B: Condensed Matter*, 2003.
- [85] K. M. Ho, C. K. Cheng, Z. Yang, X. X. Zhang, and P. Sheng, "Broadband locally resonant sonic shields," *Applied Physics Letters*, 2003.
- [86] B. Yuan, V. F. Humphrey, J. Wen, and X. Wen, "On the coupling of resonance and Bragg scattering effects in three-dimensional locally resonant sonic materials," in *Ultrasonics*, 2013.
- [87] A. O. Krushynska, V. G. Kouznetsova, and M. G. Geers, "Towards optimal design of locally resonant acoustic metamaterials," *Journal of the Mechanics and Physics of Solids*, 2014.
- [88] Y. Ding, Z. Liu, C. Qiu, and J. Shi, "Metamaterial with simultaneously negative bulk modulus and mass density," *Physical Review Letters*, 2007.
- [89] C. Ding, L. Hao, and X. Zhao, "Two-dimensional acoustic metamaterial with negative modulus," *Journal of Applied Physics*, 2010.
- [90] C. Casarini, J. Windmill, and J. Jackson, "3D printed small-scale acoustic metamaterials based on Helmholtz resonators with tuned overtones (In press)," in *IEEE Sensors Conference*, 2017.
- [91] C. Casarini, B. Tiller, C. Mineo, C. N. Macleod, J. F. C. Windmill, and J. C. Jackson, "Enhancing the Sound Absorption of Small-Scale 3-D Printed Acoustic Metamaterials Based on Helmholtz Resonators," *IEEE Sensors Journal*, vol. 18, no. 19, pp. 7949–7955, 2018.
- [92] J. M. De Bedout, M. A. Franchek, R. J. Bernhard, and L. Mongeau, "Adaptive-passive noise control with self-tuning Helmholtz resonators," *Journal of Sound and Vibration*, 1997.
- [93] M. Reynolds, Y. Gao, and S. Daley, "Experimental validation of the band-gap and dispersive bulk modulus behaviour of locally resonant acoustic metamaterials," in *Proceedings of Meetings on Acoustics*, 2013.
- [94] Z. Yang, J. Mei, M. Yang, N. H. Chan, and P. Sheng, "Membrane-type acoustic metamaterial with negative dynamic mass," *Physical Review Letters*, 2008.
- [95] C. J. Naify, C.-M. Chang, G. McKnight, and S. Nutt, "Transmission loss and dynamic response of membrane-type locally resonant acoustic metamaterials," *Journal of Applied Physics*, vol. 108, p. 114905, dec 2010.

- [96] C. J. Naify, C.-M. Chang, G. McKnight, and S. Nutt, “Transmission loss of membrane-type acoustic metamaterials with coaxial ring masses,” *Journal of Applied Physics*, vol. 110, p. 124903, dec 2011.
- [97] Z. Lu, X. Yu, S. K. Lau, B. C. Khoo, and F. Cui, “Membrane-type acoustic metamaterial with eccentric masses for broadband sound isolation,” *Applied Acoustics*, 2020.
- [98] J. Zhao, X. Li, W. Wang, Y. Wang, L. Zhu, and Y. Liu, “Membrane-type acoustic metamaterials with tunable frequency by a compact magnet,” *The Journal of the Acoustical Society of America*, 2019.
- [99] S. Chen, Y. Fan, Q. Fu, H. Wu, Y. Jin, J. Zheng, and F. Zhang, “A Review of Tunable Acoustic Metamaterials,” *Applied Sciences*, vol. 8, p. 1480, aug 2018.
- [100] A. Baz, “The structure of an active acoustic metamaterial with tunable effective density,” *New Journal of Physics*, vol. 11, no. 12, p. 123010, 2009.
- [101] A. Baz, “Active acoustic metamaterials,” *The Journal of the Acoustical Society of America*, vol. 128, p. 2428, oct 2010.
- [102] W. Akl and A. Baz, “Analysis and experimental demonstration of an active acoustic metamaterial cell,” *Journal of Applied Physics*, vol. 111, p. 44505, feb 2012.
- [103] M. Oudich and Y. Li, “Tunable sub-wavelength acoustic energy harvesting with a metamaterial plate,” *Journal of Physics D: Applied Physics*, vol. 50, no. 31, p. 315104, 2017.
- [104] H. Lissek, R. Boulandet, and R. Fleury, “Electroacoustic absorbers: Bridging the gap between shunt loudspeakers and active sound absorption,” *The Journal of the Acoustical Society of America*, vol. 129, pp. 2968–2978, may 2011.
- [105] B.-I. Popa, L. Zigoneanu, and S. A. Cummer, “Tunable active acoustic metamaterials,” *Physical Review B*, vol. 88, p. 24303, jul 2013.
- [106] B.-I. Popa, D. Shinde, A. Konneker, and S. A. Cummer, “Active acoustic metamaterials reconfigurable in real time,” *Physical Review B*, vol. 91, p. 220303, jun 2015.
- [107] A. Allam, A. Elsabbagh, and W. Akl, “Experimental demonstration of one-dimensional active plate-type acoustic metamaterial with adaptive programmable density,” *Journal of Applied Physics*, vol. 121, p. 125106, mar 2017.
- [108] G. Y. Song, Q. Cheng, B. Huang, H. Y. Dong, and T. J. Cui, “Broadband fractal acoustic metamaterials for low-frequency sound attenuation,” *Applied Physics Letters*, 2016.

- [109] G. J. Bennett, E. P. Ross, and R. Hossain, “Membrane Metamaterials For Use In Broadband Noise Attenuation,” in *25th AIAA/CEAS Aeroacoustics Conference*, Aeroacoustics Conferences, American Institute of Aeronautics and Astronautics, may 2019.
- [110] E. C. Cherry, “Some Experiments on the Recognition of Speech, with One and with Two Ears,” *The Journal of the Acoustical Society of America*, vol. 25, pp. 975–979, sep 1953.
- [111] H. Chen and C. T. Chan, “Acoustic cloaking in three dimensions using acoustic metamaterials,” *Applied Physics Letters*, 2007.
- [112] S. A. Cummer and D. Schurig, “One path to acoustic cloaking,” *New Journal of Physics*, vol. 9, no. 3, p. 45, 2007.
- [113] H. Chen and C. T. Chan, “Acoustic cloaking and transformation acoustics,” *Journal of Physics D: Applied Physics*, 2010.
- [114] S. Zhang, C. Xia, and N. Fang, “Broadband acoustic cloak for ultrasound waves,” *Physical Review Letters*, 2011.
- [115] E. Ballesterro, N. Jiménez, J. P. Groby, S. Dance, H. Aygun, and V. Romero-García, “Experimental validation of deep-subwavelength diffusion by acoustic metadiffusers,” *Applied Physics Letters*, 2019.
- [116] M. Ambati, N. Fang, C. Sun, and X. Zhang, “Surface resonant states and superlensing in acoustic metamaterials,” *Physical Review B - Condensed Matter and Materials Physics*, 2007.
- [117] S. Guenneau, A. Movchan, G. Pétursson, and S. A. Ramakrishna, “Acoustic metamaterials for sound focusing and confinement,” *New Journal of Physics*, 2007.
- [118] L. Y. Wu, L. W. Chen, and C. M. Liu, “Experimental investigation of the acoustic pressure in cavity of a two-dimensional sonic crystal,” *Physica B: Condensed Matter*, 2009.
- [119] G. Hu, L. Tang, A. Banerjee, and R. Das, “Metastructure with Piezoelectric Element for Simultaneous Vibration Suppression and Energy Harvesting,” *Journal of Vibration and Acoustics, Transactions of the ASME*, 2017.
- [120] C. W. Hull, “Apparatus for Production of Three-Dimensional Objects By Stereo Thography,” *US Patent 4,575,330*, 1984.
- [121] C. Deckard, “Method and apparatus for producing parts by selective sintering,” *US Patent 4,863,538*, 1986.
- [122] S. S. Crump, “Apparatus and Method for Creating Three-Dimensional Objects,” *US Patent 5,121,329*, 1989.

- [123] N. Cubo, M. Garcia, J. F. Del Cañizo, D. Velasco, and J. L. Jorcano, “3D bioprinting of functional human skin: Production and in vivo analysis,” *Biofabrication*, 2017.
- [124] S. Derakhshanfar, R. Mbeleck, K. Xu, X. Zhang, W. Zhong, and M. Xing, “3D bioprinting for biomedical devices and tissue engineering: A review of recent trends and advances,” 2018.
- [125] J. I. Lipton, M. Cutler, F. Nigl, D. Cohen, and H. Lipson, “Additive manufacturing for the food industry,” *Trends in Food Science & Technology*, vol. 43, no. 1, pp. 114–123, 2015.
- [126] Z. Liu, M. Zhang, B. Bhandari, and Y. Wang, “3D printing: Printing precision and application in food sector,” *Trends in Food Science & Technology*, vol. 69, pp. 83–94, 2017.
- [127] Y. L. Yap and W. Y. Yeong, “Additive manufacture of fashion and jewellery products: a mini review,” *Virtual and Physical Prototyping*, vol. 9, pp. 195–201, jul 2014.
- [128] A. Vanderploeg, S.-E. Lee, and M. Mamp, “The application of 3D printing technology in the fashion industry,” *International Journal of Fashion Design, Technology and Education*, vol. 10, pp. 170–179, may 2017.
- [129] A. Zoran, “The 3D Printed Flute: Digital Fabrication and Design of Musical Instruments,” *Journal of New Music Research*, vol. 40, pp. 379–387, dec 2011.
- [130] F. Bos, R. Wolfs, Z. Ahmed, and T. Salet, “Additive manufacturing of concrete in construction: potentials and challenges of 3D concrete printing,” *Virtual and Physical Prototyping*, vol. 11, pp. 209–225, jul 2016.
- [131] Y. Reches, J. Livingston, I. Ferguson, D. Cranor, M. Lobovsky, and N. Linder, “Three-dimensional printer,” 2015.
- [132] J. Walter-Herrmann and C. Büching, *FabLab: Of machines, makers and inventors*. transcript Verlag, 2014.
- [133] U. Cura, “Advanced 3D printing software, made accessible. <https://www.ultimaker.com/en/products/ultimaker-cura-software>,” 2018.
- [134] A. Marano, “3D Printing to Innovate the Guitar Design,” in *International Conference on Applied Human Factors and Ergonomics*, pp. 16–23, Springer, 2019.
- [135] P. Qian, X. Niu, S. Lin, L. Ma, J. Ma, S. Yu, Z. Chen, G. Li, S. Fu, and J. Lin, “A comparison on sound quality of PLA 3-D printing Ukulele and single board wooden Ukulele,” in *Proceedings of Meetings on Acoustics 178ASA*, vol. 39, p. 35007, Acoustical Society of America, 2019.

- [136] A. Kantaros and O. Diegel, “3D printing technology in musical instrument research: reviewing the potential,” *Rapid Prototyping Journal*, 2018.
- [137] R. I. Haque, E. Ogam, C. Loussert, P. Benaben, and X. Boddaert, “Fabrication of capacitive acoustic resonators combining 3D printing and 2D inkjet printing techniques,” *Sensors (Switzerland)*, 2015.
- [138] P. F. Jacobs, D. T. Reid, Computer, and A. S. A. of SME., *Rapid Prototyping & Manufacturing: Fundamentals of Stereolithography*. Society of Manufacturing Engineers, 1992.
- [139] H. Gong, M. Beauchamp, S. Perry, A. T. Woolley, and G. P. Nordin, “Optical Approach to Resin Formulation for 3D Printed Microfluidics,” *RSC advances*, vol. 5, pp. 106621–106632, dec 2015.
- [140] A. Farina, “Simultaneous measurement of impulse response and distortion with a swept-sine technique,” *Proc. AES 108th conv, Paris, France*, 2000.
- [141] C. Daraio, “Multipurpose metamaterials: designing for static, acoustic and elastic properties in a single architecture,” 2020.
- [142] C. N. MacLeod, R. Summan, G. Dobie, and S. G. Pierce, “Quantifying and Improving Laser Range Data When Scanning Industrial Materials,” *IEEE Sensors Journal*, vol. 16, no. 22, pp. 7999–8009, 2016.
- [143] C. Mineo, S. G. Pierce, P. I. Nicholson, and I. Cooper, “Robotic path planning for non-destructive testing – A custom MATLAB toolbox approach,” *Robotics and Computer-Integrated Manufacturing*, vol. 37, pp. 1–12, 2016.
- [144] A. Leblanc and A. Lavie, “3D printed membrane-type acoustic metamaterials with structured masses,” *The Journal of the Acoustical Society of America*, vol. 140, no. 4, p. 3104, 2016.
- [145] A. Leblanc and A. Lavie, “Three-dimensional-printed membrane-type acoustic metamaterial for low frequency sound attenuation,” *The Journal of the Acoustical Society of America*, vol. 141, pp. EL538–EL542, jun 2017.
- [146] A. Merkel, G. Theocharis, O. Richoux, V. Romero-García, and V. Pagneux, “Control of acoustic absorption in one-dimensional scattering by resonant scatterers,” *Applied Physics Letters*, vol. 107, p. 244102, dec 2015.
- [147] J.-P. Groby, W. Huang, A. Lardeau, and Y. Aurégan, “The use of slow waves to design simple sound absorbing materials,” *Journal of Applied Physics*, vol. 117, p. 124903, mar 2015.
- [148] F. Bongard, H. Lissek, and J. R. Mosig, “Acoustic transmission line metamaterial with negative/zero/positive refractive index,” *Physical Review B*, vol. 82, p. 94306, sep 2010.

- [149] N. Sui, X. Yan, T.-Y. Huang, J. Xu, F.-G. Yuan, and Y. Jing, “A lightweight yet sound-proof honeycomb acoustic metamaterial,” *Applied Physics Letters*, vol. 106, p. 171905, apr 2015.
- [150] S. Y. Hu, X. Zhou, and Gengkai, “Investigation of the negative-mass behaviors occurring below a cut-off frequency,” *New Journal of Physics*, vol. 12, no. 10, p. 103025, 2010.
- [151] S. Varanasi, J. S. Bolton, T. H. Siegmund, and R. J. Cipra, “The low frequency performance of metamaterial barriers based on cellular structures,” *Applied Acoustics*, vol. 74, no. 4, pp. 485–495, 2013.
- [152] C. Perala, “Active noise reduction headphone measurement: Comparison of physical and psychophysical protocols and effects of microphone placement,” apr 2006.
- [153] A. Shalool, N. Zainal, K. B. Gan, and C. Umat, “An investigation of passive and active noise reduction using commercial and standard TDH-49 headphones,” in *2016 International Conference on Advances in Electrical, Electronic and Systems Engineering (ICAEES)*, pp. 606–609, 2016.
- [154] M. Reynolds and S. Daley, “An active viscoelastic metamaterial for isolation applications,” *Smart Materials and Structures*, 2014.
- [155] J. Tan, J. Cheer, and S. Daley, “Practical realisation of an active acoustic metamaterial building block,” *Proceedings of Meetings on Acoustics*, vol. 39, p. 45006, dec 2019.
- [156] B. I. Popa and S. A. Cummer, “Non-reciprocal and highly nonlinear active acoustic metamaterials,” *Nature communications*, 2014.
- [157] A. Bacigalupo, M. L. De Bellis, and D. Misseroni, “Design of tunable acoustic metamaterials with periodic piezoelectric microstructure,” *Extreme Mechanics Letters*, 2020.
- [158] “Nissan shows new, lightweight noise-reducing technology at CES,” <https://global.nissannews.com/en/releases/nissan-shows-new-lightweight-noise-reducing-technology-at-ces>.
- [159] J. Liu, H. Guo, and T. Wang, “A Review of Acoustic Metamaterials and Phononic Crystals,” *Crystals*, vol. 10, p. 305, apr 2020.